ASSESSING THE IMPACT OF DIOXIN ON HUMAN HEALTH THROUGH MATHEMATICAL MODELING

A Dissertation

Presented to

The Academic Faculty

by

Carla Kumbale

In Partial Fulfillment

of the Requirements for the Degree

Doctor of Philosophy in Bioengineering in the

Wallace H. Coulter Department of Biomedical Engineering

at The Georgia Institute of Technology and Emory University

Georgia Institute of Technology

May 2024

ASSESSING THE IMPACT OF DIOXIN ON HUMAN HEALTH THROUGH MATHEMATICAL MODELING

Approved by:

Dr. Eberhard Voit, Advisor
Wallace H. Coulter Dept. of Biomedical Engineering
Georgia Institute of Technology and Emory University; University of Texas at Dallas

Dr. Peng Qiu
School of Wallace H. Coulter Dept. of Biomedical Engineering
Georgia Institute of Technology and Emory University

Dr. Qiang Zhang, Co-Advisor
Gangarosa Department of Environmental Health, School of Public Health
Emory University

Dr. Mark Styczynski
School of Chemical and Biomolecular Engineering
Georgia Institute of Technology

Dr. Melissa Kemp
School of Wallace H. Coulter Dept. of Biomedical Engineering
Georgia Institute of Technology and Emory University

Date Approved: April 12, 2024

In memory of our dearly departed friend, Dr. Dan Zhang.

ACKNOWLEDGEMENTS

As I close this monumental chapter of my academic journey, I am overwhelmed with gratitude for the myriad of individuals who have illuminated my path towards the completion of this dissertation. The journey to this point has been an incredibly wonderful experience; a journey that I could not have embarked upon without the support, guidance, and encouragement of many.

First and foremost, my deepest appreciation goes to my advisors, Drs. Eberhard Voit and Qiang Zhang whose expertise, understanding, and patience added considerably to my graduate experience. To Dr. Voit, my sincerest gratitude for introducing me to the captivating world of systems biology. Your guidance has been my compass throughout the entirety of my academic journey. Through the many lessons imparted, the stories shared, and the laughter that echoed in our halls, you have transformed my PhD experience into an unparalleled adventure. Your mentorship has not only enriched my academic pursuits but has also made this journey one of the most rewarding experiences any student could wish for. To Dr. Zhang, it feels like just yesterday we were sitting in your office overwhelmed with excitement over my admission to the PhD program. I sincerely thank you for the immense support you have extended to me throughout the years. Thank you for going above and beyond, making time to meet with me outside of regular working hours, and ensuring the success and progression of my research. Your dedication and effort have been truly invaluable.

I extend my heartfelt thanks to the members of my dissertation committee, Drs. Melissa Kemp, Peng Qiu, and Mark Styczynski, for their insightful comments and encouragement. Your feedback was invaluable in shaping this research. I also want to

thank our collaborators at Michigan State University, Drs. Rance Nault, John Lapres and Tim Zacharewski, and Dr. Shuo Xiao at Rutgers University, for helpful discussions throughout this research. Additionally, my gratitude extends to HERCULES at Emory/GT and the NIEHS for supporting this research.

To Drs. Jacob Davis, Luis Fonseca, Anuj Gupta, and Daniel Olivença who are not only considered my labmates but also my older brothers. Thank you for the endless laughter and for consistently looking out for me. Your support and camaraderie have been invaluable. Additionally, I wish to extend my gratitude to former members of the Voit Lab, Drs. Mojdeh Faraji and Gautam Goel, for their support and guidance, for which I will always remain thankful.

To my sister, Maya Andrea, you have been my light – always and forever. To my best friends, Lorena Magaña Zertuche, George Alexopoulos, Kyle Sullivan, Eva Kallou, Liana Hatoum, and Sarahna Moyd, who stood by me throughout this journey, thank you for your unwavering support and endless encouragement.

Lastly, but most importantly, I owe my deepest gratitude to my parents, Noelle and Murali Kumbale, my twin pillars, without whom I could not stand- I am honored to be your daughter. To Mom, thank you for your endless love and support and for instilling in me the courage to face any situation. You embody strength like no one else I know. To my Dad, thank you for your immense support, the countless lessons, and the guidance that has shaped me into the person I am today. I can hardly believe the time has come, and that I have realized my childhood dream of attending Georgia Tech, following in your footsteps. I hope to make you proud forever.

This dissertation stands as a testament not only to my efforts but to the collective support and belief of all of you in me. I am eternally grateful to each one of you. This achievement is not mine alone, but ours.

TABLE OF CONTENTS

LIST OF TABLES

LIST OF FIGURES

LIST OF SYMBOLS AND ABBREVIATIONS

AhR	Aryl hydrocarbon receptor
APOA1	Apolipoprotein A1
CTD	Comparative Toxicogenomic Database
CYP1A1	Cytochrome p450 enzyme A1
DRE	Dioxin response element
FDPS	Farnesyl diphosphate synthase
FPP	Farnesyl pyrophosphate
GPP	Geranyl pyrophosphate
HDL	High density lipoprotein
HMGCoA	3-hydroxy-3-methyl-glutaryl Coenzyme A
HMGCR	3-hydroxy-3-methyl-glutaryl-coenzyme A reductase
IDL	Intermediate-density lipoprotein
IVIVE	In vitro to in vivo extrapolations
JECFA	Joint FAO/WHO Expert Committee on Food Additives
LCAT	Lecithin–cholesterol acyltransferase
LDL	Low density lipoprotein
LSS	Lanosterol synthase
NAFLD	Non-alcoholic fatty liver disease
NAMs	New approach methodologies
ODEs	Ordinary differential equations
PBTK	Physiologically based toxicokinetics
PCBs	Polychlorinated biphenyls
POPs	Persistent organic pollutants
RfD	Reference dose
SQS	Squalene synthase
SREBP	Sterol regulatory element binding proteins
SREs	Sterol regulatory elements
T&A	Template-and-anchor (model)
T3DB	*Toxin and Toxin Target Database*
TCDD	2,3,7,8-tetrachlorodibenzo-p-dioxin
TD	Toxicodynamics
VLDL	Very low-density lipoprotein
XRE	Xenobiotic response element
E2	Estradiol
P4	Progesterone
A5	Androstenediol
T	Testosterone
LH	Luteinizing Hormone
FSH	Dioxin response element

SUMMARY

Biological systems are organized in distinct but connected layers, which makes their analysis a challenge. The higher layers usually correspond to a “big picture” of a physiological event, whereas the lower levels account for increasing granularity and detail. It is infeasible to carry along all details from lower levels, partly for technical reasons, but also because they would overwhelm insights at the higher level due to their sheer numbers and the fact that they typically run on much faster time scales.

I address the well-known challenge of biomedical multiscale analysis with a novel adaptation of the *Template-and-Anchor* (T&A) modeling paradigm. We consider a template as a high-level, coarse-grained model that focuses exclusively on the main physiological components of a system and involves correspondingly few variables, processes and parameters. Anchor models are modules of component sub-systems that provide more elaborate descriptions of specific biological details. This conceptual framework does not attempt to capture simultaneously all details within a single computable structure as many other multiscale models do. Instead, the often-overwhelming multilevel task is dissected into smaller, stand-alone models that are analyzed separately. This new adaptation of the T&A approach offers substantial advantages without losing resolution. First, the divide-and-conquer method enhances computational efficiency. Second, unlike other methods, each anchor is analyzed individually, producing a record of crucial input-output relationships that are ultimately used in the template model. Third, anchor models can be interchanged without affecting the structure of the template or other anchors. Fourth, the T&A model provides flexible guidelines for its setup and for defining variables across scales. Using this approach, we

investigate the health implications of exposure to dioxin (specifically, 2,3,7,8-tetrachlorodibenzo-p-dioxin), a persistent organic pollutant which can severely affect health, depending on the magnitude of exposure. We present a template capturing the overall effects of dioxin on the dynamics of cholesterol, a prominent target of dioxin. The anchor models that comprise the overall template model include hepatic cholesterol biosynthesis (via the mevalonate pathway), lipoprotein metabolism, and estrogen synthesis. The creation of all anchor models and the template enable a holistic evaluation of dioxin's impact on the liver, which can be translated into a tool for comprehensive computational health risk assessments.

Multiscale modeling, and more specifically T&A modeling, holds promise for a deeper understanding of complex systems and for advancing personalized medicine, interspecies translation, and virtual clinical trials.

CHAPTER 1 INTRODUCTION[1]

Biological phenomena occur and interact across multiple levels of organization, from molecules and cells to tissues, organs, organisms, and ecosystems. Each level is intricately connected and may influence others, making the study of these multiscale systems complex and challenging. As a generic example, molecular interactions govern the behavior of proteins, nucleic acids, lipids, and other biological macromolecules. These molecular interactions manifest in cellular functions such as metabolic processes, ligand binding and signal transduction. At the tissue level, cells interact through specific characteristics and play crucial roles in phenomena such as hormonal signaling, which governs many aspects of physiology. As a consequence, the collective behaviors of the various molecular processes within and among cells affect tissues, organs, organ systems and ultimately organisms that respond adequately to their environments.

Further complexity arises if one considers the interplay among different cell types, tissues, and organs, where a solid understanding of these relationships is key to deciphering biological processes such as digestion, circulation, and disease, to name just a few [1]. The intricacies of these processes are not only manifest in individual multi-cellular organisms, but quickly arise if one considers the interactions between organisms,

---

[1] Much of the material in this chapter is in revision for publication in *PLOS Computational Biology*

populations, and entire ecosystems, wherein interactions among different environments and species introduce even greater complexity. These interactions in turn influence numerous phenomena, from population growth to the spread of infectious diseases and environ-mental changes.

The often-encountered multilevel complexity implies that traditional reductionist methods alone do not provide a comprehensive understanding of biomedical phenomena and mandates an integrated approach that considers interactions and dependencies across multiple scales [1-3]. For example, unraveling diseases such as cancer requires knowledge of how molecular-level interactions translate into higher-level effects within the body. Accordingly, cancer is often rightfully described as a systemic disease, due to the intricate interplay of factors at multiple levels that contribute to its onset and progression [4]. Namely, while cancer is known to be characterized by ill-regulated cell proliferation and the invasion into healthy tissues, its manifestation and behavior are influenced by a vast network of cellular and physiological interactions, such as immune responses. Furthermore, tumors are heterogeneous cellular assemblies, whose growth and metastatic potential depend upon dynamical interactions among the cancer cells themselves and their constantly changing microenvironment. Additional systemic factors, such as hormonal responses, have profound effects on the behavior of cancers [5]. This complex web of interactions, which spans from the molecular to the organismal level, necessitates an integration of diverse processes on multiple levels for a better under-standing and treatment of this disease [6].

Not surprisingly, substantial challenges exist for the design and development of computational models describing multiscale phenomena. The fundamental reason is the

vastly increased number of components at various scales, both temporally and spatially, and the need to define, quantify, and often adjust numerous parameters of different types that possibly interrelate with one another across scales. As a part of this challenge, defining the linkage between different scales is a substantial hurdle. Often, these links are bidirectional, implying that variables, parameters, and functions characterizing the biomedical system influence one another [7]. The new complexities associated with multiscale models confound the challenges already occurring when large numbers of variables, nonlinear interactions and emergent behaviors are at play on each level. These challenges are manifest in computational demands, validation, and standardization. Simulating the dynamics across various scales can be computationally intensive, requiring specialized algorithms. A separate issue is the validation of these models, which may need unique criteria at each level, thereby potentially leading to compounded uncertainties. Finally, the lack of standardized methodologies across different domains complicates the analysis, comparison, and interpretation of multiscale systems [8].

1.1 Multiscale Modeling Approaches

In an overview on multiscale modeling in biology [1], the authors discuss the scientific progression and advances in scientific tools and technologies that have enabled the research community to explore complex biological systems that are inherently multi-scaled in nature. Future progress will require not only advancements of these methods, but also transdisciplinary collaboration among researchers in molecular and cellular biology, physiology, evolution, ecology, mathematics, bioinformatics and what is now called data science. This collaboration is needed not just to obtain, organize, and analyze

the massive volumes of data generated through experimentation, but for constructing, improving, and standardizing comprehensive models that can elucidate the functioning of life across different temporal and spatial scales. With this mandate for collaboration comes the need for improved transdisciplinary communication (Chapter 19 of [9]).

Numerous structured and *ad hoc* approaches to multiscale modeling have been proposed to capture the intricate interactions and phenomena occurring across different scales of biological systems. Two very different yet representative examples are physiologically based pharmacokinetic (PBPK) models and agent-based models (ABM).

Physiologically based pharmacokinetic (PBPK) models simulate the absorption, distribution, metabolism, and excretion of drugs or chemicals within living organisms (Figure 1). These models are structured to represent in a somewhat simplistic manner the actual physiological architecture of the organism and take the format of a hybrid between a compartment model at the organismal level and a set of kinetic models within the compartments [10, 11]. What renders PBPK models inherently multiscale is their ability to bridge different levels of biological organization. At the molecular level, they address interactions like drug-lipid partitioning, as it occurs in fatty tissue, while they account at the cellular level for processes like drug uptake and metabolism, for instance, in the liver. Moving up the scale, they define compartments for specific organs or tissues, each with its distinct drug-related parameters. Collectively, the integrative modeling of these different components enables a holistic view of how a substance behaves across the entire organism, from initial drug administration to eventual elimination, thus offering a comprehensive perspective that spans multiple biological scales and on the practical side offers guidance regarding drug doses and administration regimens.

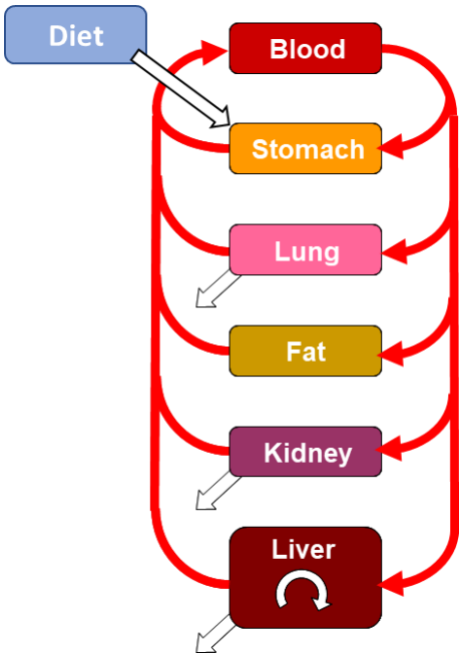

Figure 1.1 Generic PBPK model as a multiscale structure. The primary scale of granularity reflects organs and tissues, but the drug concentrations in these organs are subject to molecular and cellular events, such as sequestration and degradation in the liver.

The second example is an agent-based model (ABM), which is a generic stochastic approach that simulates the actions and interactions of autonomous agents, which are individual entities with distinct attributes and behaviors [10, 12]. The agents typically move on a grid and can represent a myriad of entities, ranging from molecules and cells in biological systems to individuals in social scenarios. Governed by predefined rules, ABM agents can adapt, learn, and evolve based on their experiences and interactions within their environment. This modeling approach is inherently multiscale because it can span a wide range from the micro-level where, for instance, agents might represent cells or individuals, to the macro-level, where tissue function or societal dynamics emerge. The temporal aspect of ABMs can capture both immediate agent

decisions and long-term system evolutions. Further, ABMs can account for spatial differences in the environment and capture behaviors that arise from numerous individuals dynamically interacting according to preset collective properties [13, 14]. More generally, multiscale modeling often adopts a "hybrid" approach in which the actions of migrating agents may be governed by systems of differential equations, which are updated at every discrete step of the ABM [15-17]. Several other types of hybrid models have been discussed in the literature [18-20]. Due to their intuitive nature and flexibility, ABMs are increasingly used as teaching tools in biology classes [21].

1.2 Technical Challenges of Multiscale Modeling

The organization of biological systems as distinct but connected layers poses one of the grand challenges for biomathematical modeling, because processes occurring at the various layers often have different time scales and almost always focus on different types of variables. The higher layers usually correspond to a "big picture" of physiological events, whereas the lower levels account for increasing granularity and detail. When investigating a system at a high level, it is often infeasible to carry along all details from lower levels, partly for technical reasons, but also because they would overwhelm insights at the higher level due to their sheer numbers and the fact that they typically run on much faster time scales. For instance, the growth of an embryo from a fertilized oocyte throughout the phases of blastula, gastrula and further development may span several weeks, during which uncounted metabolic and cellular processes occur at a much more rapid pace.

A partial solution that was proposed a long time ago is time-scale separation, which yields a reduction in model size (*e.g.*, [22]). As an explanation for the validity of this reduction, it has been argued (*e.g.*, [23, 24]) that the processes at lower levels are so fast that they are essentially always in a quasi-steady state, which permits their conversion from differential equations to explicit algebraic equations that may be entered as constraints in a much smaller set of governing equations. As an example, the clouding of the human lens is a very slow, life-long process that is caused by clearly identifiable biochemical reactions that occur on an ongoing basis at the sub-second scale. In this case, the biochemical aspects may be analyzed separately from the slow clouding process during aging [25]. While separation of time scales is certainly an option for processes with time constants at different orders of magnitude, such a separation is not feasible if the layers of biological organization are not all that distant. For instance, the dynamics of calcium exchanges in the heart is fast in comparison to macroscopic heart physiology, but it is close to impossible to separate the two [26]. In another example, discussed later in detail, the direct effects of dioxin exposure on human health are manifest at the transcriptional and metabolic levels, which have similar time scales, although their consequences may, over the span of years, lead to liver disease, reproductive dysfunction, and possibly cancer.

1.3 Template and Anchor (T&A) Modeling

To address the various challenges inherent in multiscale modeling, we propose a modeling paradigm suggested over two decades ago, but seldom actually implemented, namely Template-and-Anchor (T&A) modeling [27]. A template is a high-level model

that focuses exclusively on the main physiological components of a system and involves correspondingly few variables, processes, and parameters. It provides a coarse-grained representation of the system under investigation. Anchor models provide more elaborate views of the specific biological details characterizing the mechanisms that govern the system and are represented in the template model as variables. The original authors and proponents of T&A modeling, Full and Koditschek [27], considered this approach most useful not for multiscale modeling *per se*, but for the embedding of a generic design principle into a space of alternate implementations. Expressed differently, they considered the template model as the representation of a design principle and the anchor models as differently structured implementations of this common design. Their key example assessed the locomotion of terrestrial animals, which the authors demonstrated to have numerous, quite different manifestations (which they called "degrees of freedom"), such as the number and structure of legs. While distinctly different, all implementations had to comply with a common set of biomechanical design features. Kvalheim and Revzen [28] formally investigated this aspect of the T&A approach from a standpoint of control theory. They embedded all anchors in a high-dimensional space such that their intersection consisted of the low-dimensional template, which was thereby seen as the common design principle that all implementations had to satisfy. As the authors expressed it, "the template is not only a description of a typical subset of poses [of a galloping horse], but also a low-dimensional dynamical model that captures features of the aggregate behavior of the body." Our focus here is not on an embedding of different implementations of a design feature but on a method for taming complexity by replacing anchor models with input-output relationships that later inform the template

model. Specifically, we consider the template model as a representation of processes at some fixed level of biological organization. As is typical in dynamic modeling, this template contains variables that interact dynamically and are formulated as explicit functions with appropriate parameters. The model may be assessed with the usual steady-state analyses (*e.g.*, characterizing stability and sensitivities), as well as with computational simulations. Of importance for the T&A approach, the variables of the template model, when zoomed in, are in themselves more finely grained models, which serve as anchor models. The anchor models are analyzed separately across applicable scenarios, and the main outcome of each anchor analysis is a functional or tabulated record of all pertinent input-output relationships, which are subsequently used to connect to other anchors and to calibrate the template model. In the end, the template model can be simulated without simultaneously simulating the anchor models while retaining and utilizing pertinent results from all anchors. This strategy of "logistic level separation" is different from typical multiscale models that attempt to represent all information at once and carry it forward in some fashion.

1.4 Dioxin (2,3,7,8-tetrachlorodibenzo-p-dioxin)

To illustrate the functionality of the T&A model, we model the effects of dioxin (2,3,7,8-tetrachlorodibenzo-p-dioxin) on human health and, especially, on the dynamics of cholesterol and the sequelae of exposure.

1.4.1 Features of Dioxins and their Effects on Human Health

Dioxins are polychlorinated aryl hydrocarbons, the most toxic of which is 2,3,7,8-tetrachlorodibenzo-p-dioxin (TCDD) [29]. (Figure 2).

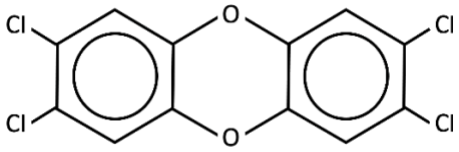

Figure 1.2: Chemical structure of 2,3,7,8-tetrachlorodibenzo-p-dioxin (TCDD).

Dioxins are widely generated as by-products in a number of industrial processes, such as chlorine bleaching of paper pulp, smelting of metals, and burning of municipal and industrial waste. Like other persistent organic pollutants (POPs), dioxins are typically very stable in the environment, and essentially every person worldwide is exposed to dioxins to some degree. The exact exposure levels vary considerably. They are usually below the reference dose (RfD) in terms of dioxin toxicity equivalency (TEQ) [30], but higher exposures have been observed. The RfD has been estimated to be between 1 and 10 pg/kg-day, which means that a lifetime average daily dose in this range is highly unlikely to cause noncarcinogenic effects; it aligns well with recommendations of the international Joint FAO/WHO Expert Committee on Food Additives [31]. Outside accidental contact, most individuals receive about 90% of their exposure from food, while 10% comes from breathing air contaminated by incineration processes [32]. The highest levels of dioxins are found in meat and dairy products because livestock and fish often take up plants to which contaminated soils and sediments are attached.

Several catastrophic incidents have exposed the general population to high levels of dioxin. During the Vietnam war, dioxin was an active ingredient in the defoliation compound Agent Orange, which was used by the American Military as a “tactical herbicide” to expose Viet Cong and North Vietnamese forces concealed by vegetation [33]. A notable accident happened in 1976 in Seveso, Italy, where high levels of dioxin were released into the environment due to an explosion in a chemical plant [34]. In 2008, dioxin-contaminated oil used in a direct-drying feed operation system led to contaminated livestock feed in a facility located in Clohamon, Ireland, causing an international recall of all pork products originating in Ireland [35].

Adverse health effects of dioxin may result from both short-term and long-term exposures [36]. It is known that short-term exposure to high levels of dioxin may cause skin conditions like chloracne. Long-term exposure is associated with impairment of the endocrine system, reproductive dysfunction, and altered cholesterol dynamics, potentially leading to non-alcoholic fatty liver disease (NAFLD). Moreover, chronic dioxin exposure has been demonstrated to pose a strongly increased risk of developing diabetes and various cancers, often in the form of soft-tissue sarcoma, non-Hodgkin lymphoma, chronic lymphocytic leukemia, and liver cancer [37]. Confounding direct effects of dioxin is its long biological half-life, which causes it to remain and gradually accumulate in human tissues for several decades after exposure [38] (Fig. 1). The impact of dioxin on human health and many contributing factors have been documented in an enormous body of toxicological studies [36].

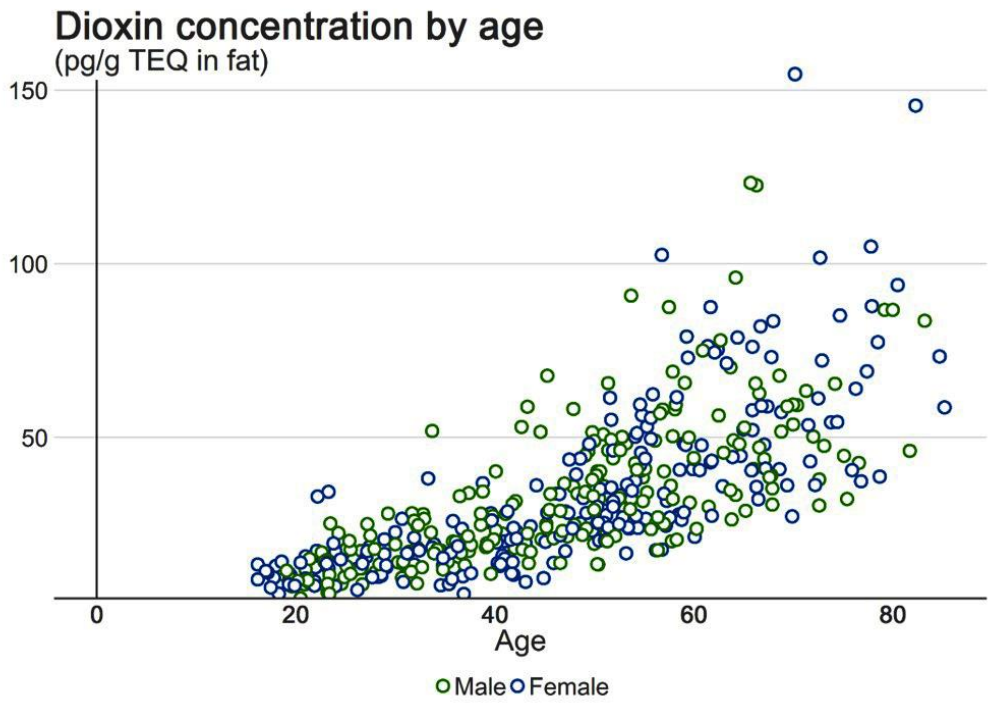

Figure 1.3: Measured gradual accumulation of dioxin concentration in humans of age 18 years and older. This is expressed as TEQ, which combines the weighted toxicity of numerous dioxins, furans, and polychlorinated biphenyls (PCBs) [38]. Image credit and source: *WikiCommons file File:Dioxin concentration by age.png* [39].

However, assessing the severity of each contribution to the overall impairment of health remains to be a challenge. As an intriguing, counterintuitive example, dioxin exposure leads to reduced *de novo* cholesterol biosynthesis in the liver, as well as reduced levels of cholesterol, HDL, and LDL in serum in mice [40, 41]. Despite these reductions, dioxin can ultimately cause fatty liver disease, which seems contradictory, but turns out to be caused by changes in processes associated with extrahepatic cholesterol. In addition, dioxin may indirectly influence fatty acid metabolism and, possibly, glycolysis to induce steatosis [40].

In comparison, epidemiological studies have shown that dioxin exposure is associated with steatosis and increased serum total cholesterol levels in humans [42-46]. Modern chemical toxicity testing and health risk assessments are steadily moving away from animal-based methods and increasingly adopt "new approach methodologies" (NAMs), which use cells, organoids, or organs-on-a-chip assays that are based on *in vitro* or *ex vivo* testing systems, machine-learning, statistical prediction algorithms, and dynamic models [47-49]. Among the latter, physiologically based toxicokinetic (PBTK) models and toxicodynamic models (TD) have become instrumental for *in vitro* to *in vivo* extrapolations (IVIVE) [50-52]. While PBTK models allow the translation of chemical concentrations in *in vitro* cultures to external exposure levels in the macroscopic world, systems-based TD models allow extrapolations of local chemical effects in cells, isolated organs or tissues to systemic-level health outcomes, which often involve multi-level, multi-organ interactions.

In an effort to address the challenge of integrating multiple distributed effects of TCDD, we propose a novel multiscale computational NAM, using the conceptual framework of "template-and-anchor" (T&A) modeling [27]. In contrast to the T&A approach proposed by Full and Koditschek though, we use the T&A approach in a different manner. Namely, instead of pursuing an embedding of different implementations of the same fundamental design [27, 53], we consider the template model as a representation of processes at some fixed level of biological organization. Generically, a template is a model that focuses on the main physiological components of a system. It provides a coarse-grained, high-level representation of the system under investigation. Like in other mathematical models, these components of a template model

are represented by state variables that are connected through functional interrelationships. By contrast, anchor models capture the dynamics of specific biological details within the template model. They characterize the mechanisms governing a subsystem at a lower level of biological organization.

In this thesis, I present three anchor models and an overall template model for the effects of TCDD toxicity on cholesterol dynamics. The three anchor models depict the biosynthesis of cholesterol via the mevalonate pathway in the liver, the metabolism and transport of lipoproteins facilitating cholesterol exchange among the liver, plasma, and peripheral tissues, and the process of steroidogenesis in the ovaries. These processes, selected for representation as anchor models, hold particular importance, as dioxin exposure influences multiple steps within these biological pathways.

I will demonstrate how the dioxin-dependent outcomes of these anchors—such as the amount of cholesterol produced under a specified dioxin exposure—integrate into subsequent variables within the overarching template model. Substituting all variables of the template model with information from the anchor models ultimately allows us to assess the global effects of dioxin exposure on the human body which has seldom been done before.

CHAPTER 2 Hepatic Cholesterol Biosynthesis and Dioxin-Induced Dysregulation[2]

The mevalonate pathway in the liver is the main source of cholesterol biosynthesis. A slightly simplified depiction is shown in (Figure 2.1) It is straightforward to design a dynamic model of cholesterol biosynthesis via this pathway, although many different mathematical representations are available [54]. This pathway model serves as one of the anchor models supporting the template model, which I will discuss in Chapter 5. It includes the following metabolic and regulatory processes:

1. Transcriptional pathways of HMGCR (3-hydroxy-3-methyl-glutaryl-coenzyme A reductase) and squalene, lanosterol, and farnesyl synthases, controlled by the transcription factor SREBP;
2. Metabolic system of the mevalonate pathway;
3. Negative feedback regulation of SREBP activity by cholesterol;
4. HMGCR degradation promoted by intermediate metabolites of the mevalonate pathway;
5. Bile formation;
6. Cholesterol storage in the form of cholesterol esters;
7. Exchange of cholesterol between liver and plasma;
8. Dietary cholesterol intake.

---

[2] Much of the material in this chapter is published in *Food and Chemical Toxicology PMID: 37820785*

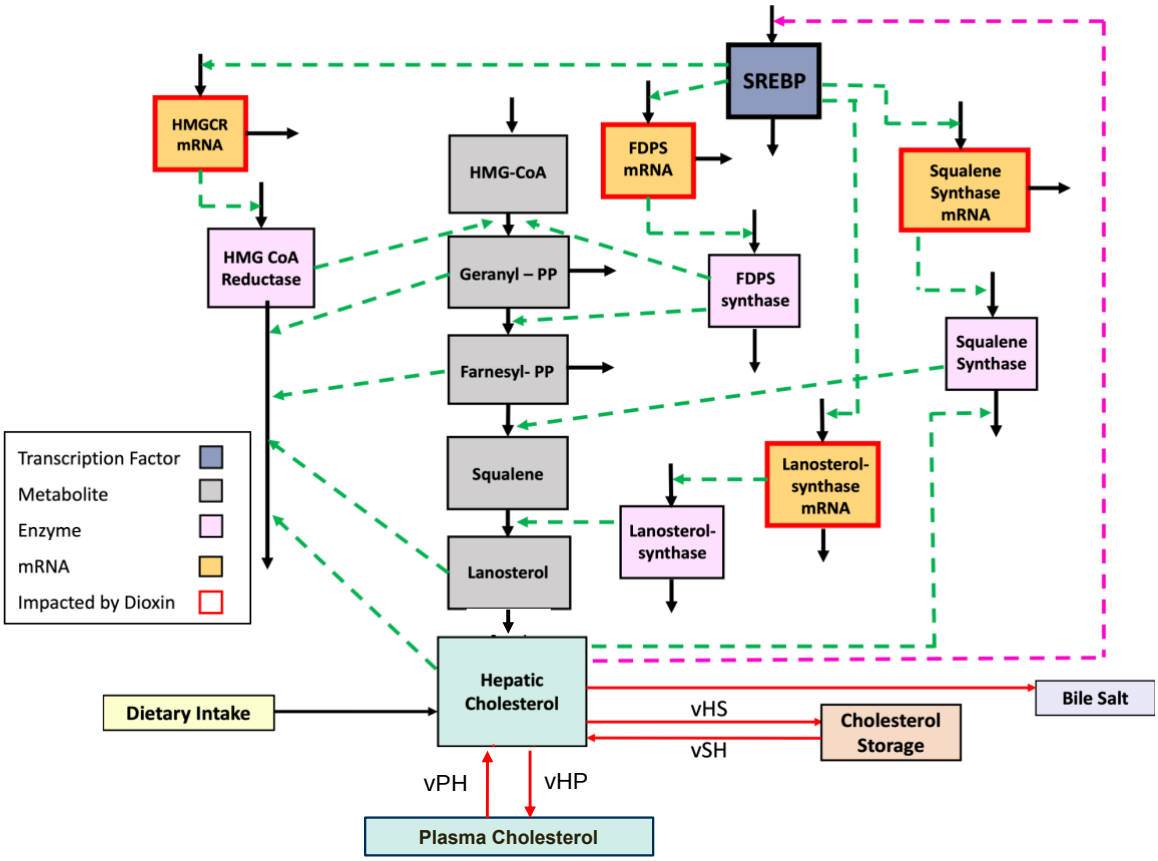

Figure 2.1: Anchor model describing hepatic cholesterol biosynthesis via the mevalonate pathway, its regulation and perturbation by TCDD. In addition to biosynthesis, this anchor accounts for bile and cholesterol storage and cholesterol exchange with the plasma. Molecules are color-coded by type, as indicated. Solid lines show metabolic reactions and transport steps, with red solid lines signifying steps impacted by TCDD. Dashed lines represent feedback inhibition (pink) and local activation (green) of transcriptional, translational, posttranslational and enzymatic processes. Boxes outlined in red represent mRNAs whose transcription is affected by TCDD. SREBP is the key transcription factor. It binds to sterol regulatory elements (SREs) in the promoter regions of its target genes and controls the mevalonate pathway together with HMG-CoA reductase, which is considered the rate-limiting step of the pathway, even though control of the pathway is distributed.

2.1 Methods

2.1.1 Molecular details of dioxin-impacted mechanisms

The nucleus of mammalian cells is protected by a membrane that prevents foreign molecules from entering. Dioxin interferes with this transport process. Specifically, dioxin binds to the aryl hydrocarbon receptor (AhR) [55]. This receptor ultimately regulates the expression of numerous genes, particularly those associated with detoxification and cell growth. AhR heterodimerizes with the AhR Nuclear Translocator ARNT [56]. The resulting complex penetrates the protective membrane barrier and, once inside the nucleus, serves as a transcription factor for genes possessing an AhR-, dioxin- or xenobiotic- responsive element (AHRE, DRE or XRE) containing the core sequence 5'-GCGTG-3. As a result of AhR binding, dioxin exposure leads to the downregulation of several genes associated with hepatic cholesterol synthesis, namely, HMG-CoA reductase (HMGCR), farnesyl-diphosphate farnesyltransferase 1 (FDFT1), squalene epoxidase (SQLE), and lanosterol synthase (LSS) [57]. In spite of this down-regulation, increased hepatic cholesterol levels have been observed after strong dioxin exposure [58]. This apparent contradiction is attributed to the upregulation of the lecithin–cholesterol acyltransferase (LCAT), apolipoprotein AI (APOA1), and low-density lipoprotein receptor (LDLR) genes that are involved in the reverse cholesterol transport pathway [59]. Furthermore, the upregulation of these genes results in an increased influx of cholesterol entering the hepatocyte and thus, contributes to the accumulation of cholesterol in the liver [60].

2.1.2 Databases documenting TCDD effects on gene expression

Over the past decade, a significant amount of information has been amassed regarding the effects of TCDD and many other toxic compounds on gene expression and regulation. Much of this information has been collected in the *Toxin and Toxin Target Database* (T3DB) [61] and the *Comparative Toxicogenomic Database* (CTD) [62]. T3DB is a bioinformatics resource that contains over 40,000 manually curated toxin-target interactions across approximately 4,000 toxins, thus providing data for investigating mechanisms and direct targets for each toxin. Complementing this information, CTD provides manually curated information about toxin-gene associations for over 10,000 toxins, thus providing expression signatures associated with downstream effects for each toxin.

According to these databases, TCDD exposure affects the expression of over 8,000 genes that are associated with numerous physiological systems in humans and/or mice, including hepatic processes involved in cholesterol biosynthesis. TCDD furthermore interacts with genes indirectly involved in cholesterol metabolism and in detoxification, including those coding for AhR, CYP1A1 (cytochrome p450 enzyme A1), and TIPARP (TCDD-inducible poly [ADP-ribose] polymerase), which is a negative regulator of AhR signaling [63, 64]. One caveat of CTD is that the cataloged outcomes of dioxin exposure on gene expression, whether an increase or decrease, may differ based on the referenced source [65, 66]. In our analysis, we mitigated this variability by selecting results that were corroborated by the highest number of references, thereby increasing the probability of reliable foundation for our assessment. Genes that are pertinent for our model and impacted by TCDD in rodents and/or humans are presented

in Table 2.1 They are the most researched genes impacted by dioxin, and ample references can be found in CTD.

Table 2.1: Dioxin-affected genes, enzymes, and other proteins related to cholesterol metabolism in the liver. The listed genes correspond to enzymes of the mevalonate pathway (shaded grey in Figure 2.1) and other pertinent pathways that are affected by dioxin.. Dioxin generally causes a decrease in expression or activity, except for the gene coding for CYP1A1, which diverts cholesterol toward secondary metabolites [67] and for genes coding for the cholesterol importers LCAT and APOA1 for which TCDD alters the expression.

Gene	Enzymes / Proteins	Impact of Dioxin on Expression	Organisms	Sources
ACAT	**Acetyl-CoA acetyltransferase**	↓	**Mus musculus**	Boutros PC (2009)
FDPS	**Farnesyl diphosphate synthase**	↓	**Homo sapiens** **Mus musculus**	Fracchiolla NS (2016)
HMGCR	**HMG- CoA Reductase**	↓	**Homo sapiens** **Mus musculus**	Boutros PC (2009)
HMGCS1	**HMG- CoA synthase**	↓	**Homo sapiens** **Mus musculus**	Iqbal K (2021)
LSS	**Lanosterol- synthase**	↓	**Homo sapiens** **Mus musculus**	Labaronne (2017)
SQLE	**Squalene-epoxidase**	↓	**Homo sapiens** **Mus musculus**	Hurst CH (1998)
APOA1	**Apolipoprotein A1**	↑	**Mus musculus**	Angrish (2013)
CYP1A1	**Cytochrome P450, family 1, subfamily A, polypeptide 1**	↑	**Homo sapiens** **Mus musculus**	Chen (2019)
LCAT	**Lecithin–cholesterol acyltransferase**	↑	**Mus musculus**	Angrish (2013)
LDLR	**Low-density lipoprotein receptor**	↑	**Mus musculus**	Angrish (2013)

2.1.3 Model formulation of cholesterol biosynthesis anchor model

The regulated pathway system in (Figure 2.1) is mathematically represented with non-linear ordinary differential equations (ODEs). They are formulated here within the framework of Mass-Action Kinetics and Biochemical Systems Theory (BST) [68-70], which has been used for a variety of biological and nonbiological systems analyses (e.g. [53, 71-79]. Details are presented in Appendix A.6. We evaluate the model mainly at the steady state, since only the long-term effects of dioxin exposure are of interest here. Each metabolite, mRNA, and protein species is modeled with an ODE that contains two types of parameters: (1) non-negative rate constants (r_i) of production and degradation, and (2) kinetic orders (a_j), whose signs directly align with the modeled function: activating or augmenting processes are modeled with a positive a_j, while inhibitory or diminishing processes are modeled with a negative a_j. Typical examples are the ODEs for Squalene (SQ), Lanosterol (L), Hepatic Cholesterol (C), and Plasma Cholesterol (Cp):

Squalene

$$\dot{SQ} = (r_{23} * FPP * SQS^{a7} - r_{24} * \mathrm{SQ} * LS^{a10}) * \mathrm{SF}$$

Lanosterol

$$\dot{L} = (r_{24} * \mathrm{SQ} * LS^{a10} - r_{25} * L) * \mathrm{SF}$$

Hepatic cholesterol

$$\dot{C} = (r_{25} * \mathrm{L} + r_{26} - r_{27} * \mathrm{C} - r_{28} * C^{a11} + r_{29} * CP + r_{33} * S - r_{34} * C) * SF$$

Plasma cholesterol

$$\dot{Cp} = r_{28} * C^{a11} - r_{29} * CP - r_{30} * CP + r_{31}$$

The complete ODEs can be found in Appendix A.4; computer code in PLAS and MATLAB format is available on GitHub.com/LBSA-VoitLab/TCDD_Chol.

2.1.4 Parameter determination and model evaluation

A summary of the parameter values for the model is provided in Appendix A.5. The model was primarily evaluated against the steady-state concentrations in human hepatocytes or plasma obtained from the literature (Table 2). Upon calibrating the model parameters, the steady-state metabolite concentrations available in the literature, *e.g.*, for 3-hydroxy-3-methyl-glutaryl Coenzyme A (HMG-CoA) and squalene, and those computed from the parameterized model were rather similar to each other (Table 2.2). Basal protein and mRNA activity levels were arbitrarily set as 100, reflecting "normal conditions." Other model parameters were based on literature information and reasonably adjusted to render model outputs consistent with published steady-state concentration data. Kinetic orders were set to default values of either 0.5, 1, or −1. A value of 0.5 corresponds to a power-law representation of a Michaelis-Menten rate law operating with a substrate concentration close to the Michaelis constant K_M. A value of 1 is appropriate for mass-action and transport processes operating in a linear range, whereas a value of −1 represents moderately strong inhibition [69, 70]. The remaining parameter values were manually adjusted to align roughly with the expected half-lives of metabolites, proteins, and mRNAs. Finally, we calibrated the percent reduction in hepatic cholesterol biosynthesis under TCDD exposure based on animal studies for each TCDD dose [80, 81]. Because we are not considering the short-term dynamics of the pathway, specific values of rate constants are not as critical as they would be otherwise, as long as their ratios are adequate, and we used rounded values rather than attempting to match observed values precisely.

Table 2.2: Comparison of the steady-state concentrations of key metabolites in the mevalonate pathway from the literature with results from model simulations. Steady-state values cited in the literature and corresponding values obtained for the model with parameter values presented in the Supplementary Materials. GPP: Geranyl pyrophosphate, FPP: Farnesyl pyrophosphate.

	Steady State Simulation (µM)	Steady State Literature (µM)	References
HMG-CoA	30	33	Turley (1995)
GPP	90	95	Turley (1995)
FPP	71	78	Turley (1995)
Squalene	73	73	Turley (1995)
Lanosterol	75	70	Turley (1995)
Hepatic Cholesterol	11200	11638	Sniderman (2013)
Plasma Cholesterol	5502	5170	Griffin (2013)

2.2 Results

Using the parameter values listed in Appendix A.5 and methods presented in the A.2, numerical simulations and sensitivity analyses were conducted to examine the impact of various doses of dioxin exposure on hepatic and serum cholesterol homeostasis. We also analyzed the effect of normal, high, and very high dietary cholesterol intake on the system and tested how these dietary variations, combined with dioxin exposure, impact hepatic and serum cholesterol levels.

2.2.1 Sensitivity analysis for the cholesterol biosynthesis anchor model

Parameter sensitivity analysis for the biosynthesis anchor model, comprising the mevalonate pathway and cholesterol transport into and out of the liver, revealed that 44 of the 45 model parameters yielded changes in steady-state hepatic cholesterol concentration of less than 10% in magnitude when their values were increased or decreased by 10% (absolute values of relative sensitivity <1; Figure 2.2). Thus, the impacts of alterations in most parameter values are attenuated by the system, consistent with the stabilizing negative feedback structure of the mevalonate pathway. Only one parameter, a_6 a kinetic order with a value of −1, turned out to be relatively influential. This parameter reflects the strength of the negative feedback signal exerted by hepatic cholesterol on the inhibition of the transcription factor SREBP (*cf.* In in Figure 2.1). Upon a 10% increase in this parameter, hepatic cholesterol decreases by about 35%. This somewhat higher relative sensitivity of 3.5 appears to be a reasonable compromise between extreme signal amplification (say, with an absolute value of 10 or 20) and a

systemic lack of adequate responsiveness to changing cellular demands (such as an absolute value < 1). The positioning of this feedback is consistent with the typical natural design of negative feedback loops, in which the end product regulates the first step in the pathway [82, 83].

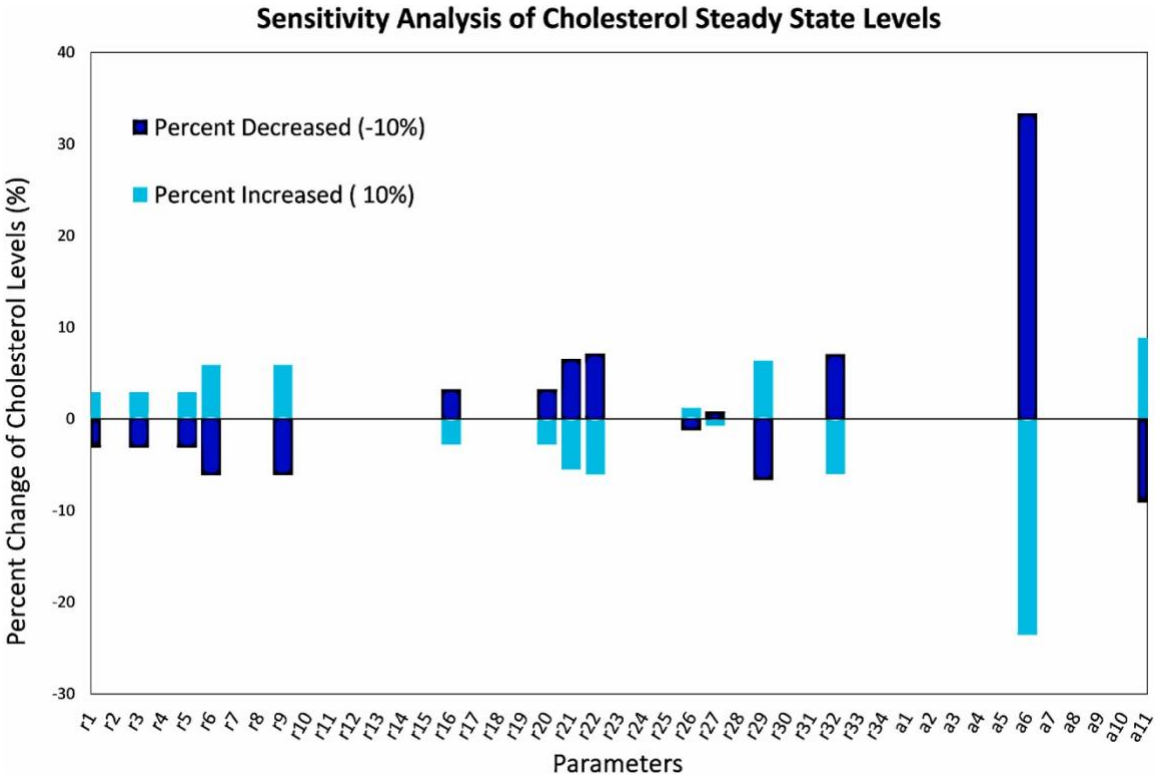

Figure 2.2: Results of a relative sensitivity analysis addressing the steady-state level of *de novo* generated hepatic cholesterol by varying each parameter in the mevalonate pathway model by ±10%.

2.2.2 Effects of TCDD on hepatic and plasma cholesterol

To quantify the impact of TCDD on cholesterol biosynthesis, we analyzed the effects of different practically relevant doses of TCDD, ranging from 0 to 50 μg/kg body weight. Specifically, we varied the values of the rate constant parameters of each flux altered by TCDD such that the outcome matched literature information based on experimentation in rodents, such as the percentage inhibition of hepatic cholesterol synthesis rate for each TCDD dose [80, 81]. The hepatic cholesterol concentrations resulting from these alterations were recorded and used to construct a dose-response relationship.

The model analysis of TCDD impact was performed in two variants. The first targeted a "partial model," which included only the TCDD effects on the biosynthesis of hepatic cholesterol via the mevalonate pathway, along with cholesteryl ester and bile formation. The second analysis addressed the entire system ("full model"), which also included the TCDD effects on the transport of cholesterol between the liver and plasma. The dose-response curves for TCDD exposure and the resulting effects on hepatic and plasma cholesterol are shown in Figure 2.3.

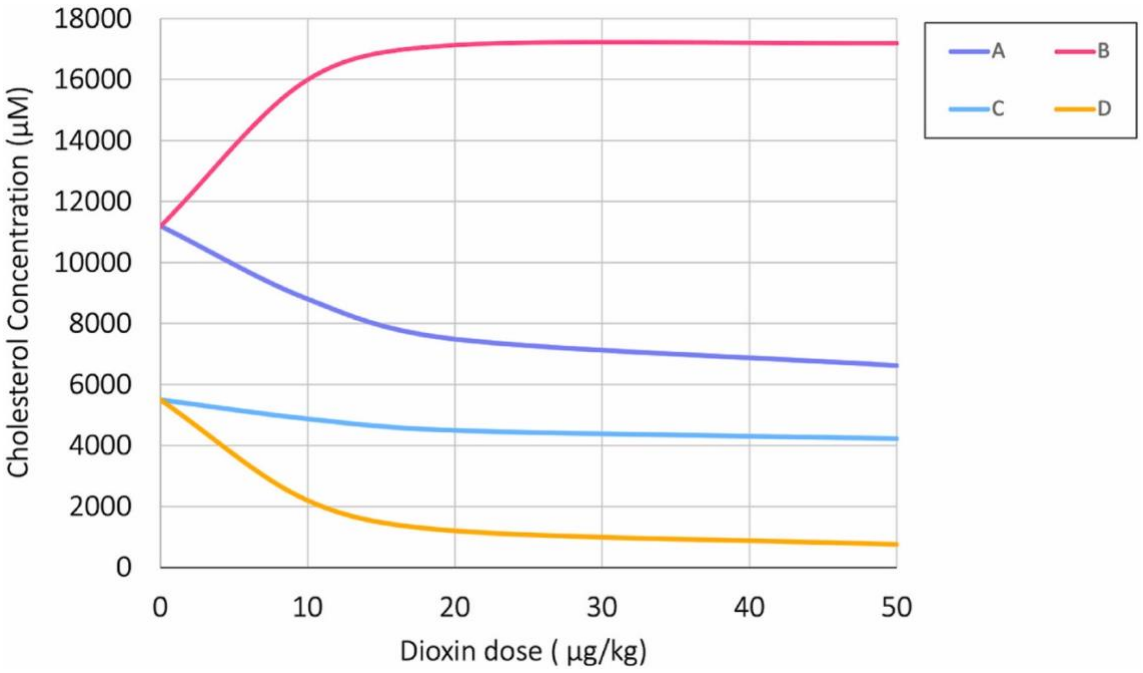

Figure 2.3: Dose-response curves quantifying the effects of increasing dosage of TCDD on hepatic and plasma cholesterol concentrations. The partial model, accounts for the mevalonate pathway along with cholesterol storage and bile formation, and the full model, additionally accounts for the effects of TCDD on the hepatic exchange of cholesterol with the plasma. (A–B) Effect of dioxin on hepatic cholesterol according to the partial (A) versus the full (B) model; note the opposite trends. (C–D) Effect of dioxin on plasma cholesterol according to the partial (C) versus the full (D) model.

With increasing doses of TCDD exposure, hepatic cholesterol decreases noticeably in the partial model, which does not consider the impact of TCDD on the exchange of cholesterol between liver and plasma. This decrease is clearly attributable to the downregulation of several biosynthesis genes including those encoding HMGCR, FDPS, SQS and LSS. Importantly, this downregulation affects the key enzyme HMGCR, which catalyzes the alleged rate-limiting step of the pathway [84]. The change in the relative rate of cholesterol biosynthesis *versus* the dioxin dose, calculated as a percent change with respect to control, is shown in (Figure 2.4) . It aligns with the trend in

hepatic cholesterol concentration in the partial model (Figure 2.3, line A) and with experimental data in mice [80, 81].

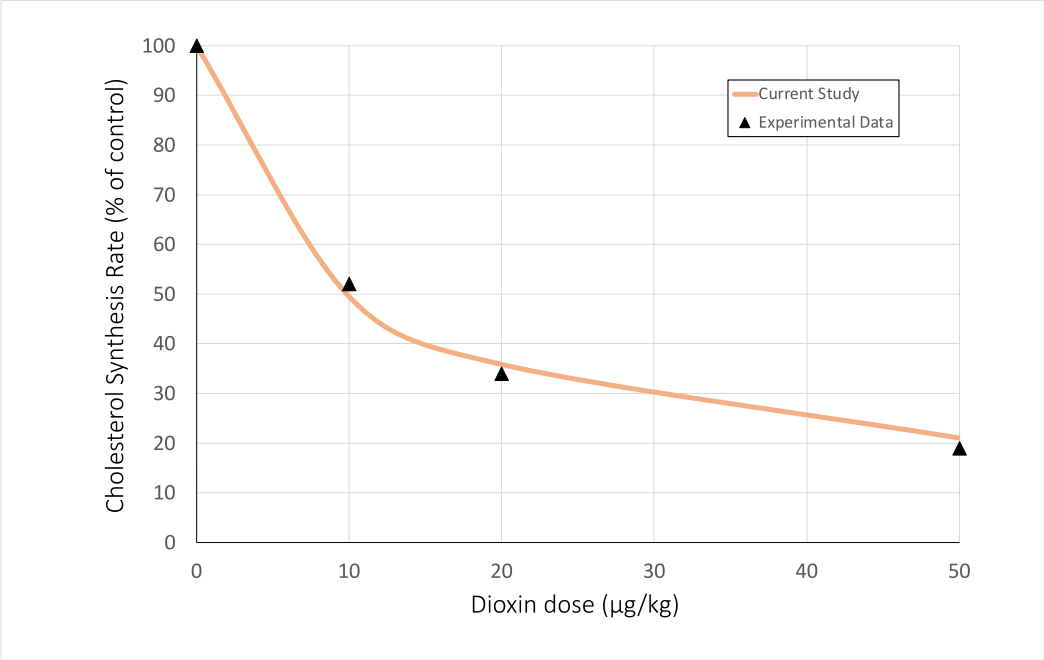

Figure 2.4: Dose-response curve of the effect of TCDD on the rate of hepatic cholesterol biosynthesis. This rate is expressed as the percent of remaining activity in comparison with the control. The trendline was matched to fit experimental data (triangle) in mice [80, 81].

In contrast to the partial model, analysis of the full model, which accounts for the interactions with the plasma, reveals that hepatic cholesterol levels accumulate under TCDD exposure. This increase is primarily due to the upregulation of the transport of cholesterol from the plasma into the liver (vPH, *cf.* Figure 2.1), which can be contributed mainly to the upregulation of LCAT and LDLR. This accumulation is consistent with the onset of NAFLD following strong TCDD exposure [85]. Confounding the risk of NAFLD is the observation that bile formation decreases [85], which decreases the usage

of hepatic cholesterol. The hydrolysis of cholesteryl ester to cholesterol is reduced under TCDD, but the effect is apparently minor in comparison to the other effects [86]. In both the partial and full models, plasma cholesterol decreases, with the full model suggesting a greater reduction than the full model (Figure 2.3, line C *vs*. D). This decrease of plasma cholesterol in the model simulation is consistent with results from mouse models [87]. It is interesting to note that the TCDD effect on hepatic cholesterol accumulation is strong for low exposures and that the effect ultimately seems to approach saturation for high exposures. Indeed, it appears that the dose-response is biphasic, with a robust increase in severity for low doses (below ~10 μg/kg) and limited further increases for higher doses (Figure 2.3, line B). However, these reductions in biosynthesis may not be of clinical significance, especially if other compensatory mechanisms are included, such as cholesterol storage and bile production, which are affected by TCDD as well. Like in animals, human exposure to dioxins including TCDD is also associated with steatosis (fat build-up) in the liver steatosis [45, 46]. However, except for a few studies showing no significant differences [88], most epidemiological studies indicate that serum total cholesterol levels increase in individuals exposed to high levels of dioxins [42-46]. This is in contrast to the rodent studies where TCDD caused a decrease in serum cholesterol levels [40, 41]. Therefore, one must use caution interpreting the these predictions. Further investigations are needed to differentiate the species differences before inter-species extrapolations can be applied with confidence.

2.2.3 Effects of dietary cholesterol on hepatic and plasma cholesterol

The model allows us to assess the potential additional role of dietary cholesterol intake. The recommended range of dietary cholesterol intake is < 300 mg/day, which is reduced to < 200 mg/day for individuals with risk factors for heart disease [89]. The model indicates that cholesterol intake increases both hepatic and plasma cholesterol (Figure 2.5) but in a much more insensitive manner, which is consistent with literature reports [90].

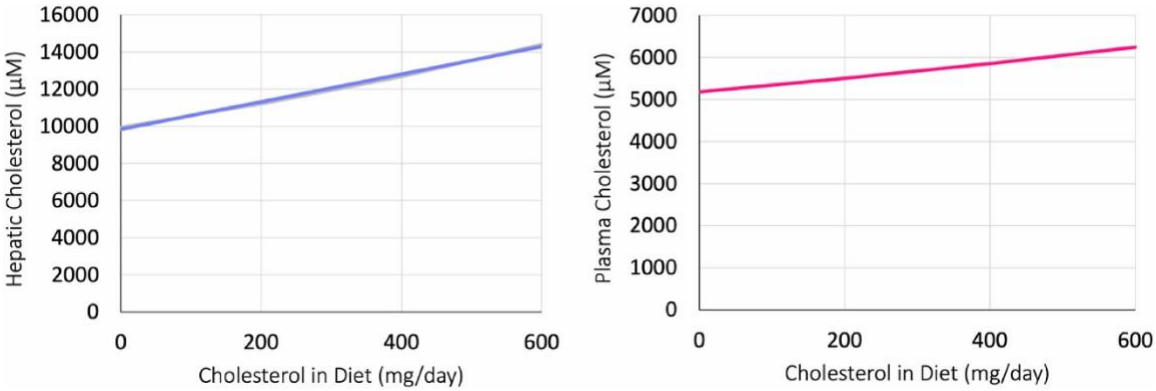

Figure 2.5: Effect of increased dietary cholesterol intake on hepatic and plasma cholesterol in the model. Note different scales of the Y-axes.

Using these results, we explored with simulations the effects of combinations of dietary intake and TCDD exposure. Without TCDD exposure, the steady-state value of hepatic cholesterol under a normal daily consumption of ~250 mg cholesterol is about 11,200 µM (Table 2.2). As expected, the hepatic cholesterol levels rise with both increased dietary intake and increasing doses of TCDD (Figure 2.6). For the recommended cholesterol intake, the model predicts a rise in hepatic cholesterol concentration to about 18,000 µM, if the individual is exposed to a high dose of 50 µg/kg of TCDD. In comparison, the concentration reaches only approximately 14,000 µM if no cholesterol

comes from the diet. For the same dose of TCDD, but with 600 mg/day of dietary cholesterol intake, the model predicts approximately 27,000 μM of hepatic cholesterol, which is more than twice the normal concentration.

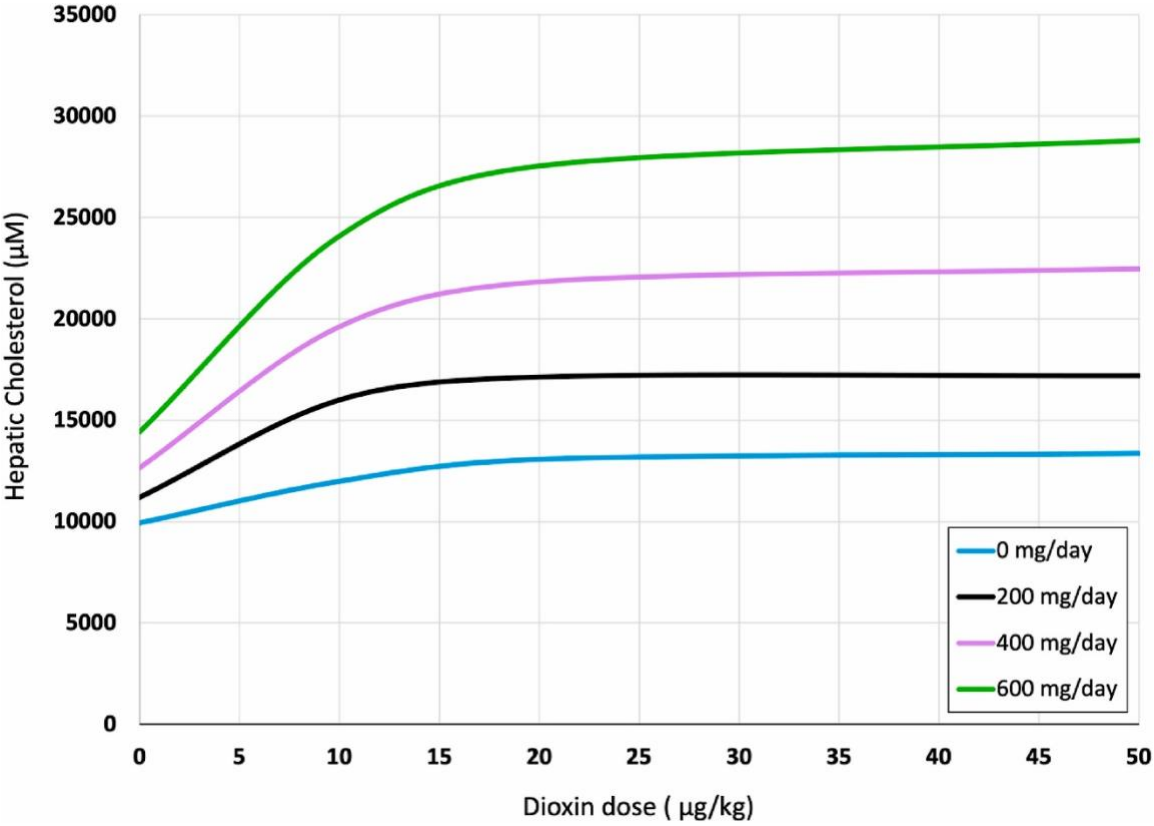

Figure 2.6: Combined effects of TCDD exposure and dietary intake of cholesterol on hepatic cholesterol as indicated.

2.3 Discussion

2.3.1 Summary of Findings

2.3.1.1 Impact of dioxin on exposure and changes in gene expression

The current model of cholesterol biosynthesis accounts for pathway features that are known to be relevant, including important regulatory steps, such as feedback inhibition of the main transcription factor, SREBP, by hepatic cholesterol. Importantly, the model permits us to study the effects of TCDD exposure on the biosynthetic pathway in detail. For instance, it is known that several genes involved in cholesterol biosynthesis in the liver are downregulated under TCDD exposure, and the model enables us to assess the consequences of the downregulation. As is to be expected, and confirmed by the model, the overall result is a decrease of hepatic cholesterol synthesis *de novo*. However, it has also been observed that TCDD exposure leads to a build-up of hepatic cholesterol and, possibly, NAFLD [91]. Dietary intake and TCDD effects on the mevalonate pathways alone cannot explain this observation, but the model demonstrates a mechanism of reconciliation explaining the apparent discrepancy. It reveals that the upregulation of genes outside the mevalonate pathway, such as LCAT and LDLR, which are involved in cholesterol transport between plasma and the liver (vPH and vHP in Figure 2.3), not only compensates for the reduction in cholesterol biosynthesis but indeed results in hepatic cholesterol accumulation.

2.3.1.2 Impact of dietary cholesterol and dioxin exposure on gene expression and cholesterol levels

As an illustration of the use of the proposed types of models, we studied the interrelations between diet and TCDD exposure. Studies in the literature [92] had suggested synergistic effects between the two, and the model permitted us to assess this synergism quantitatively. Consistent with observations, the model revealed that increased cholesterol in the diet has a greater impact on hepatic cholesterol levels than on plasma levels [92]. Introducing various doses of TCDD, along with increased levels of cholesterol in the diet, resulted in enhanced accumulation of cholesterol in the liver.

2.3.2 Limitations of the biosynthesis anchor model

While the biosynthesis anchor model appears to function properly, it is obviously simplified, like any other model. For instance, further complexity could be added to the mevalonate pathway model by including other sterol intermediates of the cholesterol derivatives, such as 25-hydroxycholesterol, which can also inhibit SREBP-2 through binding to an oxysterol-sensing protein [93]. Numerous other extensions would be possible. Nonetheless, we believe the approach is sufficient for revealing the essence of the complex phenomenon of dioxin impact on cholesterol biosynthesis.

The mathematical structure of the model is, as in all modeling efforts, debatable. We use a straightforward and essentially unbiased combination of mass-action and power-law representation for the design of the differential equations governing the model, which numerous times has proven to be effective for capturing complex phenomena in biology and medicine while, at the same time, being mathematically tractable (see ([54]) as well as references therein and above).

Even the best model is only as good as the data that are available for its calibration. In our case, there are clearly numerical uncertainties regarding parameter values and the slightly simplified structure of the model. In particular, human data are scarce, and our supplanting them with mouse data poses a clear limitation. Given the differential serum cholesterol changes in response to TCDD between humans and mice, as mentioned above, additional sites of action of TCDD in extrahepatic organs may need to be introduced for the model to account accurately for increasing cholesterol levels in circulation while the liver continues to accumulate cholesterol in humans.

2.3.3 Significance and Future Directions

Future implementations of the model will allow us to overcome shortcomings of the current set-up. For instance, we presently introduce high levels of dioxin into the system within a short time frame, which may be relevant for acute high-dose exposure scenarios but is not realistic for the average population. It has been reported [94] that the typical average daily intake of dioxin in the U.S. ranges from 28 to 41 ng of TEQ/kg lipids and from 36 to 58 ng of TEQ/kg lipids if dioxin-like PCBs are included. Considered in comparison with the RfD of 70 pg/kg-bodyweight per month [36], these numbers will become important for risk assessments in public health.

As a potentially very powerful new NAM, the T&A approach—with future refinements—will allow us to analyze *in vitro* findings regarding dioxin effects in primary hepatocyte culture. For instance, it will help us predict and explain system-level responses when it is used in conjunction with a PBTK model of TCDD or dioxin-like compounds for toxicokinetic IVIVE [95, 96].

The T&A approach will eventually permit the exploration of personalized health risk scenarios, which will require an examination of the various heterogeneities that are inherent in all complex biomedical systems, including gender, age, race, diet, genetics and comorbidities.

While the current T&A model focuses on liver and plasma cholesterol, future iterations may include other tissues/organs such as the brain, where disruptions of cholesterol metabolism have been linked to multiple neurogenerative diseases including Parkinson's diseases and dementia [97, 98]. As personalized data including dioxin exposure data become more widely available, one may even envisage that models might allow us to predict cholesterol levels in different tissues and screen for at-risk individuals and populations, thereby contributing to the public health of environmental exposure to dioxins.

Lastly, as the hepatic cholesterol synthesis pathway model is further improved, the mechanistically based T&A model may be applied to make predictions for other cholesterol-altering chemicals that induce different molecular initiating events that ultimately impact cholesterol biosynthesis.

CHAPTER 3 The Impact of Dioxin on Lipoprotein Metabolism and Cholesterol Transport

Lipids are hydrophobic and therefore require special carriers to travel in the aqueous environment of the blood [99]. Lipoproteins serve as these carriers. They consist of a core of cholesterol esters and triglycerides surrounded by a shell of phospholipids, free cholesterol, and apolipoproteins [99]. The apolipoproteins play an important role in classifying the lipoprotein into one of five classes: chylomicrons, very low-density lipoproteins (VLDL), VLDL remnants (IDL), low-density lipoproteins (LDL), and high-density lipoproteins (HDL) [99].

The transport of lipoproteins is essential for maintaining a proper lipid balance within the body and ensuring that lipids are delivered to various tissues where they are needed for cell growth and repair, bile production, which is essential for digestion, and the production of hormones such as estradiol, testosterone, and vitamin D [100].

3.1.1 Cholesterol transport and delivery

Lipoprotein metabolism is divided into two generative pathways: exogenous, which pertains to lipids obtained from dietary sources, and endogenous, which includes synthesis by the liver. Lipoprotein metabolism furthermore includes degradation and utilization. In the endogenous pathway, lipoproteins are assembled within the liver and intestine by combining lipids with apolipoproteins [101]. The latter help stabilize the lipoprotein structure and facilitate their transport in the bloodstream. Once assembled, lipoproteins are secreted into the bloodstream. Lipoproteins transport lipids for utilization and storage through the bloodstream to various tissues and organs, including adipose and

muscle tissue, and facilitate lipid reentry into the liver [102]. As they travel, lipoproteins release their cargo of triglycerides and cholesterol to these peripheral tissues. Lipoproteins undergo various metabolic processes as they circulate through the bloodstream. Enzymes and lipoprotein receptors on cell surfaces interact with lipoproteins to metabolize them, remodel their composition, and regulate lipid uptake by cells. The lipoprotein pathway plays a critical role in maintaining a proper lipid balance in the body. Disruption such as an increase in LDL cholesterol due to environmental toxin exposure such as dioxin and/or poor diet, can contribute to the development of diseases such as atherosclerosis [103], non-alcoholic fatty liver disease (NAFLD) [104], and polycystic ovary syndrome (PCOS) [105].

3.1.2 A model of lipoprotein cholesterol metabolism and transport

A simplified depiction of lipoprotein metabolism and transport is shown in Figure 3.1. A mathematical representation of this diagram serves as one of the anchor models supporting the template model which I discuss further in Chapter 5. A simplified version of this system was included into the biosynthesis anchor model, which demonstrates the flexibility of the template-and-anchor approach.

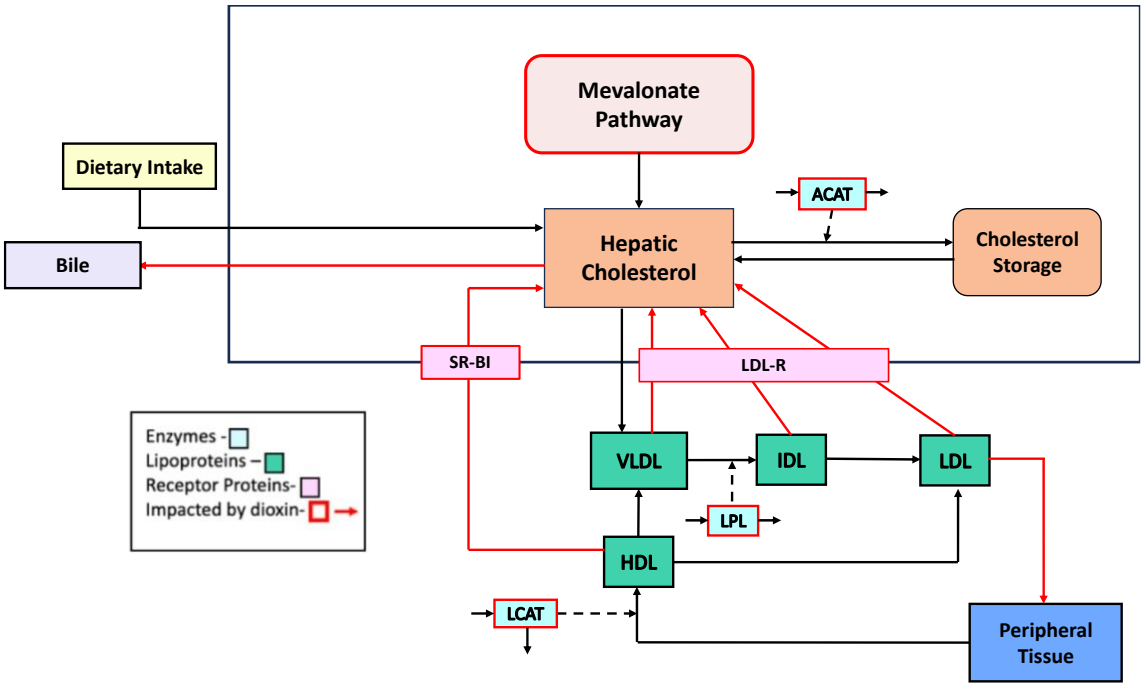

Figure 3.1: Overview of cholesterol metabolism and transport pathways. This diagram illustrates the process of cholesterol dynamics, highlighting the lipoproteins VLDL, IDL, LDL, and HDL responsible for the transport of cholesterol between the liver and peripheral tissues. The receptors proteins SR-BI and LDL-R along with enzymes such as LPL and ACAT are also depicted. Notably, the impact of dioxin on specific processes are depicted.

The main types of lipoproteins involved in this pathway system include:

- **Very Low-Density Lipoproteins (VLDL):** They transport cholesterol and triglycerides synthesized in the liver to tissues throughout the body. As they release triglycerides, VLDLs shrink in size and become denser.
- **Low-Density Lipoproteins (LDL);** often referred to as "bad cholesterol." They are formed from VLDL remnants (IDL) and contain a higher proportion of cholesterol in comparison to VLDL. LDL particles deliver cholesterol to various peripheral tissues and the liver. High levels of LDL cholesterol are associated with an increased risk of cardiovascular disease.

- **High-Density Lipoproteins (HDL);** often termed "good cholesterol." They are smaller and denser than LDL particles and remove excess cholesterol from the bloodstream and transport it back to the liver for excretion, a process known as reverse cholesterol transport.

In the liver, cholesterol is synthesized *de novo* (see Chapter 2) or taken up from the bloodstream via low-density lipoprotein receptors (LDLR). Hepatic cholesterol can then be converted to cholesterol esters and stored, a process catalyzed by the enzyme acetyl-CoA acyltransferase (ACAT), or it can be incorporated into VLDL for secretion into the bloodstream. Once in the bloodstream, VLDL is hydrolyzed by lipoprotein lipase (LPL) leading to the formation of IDL. IDLs are either taken up by the liver or further catabolized to LDLs by an enzyme called hormone sensitive lipase (HSL). LDLs are then taken up by the liver or peripheral cells where they can be utilized for various cellular processes, including membrane synthesis and steroid hormone production [106]. The LDL receptor (LDLR) facilitates the uptake of VLDLs, IDLs, and LDLs into the liver [107]. Additionally, HDL acquires free cholesterol from the cell membranes of peripheral tissues, which allows it to be esterified by lecithin: cholesterol acyltransferase (LCAT). Furthermore, it is believed that the esterification of cholesterol by the action of LCAT promotes the net removal of cholesterol from peripheral tissue and incorporation into HDL [108]. HDLs then transport the excess cholesterol from peripheral tissues back to the liver for excretion, storage or recycling in a process termed reverse cholesterol transport [109]. This process is facilitated by scavenger receptor class B type 1 (SR-B1), which mediates selective uptake of cholesterol from HDL particles by hepatocytes [110].

3.1.3 Effects of dioxin on lipoprotein cholesterol metabolism and transport

Dioxin (TCDD) exerts a complex influence on the lipoprotein transport pathway, which is critical for the distribution and regulation of lipids in the body, as described above. Through its interaction with the aryl hydrocarbon receptor (AhR), dioxin can alter the expression of genes that are integral to the production, conversion, and uptake of lipoproteins. The changed expression can lead to disruptions in the normal balance and function of lipoproteins including VLDL, LDL, and HDL. According to the Comparative Toxicogenomic Database (CTD) (refer to Chapter 1), dioxin interacts with several genes that are directly or indirectly involved in lipoprotein formation and transport. Genes that are pertinent for our model and impacted by dioxin in rodents and/or humans are presented in Table 3.1.

Table 3.1: Dioxin-affected genes, enzymes, and other proteins related to lipoprotein cholesterol transport between the liver and peripheral tissues.

Gene	Enzymes / Proteins	Impact of Dioxin on Expression	Organisms	Sources
ACAT	Acetyl-CoA acetyltransferase	↓	Mus musculus	Mathjis K (2009)
LDLR	Low-density lipoprotein receptor	↑	Mus musculus	Nault R (2017) Angrish (2013)
LPL	Cytochrome P450 family 7 subfamily A member 1	↑	Homo sapiens Mus musculus	Fader KA (2015) Nault R (2017)
LCAT	Lecithin–cholesterol acyltransferase	↑	Mus musculus	Angrish (2013)
SR-B1	Scavenger receptor class B	↑	Mus musculus	Boutros PC (2009)

3.2 Methods

3.2.1 Model formulation of the lipoprotein cholesterol transport pathway

The lipoprotein transport pathway depicted in Figure 3.1 is mathematically represented with nonlinear ordinary differential equations (ODEs) in the same fashion as for the mevalonate pathway anchor model (Chapter 2). Thus, the equations are formulated within the framework of Biochemical Systems Theory (BST) [68-70], and its special case, Mass-Action Kinetics. Details are presented in Appendix A.2. The model is evaluated at the steady state, as with the previous anchor model since we are only interested in the long-term effects of dioxin exposure. Each lipoprotein and enzyme is modeled with an ODE that contains two types of parameters: (1) non-negative rate constants (c_i) of production and degradation, and (2) kinetic orders (k_j), whose signs directly align with the modeled function as described in Chapter 2. Typical examples are the ODEs for LDL and HDL:

LDL Cholesterol:

$$x_5' = v_{65} * x_6 * DR_9 - v_{51} * x_5 * DR_6 + v_{35} * x_3 * DR_{11} - v_{57} * x_5 * DR_{12}$$

HDL Cholesterol:

$$x_6' = v_{76} * x_7 * DR_{10} - v_{61} * x_6 - v_{65} * x_6 * DR_9 - v_{62} * x_6 * DR_7$$

Here, the indexed quantities DR_i are placeholders that have a value of 1 at the baseline but allow us later to modify rates according to process-specific dioxin dose-response relationships.

The complete ODEs can be found in Appendix A.6; computer code in PLAS and MATLAB format is available on GitHub.com/LBSA-VoitLab/TCDD_Chol.

3.2.2 Parameter determination and model evaluation

A summary of the parameter values for the model is provided in Appendix A.7. The model was primarily evaluated against the steady-state concentrations in human hepatocytes or plasma obtained from the literature Table 3.2. Upon calibrating the model parameters, the steady-state lipoprotein concentrations obtained from the literature and those computed with the parameterized model were quite similar to each other (Table 3.2). Basal protein activity levels were arbitrarily set as 100, reflecting "normal conditions." Values of other model parameters were based on previously set parameters from the mevalonate anchor model, where applicable, and from literature information; they were reasonably adjusted to obtain model outputs consistent with published steady-state concentration data. The remaining parameter values were manually adjusted to align roughly with the expected half-lives of the lipoproteins and enzymes. Finally, we calibrated the percent change in lipoprotein cholesterol concentration under TCDD exposure based on animal studies for a TCDD dose of 30 ug/kg [40]. For simplicity, and due to the lack of information, we then used linear interpolation to obtain lipoprotein cholesterol concentrations at other doses of dioxin. It is important to note, as previously mentioned in Chapter 2, that we are not considering the short-term dynamics of the pathway, so that specific values of rate constants are not as critical as they would be otherwise, as long as their ratios are adequate.

Table 3.2: Comparison of the steady-state concentrations of key lipoproteins from the literature with results from model simulations. Steady-state values cited in the literature and corresponding values obtained for the model with parameter values presented in the Appendix A.7

	Steady State Simulation (μM)	Steady State Literature (μM)	References
Hepatic Cholesterol	11635.47	11638	Sniderman (2013)
VLDL	775.46	775.90	Lee (2023)
IDL	387.53	387.95	Lee (2023)
LDL	2585.55	2586.32	Lee (2023)
HDL	1293.10	1293.16	Lee (2023)

Using the parameter values listed in Appendix A.7 and methods presented in Appendix A.2, numerical simulations and sensitivity analyses were conducted to examine the impact of various doses of dioxin exposure on hepatic and lipoprotein cholesterol homeostasis.

3.3 Results

3.3.1 Sensitivity analysis for the lipoprotein cholesterol metabolism and transport anchor model

Local sensitivity analysis for the lipoprotein anchor model, comprising the formation transfer of cholesterol between VLDL, IDL, LDL and HDL, and the transport of lipoproteins between hepatocytes plasma and peripheral tissue, was conducted to quantify the influence of model parameters for LDL, HDL and total plasma cholesterol (Figure 3.1). Total plasma cholesterol was calculated as the sum of VLDL, IDL, LDL, and HDL cholesterol steady-state concentrations. The sensitivity analysis was performed by

increasing and decreasing one parameter at a time by 10% from the default value and calculating the percentage change of LDL HDL, and total plasma cholesterol. The relative sensitivity coefficient was calculated by averaging the ratios of the percentage change of the cholesterol concentrations to 10% in both directions.

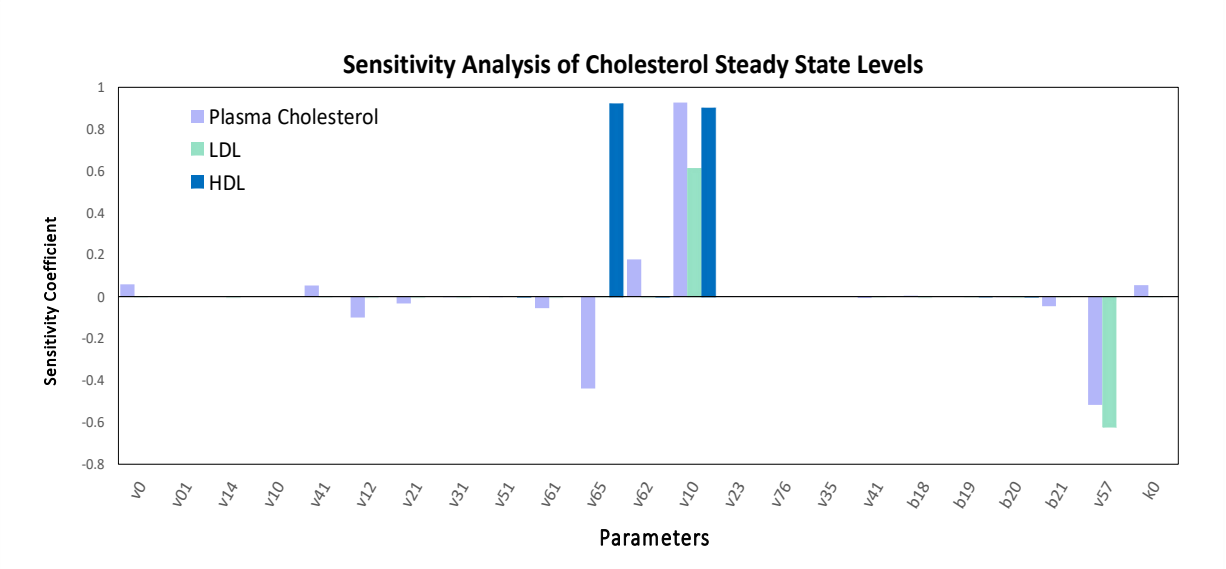

Figure 3.2: Sensitivity analysis of plasma cholesterol, LDL, and HDL. All parameters have a sensitivity coefficient below 1 in magnitude.

v65, reflecting the transfer of cholesterol from HDL to LDL; v62, reflecting the transfer from HDL to VLDL; v10, reflecting the hepatic removal of cholesterol for excretion; and v57, reflecting the transport of LDL cholesterol to peripheral tissues. All parameters exhibited sensitivity coefficients of less than ± 0.9 when adjusted by 10%. Therefore, these parameters can be considered as relatively influential, although the relative sensitivity is still below 1 in magnitude. The low sensitivities indicate that inaccuracies in parameter determination are not particularly influential.

3.3.2 Impact of dioxin on lipoprotein, hepatic, and plasma cholesterol

To evaluate the influence of dioxin on the lipoprotein transport pathway, we assessed the effects of varying doses of TCDD, spanning a range from 0 to 50 μg/kg body weight. Specifically, the assessment was executed by adjusting the parameters DR_i for each TCDD-impacted flux such that the outcome matched literature information, which was only available for a dose of 30 μg/kg [40]. Additionally, we calibrated the model against the dioxin-*versus*-hepatic cholesterol dose-response curve, which was previously reported in Chapter ## for the mevalonate anchor model. In response to these dose-specific adjustments, the total plasma cholesterol, LDL, and HDL all decreased by ~25% following treatment with 30 μg/kg TCDD. At the same time, this increasing "loss" of plasma cholesterol is reflected in strong increases in hepatic cholesterol, as they have been observed (Figure 2.3).

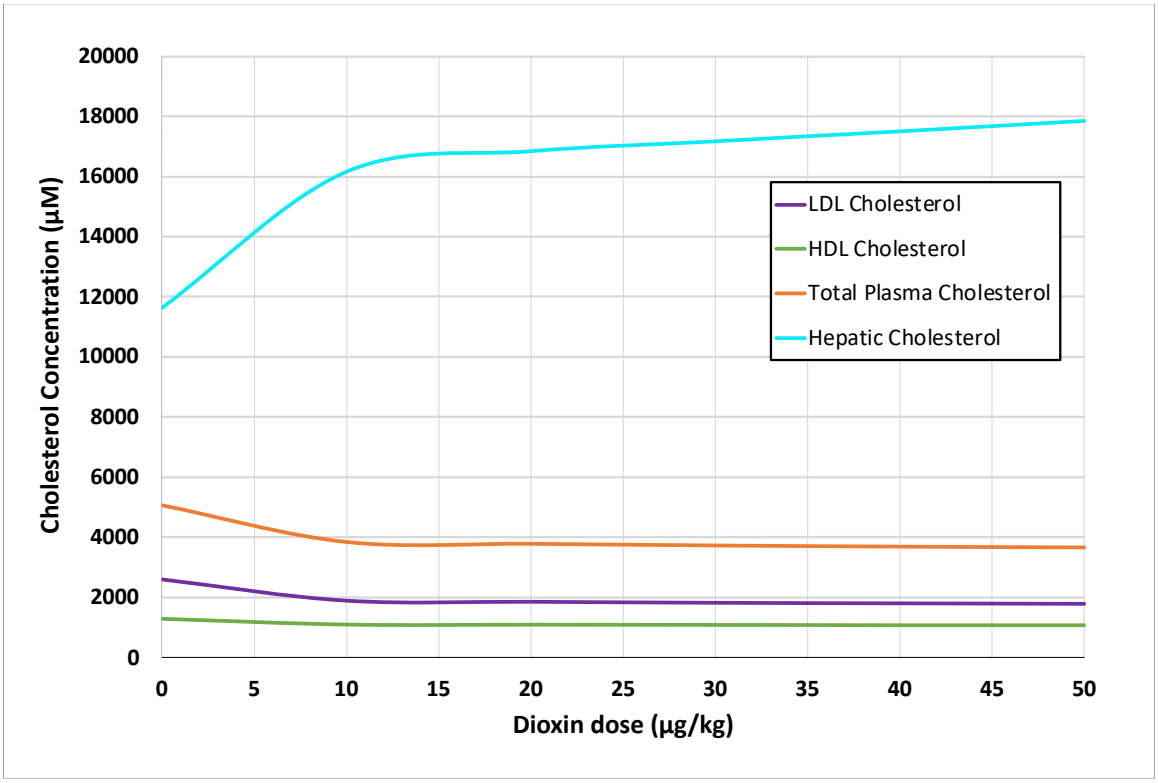

Figure 3.3: Dose-response curves quantifying the effects of increasing dosage of TCDD on LDL, HDL, hepatic, and plasma cholesterol concentrations.

Thus, similar to the dose response curves reported in Chapter 2 (Figure 2.4), the dioxin effect on hepatic cholesterol accumulation is strong even for low exposures and ultimately approaches saturation for high exposures. This increase in hepatic cholesterol under higher doses of dioxin is in some sense compensated by a concomitant reduction in the concentrations of total plasma cholesterol, HDL, and LDL. Specifically, at a dose of 30 µg/kg an approximate ~26% decrease of total plasma cholesterol, ~17% decrease of HDL, and ~30% decrease of LDL is observed which is consistent with the literature [40].

3.3.3 Effects of dietary cholesterol on LDL and HDL

The model allows us to assess the potentially synergistic role of dietary cholesterol intake and its effects on hepatic and serum cholesterol. As mentioned before, the recommended range of dietary cholesterol intake is approximately <200 mg/day [89]. The model indicates that cholesterol intake increases hepatic, VLDL, IDL, HDL, LDL, and total plasma cholesterol (Fig. 3.4) but again, in a rather insensitive manner, which is consistent with literature reports [90].

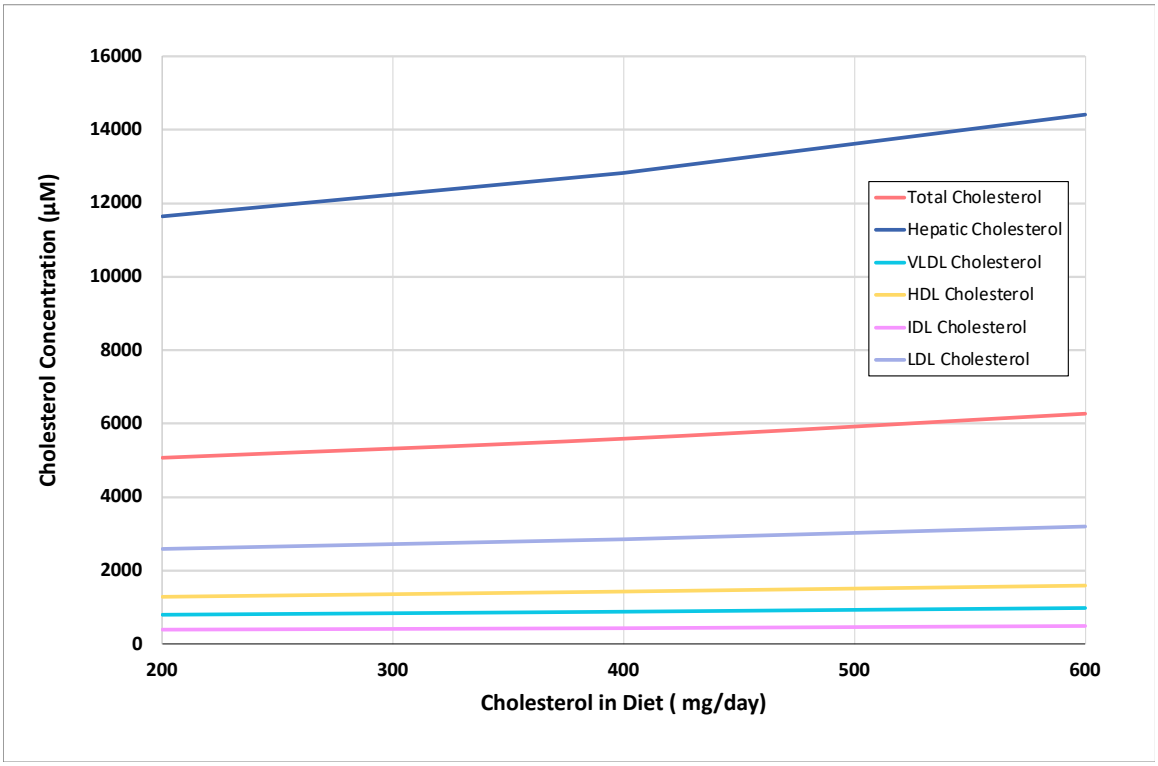

Figure 3.4: Effect of increased dietary cholesterol intake on LDL, HDL, IDL, VLDL hepatic, and plasma cholesterol concentrations in the model.

Using these results, we explored with simulations the effects of combinations of dietary intake and dioxin exposure. Without dioxin exposure, the steady-state value of LDL and HDL cholesterol under a normal daily consumption of ~200 mg cholesterol is about 2,600 μM and 1,300 μM respectively (Table 3.2) As expected, both LDL and HDL cholesterol levels increase with increasing dietary intake but show a decrease with increasing doeses of dioxin (Fig. 8). For the recommended cholesterol intake, the model predicts a decrease in LDL and HDL 1782 μM and 1064 μM respectively, if the individual is exposed to a relatively high dose of 50 μg/kg of dioxin. In comparison, for the same dose of TCDD, but with 600 mg/day of dietary cholesterol intake, the model predicts approximately 2,200 μM and 1,315 μM of LDL and HDL cholesterol respectively, which is close to the concentrations observed with the recommended dietary intake but with no dixoin exposure. Again, these decreases are accompanied by increases in hepatic cholesterol.

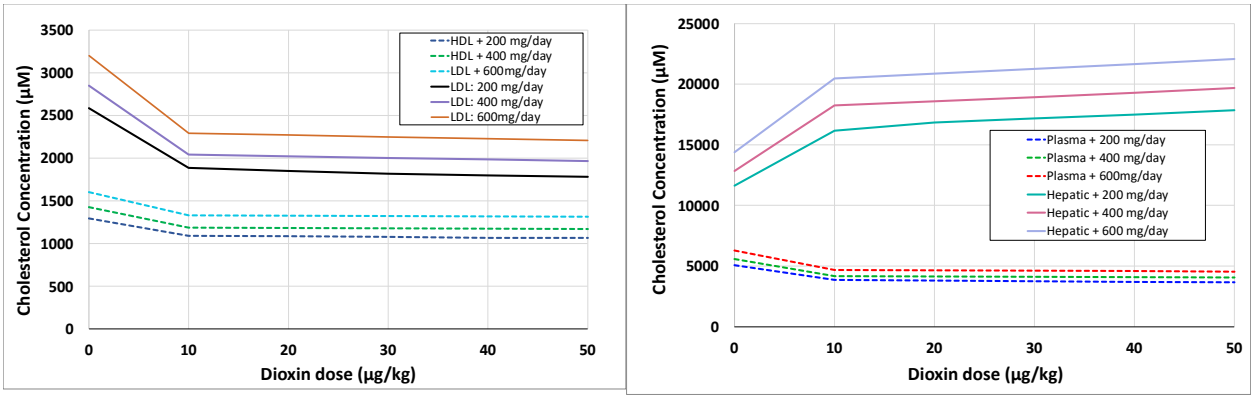

Figure 3.5: Dose response curves accounting for the effect of dioxin and increased diet on the lipoprotein transport pathway. The lipoproteins included are LDL and HDL (A). We also consider the response of hepatic and plasma cholesterol (B). 200 mg/ day is the recommended amount of cholesterol in diet/ day while 400 mg/day is high and 600 mg/day is considered very high.

3.4 Discussion

3.4.1 Summary of Findings

3.4.1.1 Impact of dioxin exposure and changes in gene expression

The presented lipoprotein model encompasses features known to be relevant, such as the synthesis of IDL, LDL, and VLDL, the reverse cholesterol transport process—encompassing the generation of HDL from peripheral cholesterol and its return to the liver—, and the exchange of cholesterol between the liver and plasma mediated by LDLR and SR-B1. Importantly, this model permits us to study the effects of dioxin exposure on this mechanism in detail. In particular, we can assess the balance between downregulation of pertinent genes, such as LDLR, LCAT, SR-B1 and LPL, and the upregulation of ACAT, and investigate the effect of this balance on various forms of cholesterol.

As the model demonstrates, the overall result is an increase in hepatic cholesterol and a decrease in plasma cholesterol. The same effect was observed in the mevalonate anchor model (Figure 2.4), which employed a drastically simplified plasma lipid module. As in the mevalonate model, the upregulation of genes such as SR-B1 and LDLR, involved in cholesterol transport between the plasma and liver, contribute to a decrease in serum cholesterol concentrations and the accumulation of hepatic cholesterol.

3.4.1.2 Impact of dietary cholesterol and dioxin exposure on gene expression and cholesterol levels

To illustrate the utility of the proposed types of models further, we studied the interrelations between dietary cholesterol intake and dioxin exposure. As mentioned previously, studies suggested synergistic effects between diet and dioxin exposure [92], and this model permitted us to assess this synergism quantitatively. Indeed, the results were more nuanced, as there is synergism with respect to hepatic cholesterol but antagonism with respect to plasma lipoproteins. Aligning well with findings from both the literature and simulations using the mevalonate anchor model, the model demonstrates that dietary cholesterol exerts a substantial impact on hepatic cholesterol levels, while having a slightly compensatory effect on plasma cholesterol levels.

3.4.2 Limitations of the lipoprotein cholesterol metabolism and transport anchor model

While the lipoprotein anchor model appears to function properly, it is obviously simplified, like any other model. For instance, further complexity could be added to include the intricacies of cholesterol absorption from diet, which involves a large number of enzymes and transport proteins in a multi-step process [111]. Additionally, the complexities involved in the formation of bile from hepatic cholesterol, which plays an important role in the excretion of excess cholesterol-containing lipoproteins, have been simplified [112]. Other complexities could be added to the model to include more detailed steps of reverse cholesterol transport which governs the flux of cholesterol from the peripheral tissues to the liver via HDL.

It goes without saying that the quality of any model, regardless of its sophistication, is fundamentally limited by the availability and accuracy of the data used for its calibration. In our situation, there are obvious uncertainties related to the values of parameters and the model's simplified structure. In particular, the scarcity of human data and our reliance on mouse data represent a significant constraint. This aspect is somewhat worrisome, considering the different responses to TCDD in serum cholesterol levels observed between humans and mice. To capture these observed changes in circulating plasma cholesterol levels accurately, while concurrently accounting for the accumulation of cholesterol in the human liver and integrating into the model additional pathways of TCDD's impact on organs besides the liver , it would be desirable to develop separate human-only or mouse-only models.

While certainly not complete or perfect, the approach was shown to be sufficient for revealing the essence of the complex phenomenon of dioxin affecting cholesterol handling. As mentioned in other anchor models (see Chapters 2, 4, and 5), and as is true in all modeling efforts, the mathematical structure of the model is debatable. Nonetheless, the use of mass-action and power-law representations for the design of the differential equations in the model is arguable the most straightforward and least biased approach (see ([54]) as well as references therein and above).

3.4.3 Significance and Future

The current model serves as a foundational platform for studying lipoprotein metabolism and cholesterol transport and the impact of dioxin on this process. Once the requisite data are available, future iterations of this anchor model will aim to incorporate the complex multi-step process of dietary cholesterol absorption and bile formation more accurately. By integrating a

more comprehensive set of enzymes, transport proteins, and biochemical pathways, the model has the potential of achieving greater fidelity with biological reality.

Given the species-specific responses to dioxin, there is a compelling need for separate models that can singularly represent human and mouse physiology [113]. This separation will allow for a more nuanced analysis of TCDD's effects on cholesterol levels across the different species.

Overall, the dynamics of this model is linked to the other anchor models (see Chapters 2 and 4) in the template model, enabling a comprehensive evaluation of the effect of dioxin on cholesterol dynamics (see Chapter 5).

CHAPTER 4 The Impact of Dioxin on Ovarian Steroidogenesis

4.1 Introduction

4.1.1 The menstrual cycle

4.1.1.1 Background

Menstruation is the cyclic shedding of the uterine lining in response to the interactions of hormones from the hypothalamus, pituitary gland, and ovaries. The menstrual cycle is divided into two phases: the follicular, also known as the proliferative, phase, and the luteal, also known as the secretory, phase. The length of the menstrual cycle is defined as the number of days between the start of menses of one cycle to the beginning of the next cycle. On average, the menstrual cycle spans 28 days, with individual variations commonly ranging from 25 to 30 days [114, 115].

The follicular phase is the preparatory stage of the menstrual cycle that starts on the first day of menstruation and ends with ovulation. At the end of the previous cycle, accompanied by the breakdown of the corpus luteum, there is a decrease in the hormones estrogen (E2), progesterone (P4), and inhibin A. This decrease allows disinhibition of the negative feedback action of these ovarian hormones in the hypothalamus and anterior pituitary, leading to an increased release of follicle-stimulating hormone (FSH) into the bloodstream [116]. The rise in FSH stimulates the granulosa cells of the antral follicles and thus facilitates the recruitment and maturation of the follicles. Among them, a single follicle emerges as dominant, continues to grow, and ultimately progresses to ovulation within that cycle [117, 118]. Additionally, as the dominant follicle grows, it secretes increasing amounts of estradiol and inhibin B into the bloodstream. These hormones act

to suppress FSH levels, which diminish until ovulation occurs. [118]. When the circulating estradiol level secreted by the dominant antral follicle reaches a sufficiently high level, it signals the hypothalamus and anterior pituitary that the follicle is mature and ready for ovulation. At this stage, estradiol begins to stimulate the hypothalamus and anterior pituitary gland, leading to a surge in both LH and FSH . The LH surge initiates the release of the oocyte from the dominant follicle—known as ovulation—after which the residual follicular tissue collapses. Subsequently, the granulosa and theca cells contained within differentiate to form the corpus luteum. Finally, the corpus luteum starts to secrete progesterone along with estrogen. This rise in progesterone thickens the uterine lining during the luteal phase, providing an ideal environment for a fertilized egg to implant and pregnancy to occur. If pregnancy does not occur, the corpus luteum dissolves and hormone levels decline, thus causing the uterine lining to shed and producing menses [119].

4.1.1.2 Ovarian steroidogenesis pathway

The female sex steroid hormones, mainly E2 and P4, are synthesized in the ovary, specifically by the antral follicles during the follicular phase and by the corpus luteum during the luteal phase. Antral follicles are composed of an inner layer of granulosa cells and an outer layer of theca cells. The two types of cells work together to produce steroid hormones according to a well-known two-cell, two-gonadotropin principle [120], where the theca cells utilize cholesterol to make progesterone and androgen, the latter of which diffuses into the granulosa cells where it is converted to estrogen. The steroidogenesis in the corpus luteum works in a similar fashion involving luteinized/differentiated theca and granulosa cells [121].

The initial and rate-limiting step in the steroidogenesis pathway is the transport of cholesterol from the mitochondrial outer membrane to the inner membrane, mediated by the steroidogenic acute regulatory protein (StAR). Subsequently, cholesterol is converted to pregnenolone (P5) by the enzyme CYP11A1, which is located at the inner membrane. [122-124]. P5 then moves out of the mitochondrion and into the endoplasmic reticulum where it is converted to P4 by 3β-hydroxysteroid dehydrogenase (HSD3B1), or to dehydroepiandrosterone (DHEA) by CYP17A1. P4 can either be released into the bloodstream or partially transformed into androstenedione (A4) by the enzyme CYP17A1. Additionally, DHEA can be converted into A4 by the enzyme HSD3B1.

A4 is then converted to testosterone (T) by HSD17B1, and T is converted to E2 by the aromatase. CYP19A1. An alternative path in the last two steps is that A4 is first converted to estrone (E1) by CYP19A1, and then E1 is converted to E2 by HSD17B1. E2 is eventually secreted into circulation.

4.1.2 Dioxin's impact on steroidogenesis and the menstrual cycle

Exposure to dioxin has been demonstrated to cause a variety of adverse reproductive outcomes, including altered sex hormone dynamics, anovulation, reduced fecundity, delayed fetal growth and development, and endometriosis [125]. While TCDD has multiple toxicity targets within the female reproductive system, inhibition of female steroid hormone production and disruption of the reproductive cycles appear to be a common theme in a variety of species. Earlier studies showed that exposure of rhesus monkeys to 500 ppt TCDD in the diet for 6 months caused decreases in both E2 and P4 levels [126]. Chronic exposure to TCDD dose-dependently induced decreases in E2 level

on proestrus in rats [127]. In human luteinizing granulosa cells, TCDD caused E2 to decrease [128]. In mouse antral follicles studied *in vitro*, TCDD exposure suppressed the secretion of progesterone (P4), androstenediol (A5), testosterone (T), and estradiol (E2) over a period of 96 hours, showing a concentration-dependent and non-monotonic pattern of inhibition. [129].

Exposure to TCDD in rats has been observed to interfere with the estrous cycle, resulting in an extended duration of the diestrus phase [130]. Furthermore, rhesus monkeys exposed to TCDD through their diet exhibited a trend toward longer menstrual cycle lengths, increasing from 27.3±4.3 to 27.8±3.9 days, although this increase was not statistically significant [126]. Epidemiological studies showed that the menstrual cycle length of women living in dioxin-polluted areas in Seveso, Italy, was positively associated with serum TCDD concentrations [131], and women with high serum TCDD concentration experienced increased time to pregnancy and risk of infertility [131]. Serum levels of estrogenic PCBs, some of which are dioxin-like compounds, were significantly associated with increased menstrual cycle length, which can be prolonged by approximately 3 days [132].

While animal and *in vitro* studies showed that exposure to dioxin generally leads to suppression of ovarian E2 secretion, the steroidogenic enzymes altered by dioxin appear to vary depending on the species and experimental conditions. In human luteinizing granulosa cells, TCDD caused E2 to decrease without changing either aromatase protein or its enzyme activity [128], however, there was a decrease in CYP17A1 protein abundance and activity [133]. In these cells, it was shown recently that TCDD decreased mRNA expression of CYP11A1 and CYP19A1. Similarly, in granulosa

cells from young or adult rats, TCDD also reduced CYP11A1 and CYP19A1 mRNA expression [134]. In rats chronically exposed to TCDD, CYP17A1 mRNA expression was significantly inhibited while the expression of genes of other steroidogenic enzymes were not altered [127]. In mouse antral follicles, TCDD inhibited CYP11A1, CYP17A1, HSD17B1, and CYP19A1 mRNA expression, and increased HSD3B1 mRNA expression; however, at the protein level only the abundance of HSD17B1 was significantly reduced [135].

In summary, exposure to dioxin can dysregulate the steroidogenic enzymes, inhibit steroid hormone production, and alter the ovarian cycle.

4.1.3 Modeling approach for understanding the dioxin effects on steroidogenesis and female reproduction

Based on toxicological studies in animals and epidemiological studies, we hypothesize that (1) dioxin dysregulates the enzymes participating in the female steroidogenesis pathway in the ovarian follicles by inhibiting E2 synthesis and secretion, and (2) as a result, it takes a longer time for the circulating E2 to rise to levels sufficiently high to trigger the LH surge, leading to delayed ovulation and longer follicular phase. There are many existing models of menstrual cycles focusing on different aspects, including follicle development, hormonal dynamics, and potential applications [136-149]. However, rarely do these models incorporate biochemical details of the steroidogenesis pathway starting from cholesterol as the source substrate to the final production of E2, with P4 and T as the intermediate steroids.

In the present study, we propose a mathematical model of the menstrual cycle containing the steroidogenesis pathway so that the effects of dioxin on the metabolic

enzymes in the pathway can be simulated and the outcome of follicular phase length can be predicted. The model will serve as the anchor model for a higher-level template model.

4.2 Methods

4.2.1 Model formulation of the steroidogenesis anchor model

The overall structure of the model is illustrated in Figure 4.1. It contains the essential feedback interactions between the pituitary gonadotropins FSH and LH and the ovarian hormones E2 and P4, the antral follicle and corpus luteum dynamics, and the steroidogenesis pathway.

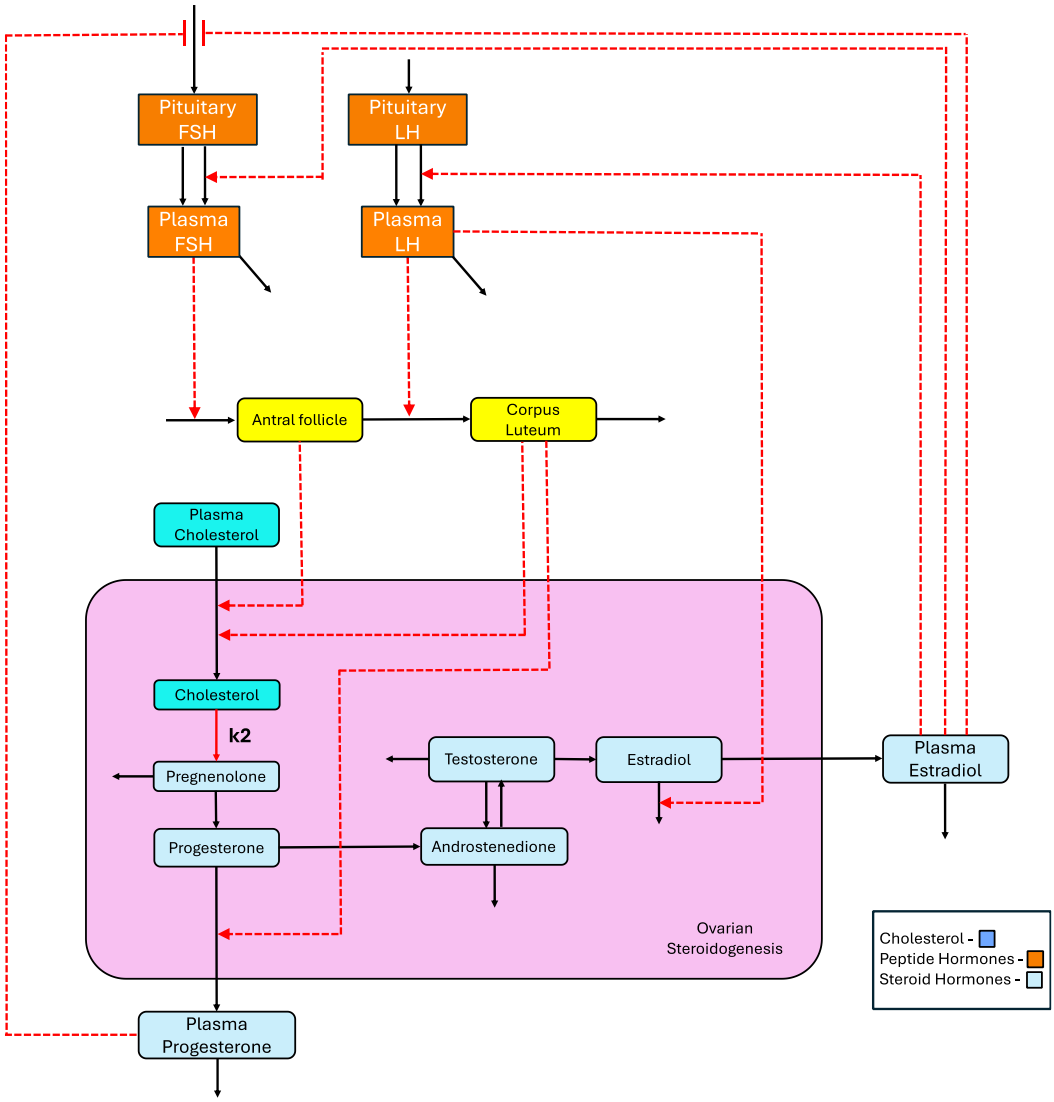

Figure 4.1 Steroidogenesis anchor model describing the estradiol synthesis pathway, it's regulation, and perturbation by TCDD. Molecules are color-coded by type, as indicated. Solid lines show reactions and transport steps, with the red solid line (k2) signifying a step impacted by TCDD. Dashed lines represent feedback regulation (red) from estradiol and progesterone on the synthesis and release of FSH and LH hormones from the pituitary to plasma, exerting control over the development of the antral follicles and the corpus luteum.

The steroidogenesis pathway module contains the following key enzymatic steps: The initial rate-limiting step, which includes the StAR-mediated cholesterol transfer from the mitochondrial outer membrane to the inner membrane and the CYP11A1-mediated conversion of cholesterol to P5, is represented by the step k2, as illustrated. P5 is converted to P4 by HSD3B1. P4 can be secreted into the circulation and a fraction is further converted by CYP17A1 into A4. A4 is then converted to T by HSD17B1 and T is converted to E2 by CYP19A1. E2 is eventually secreted into the plasma. All steroid conversion steps were modeled as first-order processes, without explicit concern for the specific enzymes involved.

FSH stimulates the growth of the antral follicle. As the follicle increases in mass, its steroidogenic activity will increase because more theca and granulosa cells are formed. The follicle growth-driven increase in steroid synthesis is implemented by increasing the supply of plasma cholesterol as the substrate to the first step of the steroidogenesis pathway described above. As the plasma E2 increases, it feedback-inhibits the production of pituitary FSH, causing FSH to decrease. As the plasma E2 increases to a certain threshold level, it triggers the release of LH stored in the pituitary into the blood circulation, producing an LH surge. A similar FSH surge is also triggered. The E2 threshold was implemented here by an intermediate signaling (S, not shown) that functions as a bistable switch in response to E2. The LH surge converts the antral follicle to the corpus luteum which eventually regresses. The corpus luteum drives the steroid synthesis also by increasing the supply of plasma cholesterol. In addition, the corpus luteum promotes the release of P4 to the circulation engendering the P4 rise in the luteal phase.

The current model is not intended to produce a spontaneous oscillator of the menstrual cycle. Its main purpose is to recapitulate the hormonal dynamics in the follicular phase, at least semi-quantitatively [150, 151], which is sufficient to allow us to mimic the effects of dioxin on antral follicle steroidogenesis and the time to the LH

surge. Most of the reactions in the model were formulated as either first-order mass action, Michaelis-Menten kinetics, or Hill functions. The reactions were parameterized so that the state variables are described as fold-change rather than concerned with their absolute values. The model's ODEs and parameter values are listed in Appendix A.8.1 and A.9 respectively. For Monte Carlo simulations of population responses, a few key parameters were randomly sampled from pre-defined lognormal distributions as indicated in Appendix A.8.3.

4.2.2 Modeling the effects of dioxin on steroidogenesis

Given the fact that the steroidogenic enzyme targets of dioxin can vary depending on the species and state of the ovarian cells [128, 134, 135, 152], it is challenging to implement the inhibitory effect of dioxin in an enzyme-specific manner. For simplicity, the impact of dioxin is implemented in the current model at the rate-limiting step of the steroidogenesis pathway, which is the conversion of cholesterol to P5 (k2 step in our model). This approach is consistent with research findings showing that the inhibitory effects of TCDD on P4, A4, T, and E2 in mouse antral follicles can be reversed completely by oversupplying P5, suggesting that the main inhibition site of dioxin is upstream of P5 [129]. In our model, the effect of dioxin is simulated by altering k2 to different fold-change levels relative to the default value. To link the dioxin exposure level to k2, we utilized an epidemiological study [131]. This study investigated the association between menstrual cycle length and serum TCDD level in women who were prepuberty at the time of occurrence of an industrial explosion causing dioxin pollution in the area in 1976 and had lived there since for 20 years. The study showed that for every 10-fold increase in serum TCDD concentration, the menstrual cycle is lengthened by 0.92 days. With the serum TCDD ranging between 10-10,000 part per trillion (ppt) in these subjects, the mean menstrual length can vary by nearly 3 days. We implemented the TCDD dose response by specifying a Hill function between TCDD concentration and k2 fold-change

so that at high TCDD concentration k2 is lowered to a value that causes the follicular phase length to be increased by 3 days, with the assumption that the menstrual cycle length increase is caused solely by follicular phase increase.

4.3 Results

4.3.1 Standardized model of the menstrual cycle

The model outlined in section *4.2.1* effectively delineates the hormonal interplay over the course of one menstrual cycle, capturing the fluctuations of steroid hormones—E2 and P4—as well as the gonadotropins—FSH and LH. The model was calibrated using literature that benchmarks the average menstrual cycle at 28 days, with ovulation typically occurring around day 15 shortly after the LH surge. This calibration allows us to track the progression of E2, P5, FSH, and LH during the follicular phase from days 1 to 15, leading up to ovulation, and subsequently through the luteal phase from days 15 to 28.

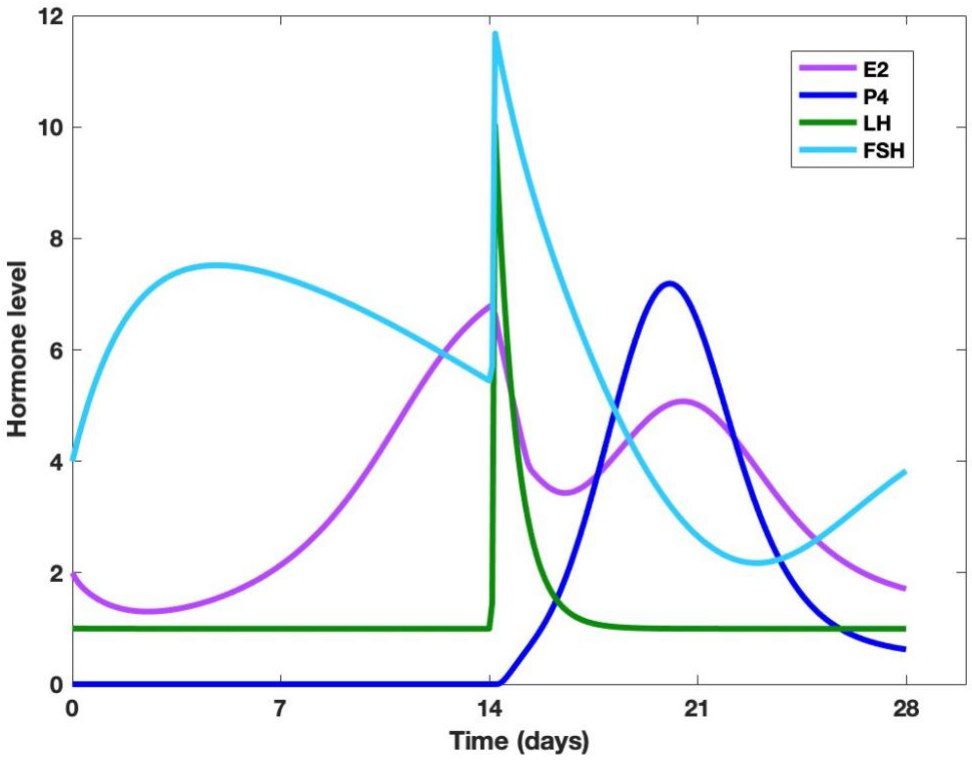

Figure 4.2: Dynamics of gonadotropins (FSH and LH) and steroid hormones (E2 and P4) as indicated through one menstrual cycle in the average model.

4.3.2 Sensitivity analysis for the steroidogenesis pathway model

Local sensitivity analysis was conducted to quantify the influence of model parameters on the length of the follicular phase. (Figure 4.3) The length of the follicular phase is defined as the duration from the start of the follicular phase to the time of the peak of the LH surge. The sensitivity analysis was performed by increasing and decreasing one parameter at a time by 10% from the default value and calculating the percentage change of the follicular phase length. The relative sensitivity coefficient was calculated by averaging the ratios of the percentage change of the follicular phase length to 10% in both directions.

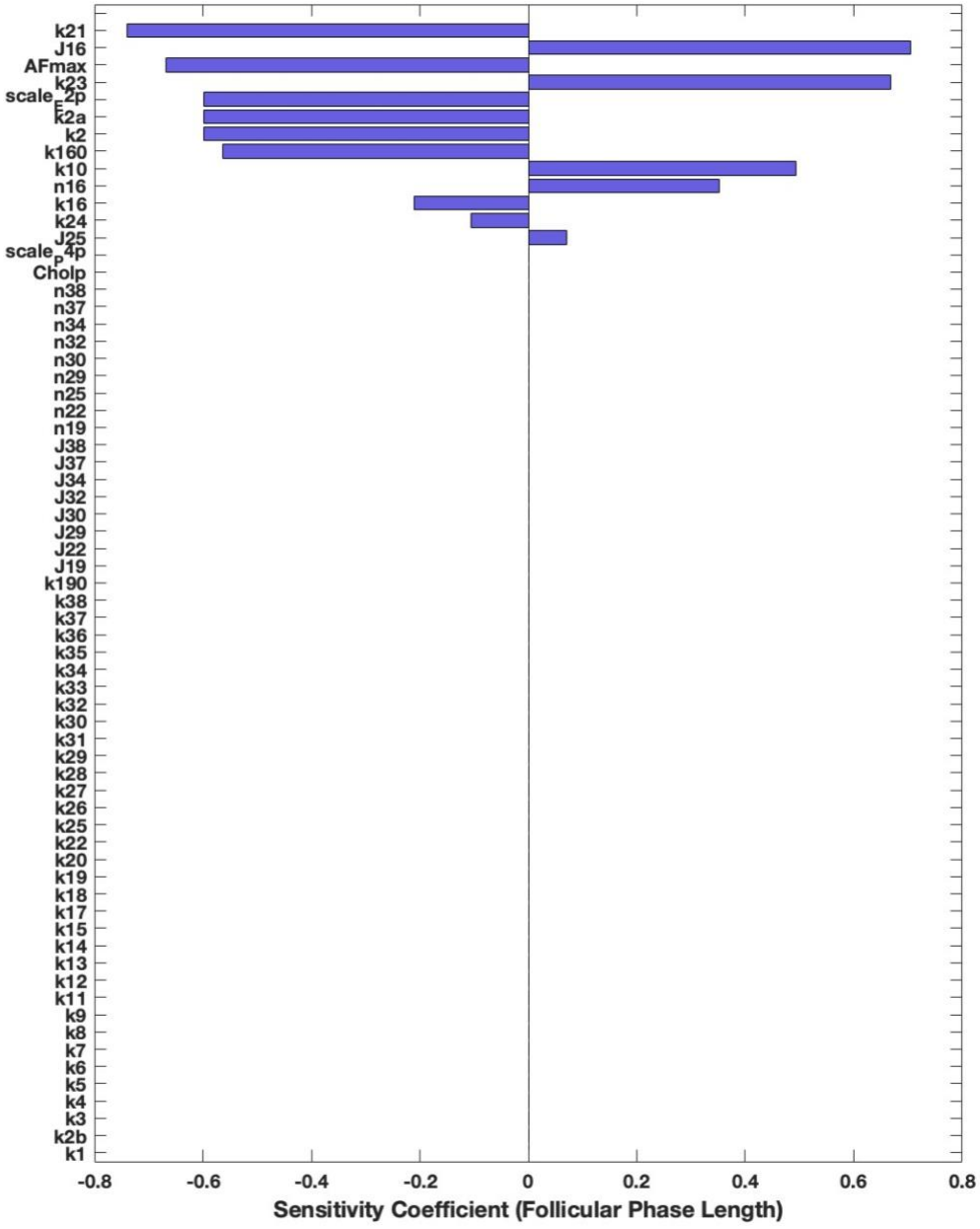

Figure 4.3: Results of a local sensitivity analysis for the steroidogenesis pathway anchor model. All parameters have sensitivity coefficients below 1 in magnitude.

Of the 66 parameters, 13 parameters demonstrated a sensitivity coefficient of greater than ± 0.1. The parameters that exert the most influence on the model include k21 a rate constant reflecting the antral follicle growth rate and J16, the affinity constant reflecting the E2 threshold that triggers the LH surge.

Moreover, all parameters exhibited sensitivity coefficients of less than ± 0.8 when adjusted by 10%. Therefore, the parameters can be considered to exhibit low sensitivity indicating that inaccuracies in parameter determination are not particularly influential.

4.3.3 Population-based modeling of menstrual cycle variability

Considerable variability of the menstrual cycle length exists with both intra- and inter-individual differences [114, 115, 153, 154], particularly in the duration of the follicular phase [114, 155]. Furthermore, there is a broad range of what constitutes normal hormonal levels across different individuals [150, 151]. Considering the documented effects of dioxin on menstrual cycle duration and estradiol levels, constructing a population-based model that accounts for these variations provides us with a comprehensive understanding of the menstrual effect of dioxin via the altering of ovarian steroidogenesis. The population dynamic trends of E2, P4, FSH, and LH, are presented in Figure 4.4 across one menstrual cycle. This model accounts for 100 individuals (grey); the figure also shows the means (solid lines) and 95% ranges (dashed lines).

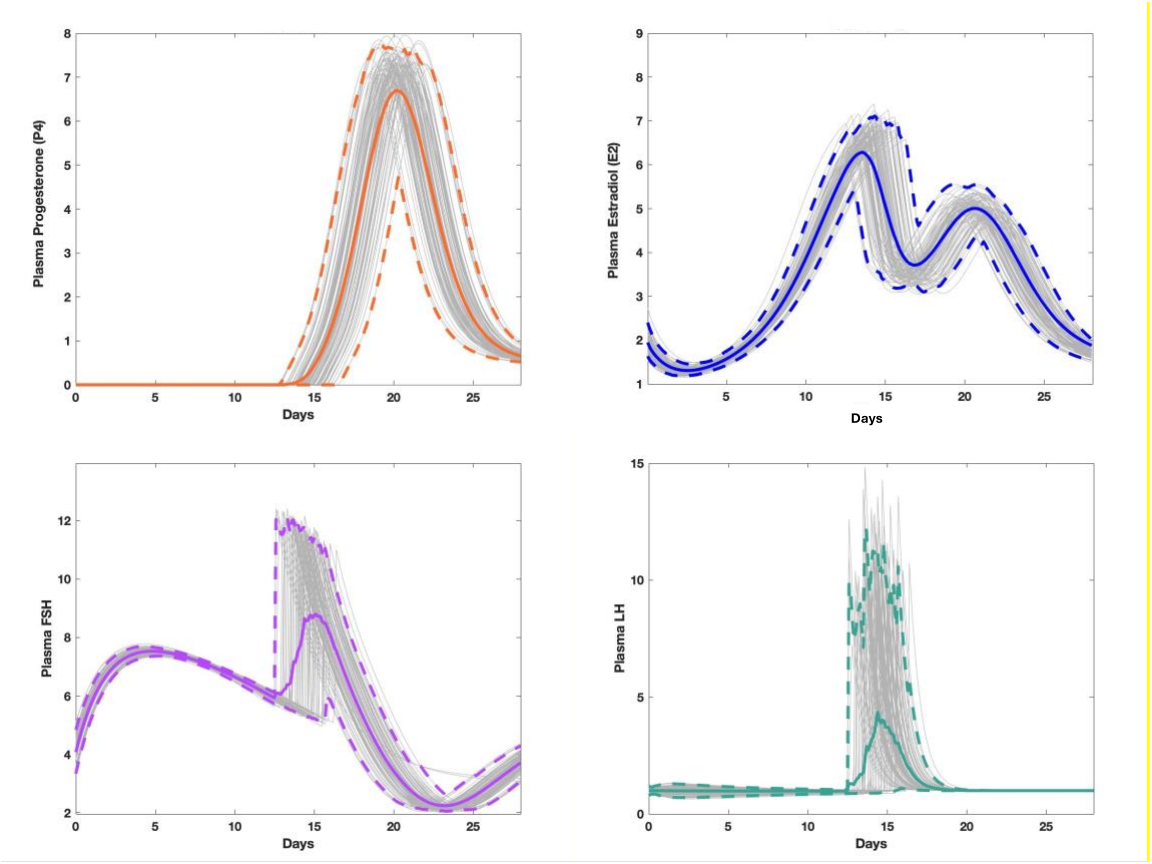

Figure 4.4: Population model dynamics of gonadotropins (FSH and LH) and steroid hormones (E2 and P4) as indicated through one menstrual cycle. Grey lines represent the data for 100 individual cases. The solid line denotes the average value across these cases, while the dashed lines define the 95% range within which most values lie.

4.3.4 Impact of dioxin exposure on the standardized menstrual cycle model

We evaluate the influence of dioxin on steroidogenesis by altering k2 as explained in the methods section, which accounts for the rate-limiting conversion of cholesterol to P5, to different fold-change levels relative to the default value as indicated in Figure 4.5. For instance, a 0.8-fold change of k2 corresponds to a 0.79-fold change in the peak E2 level, while also delaying the LH peak occurrence from the original day 14 to day 16.

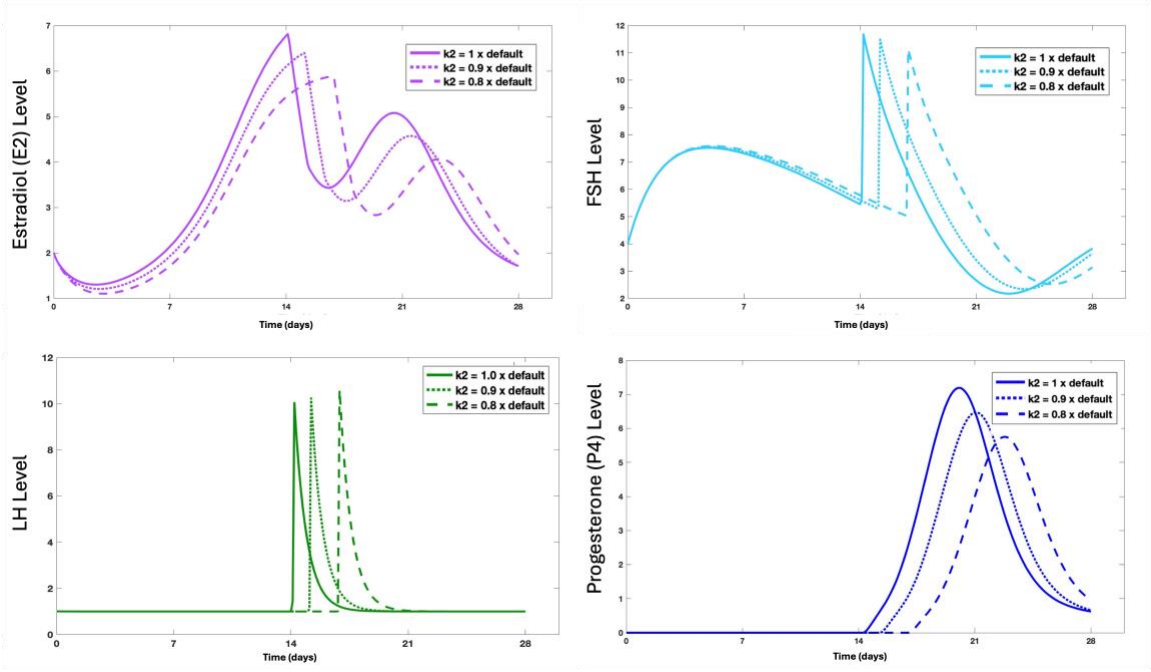

Figure 4.5: Effect of varying k2 (conversion of cholesterol to P5) on hormone dynamics based on the standardized menstrual cycle model.

4.3.5 Effect of dioxin on the population model

To quantify the impact of TCDD on the population steroidogenesis model, the serum TCDD level is mapped to fold decreases in k2 values as detailed in the methods. The simulation indicated that the length of the follicular phase appears to have a right-skewed distribution, as depicted in Figure 4.6, with the mean increasing as TCDD levels rise. Within the serum TCDD concentration range of 1 – 10,000 ppt, the follicular phase lengthens by approximately 3 days, starting from a mean of 14.4±0.8 days to 17.3±2.4 days, accompanied by increased variability, which includes instances of individuals displaying a 24-day follicular phase. The cumulative probability distribution of follicular phase lengths skews rightward as TCDD levels rise, suggesting that TCDD exposure impacts nearly the entire population under study.

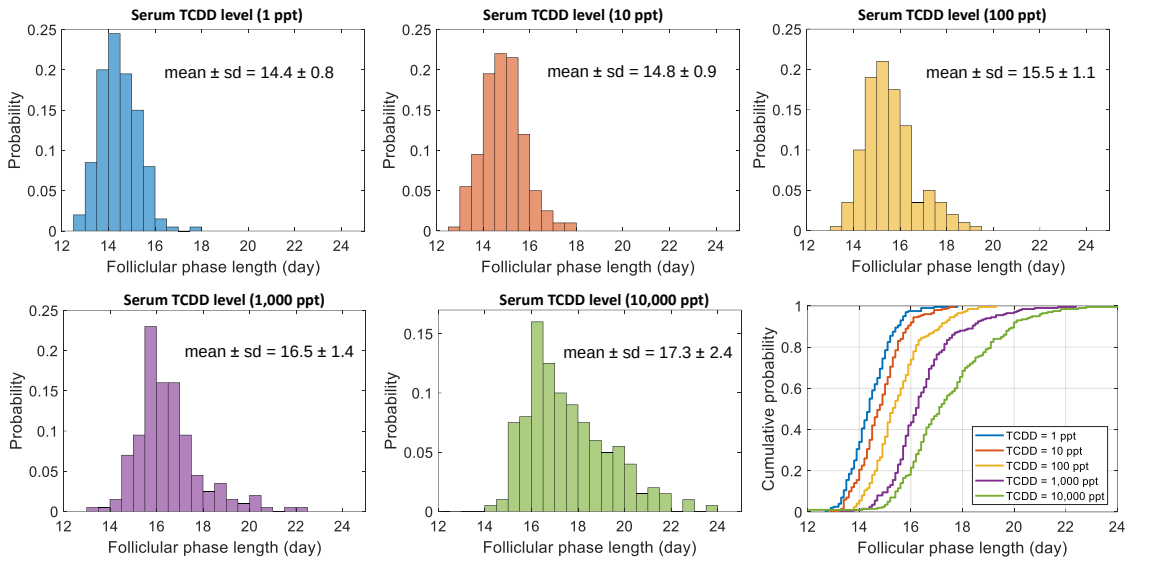

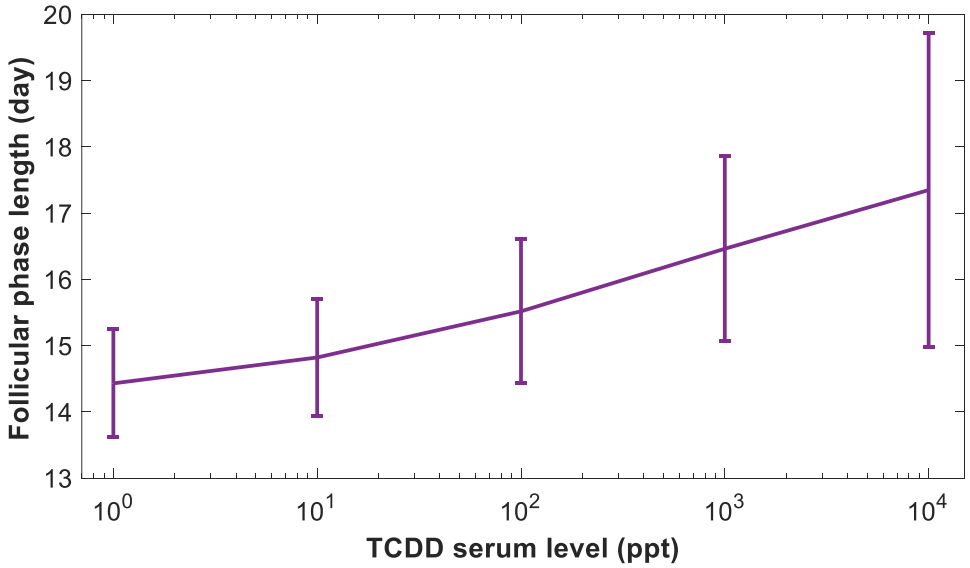

Figure 4.6: Dose response curve depicting the influence of TCDD serum level *vs.* follicular phase length expressed as the mean +/- SD in the population model. We include the probability distributions and the corresponding cumulative probability describing the relationship between dioxin serum levels (ppt) and follicular phase length.

4.4 Discussion

4.4.1 Summary of findings

The presented steroidogenesis anchor model effectively captures the dynamics of key hormones throughout one menstrual cycle, specifically illustrating the oscillations of gonadotropins LH and FSH, as well as the steroid hormones E2 and P4, across both the follicular and luteal phases. Moreover, the model is adept at simulating both average hormonal patterns and population variations, thereby accounting for individual differences in cycle length due to the variable duration of the follicular phase [156]. Importantly, this model permits us to study the effects of dioxin exposure on steroidogenesis in detail. In particular, we can assess the downregulation of CYP11A1, an enzyme that catalyzes the rate-limiting step of the steroidogenesis pathway, and investigate the effect on follicular phase length. As the model demonstrates, the overall result is an increase in the menstrual cycle by nearly 3 days with the maximum dioxin serum level of 10^4 ppt which is consistent with findings based on epidemiological studies [157]. Additionally, we were able to notice a decrease in E2 levels with increasing doses of TCDD, consistent with studies found in the literature [157].

4.4.2 Novelty of the model

A number of established models of the menstrual cycles exploring various aspects of follicle development and hormonal dynamics are currently available, along with their respective applications [128, 134, 135, 152]. Yet, such models seldom integrate the biochemical details of the steroidogenesis pathway, which includes the process from cholesterol, as the source substrate, to the final synthesis of E2, with intermediates involving the production of P4 and T. Moreover, to our knowledge, none have explored the TCDD-mediated effects on steroid hormone synthesis and on the menstrual cycle. To

address this aspect, we developed a mathematical model that not only integrates the steps of the steroidogenesis pathway but also captures the influence of dioxin on menstrual cycle dynamics. This strategy allows us to simulate and predict how varying dioxin doses may affect the length of the follicular phase. The model's effectivness is further emphasized by its capacity to reflect population-wide hormonal responses to dioxin, offering a comprehensive view that acknowledges the heterogeneities observed among individuals.

4.4.3 Limitations

The model we developed examines the effects of dioxin during the follicular phase and helps us understand its impact on menstrual cycle duration. Although it is noted that most variability of cycle length is usually derived from varying lengths of the follicular phase [156], our assumption does not reflect physiological reality, considering that the corpus luteum also synthesizes steroid hormones similarly to the antral follicles during the follicular phase, and thus could potentially be influenced by dioxin exposure. Additionally, our current understanding of the specific enzymatic dysregulation caused by dioxin is incomplete. As more information becomes available, the model can be refined accordingly to include these targets, thereby enhancing its accuracy and predictive capability.

4.4.4 Significance and future directions

In the future, this model can be used for *in vitro* to *in vivo* extrapolation (IVIVE) in the risk assessment of dioxin and other potential endocrine disrupting chemicals. Additionally, the dynamics of this model can be linked to other anchors in the template model, which allows us to evaluate the effect of estradiol levels on cholesterol along with the overall effects of dioxin on estrogen and cholesterol synthesis (see Chapter 5).

CHAPTER 5 The Template Model[3]

Dioxin is known to alter the expression of a wide range of genes, including those involved in cholesterol biosynthesis, lipoprotein transport, and steroid hormone synthesis. Its ultimate effect is mediated by the xenobiotic aryl hydrocarbon receptor AhR [40, 158]. The complexity of this broad spectrum of effects on various processes and organ systems poses a challenge for modeling the overall, "global" effect of "local" changes, thus necessitating a multiscale approach. As briefly introduced in Chapter 1, the Template-and-Anchor (T&A) modeling paradigm provides a structured framework for exploring both the overarching dynamics and the intricate details of these complex biological systems.

Several options are feasible for structuring the problem space of dioxin effects as a T&A system. The biomedical interaction system for a template specifically focusing on the cholesterol handling by various organs in the human body is shown in Figure 5.1. The boxes represent the dependent variables of this template model, while the arrows indicate fluxes among them. Ultimately, each box (variable) is modeled separately as an anchor model.

---

[3] Much of the material in this chapter is in revision for publication in *PLOS Computational Biology*

The prominent anchor models considered here are:

1) Cholesterol biosynthesis in hepatocytes, cholesterol storage through reversible formation of cholesterol esters, and transport among liver, plasma, and peripheral tissues [159]; see Chapter 2.
2) The lipoprotein pathway governing the dynamics of LDL, HDL, VLDL and IDL cholesterol in the plasma; see Chapter 3.
3) Endocrine dynamics pertaining to the synthesis of progesterone, testosterone, estradiol, and related steroids in gonads; see Chapter 4.

As a future refinement, one could explicitly consider further anchor models, which are presently not addressed or subsumed in the three anchors above, such as cholesterol storage and utilization in peripheral tissues.

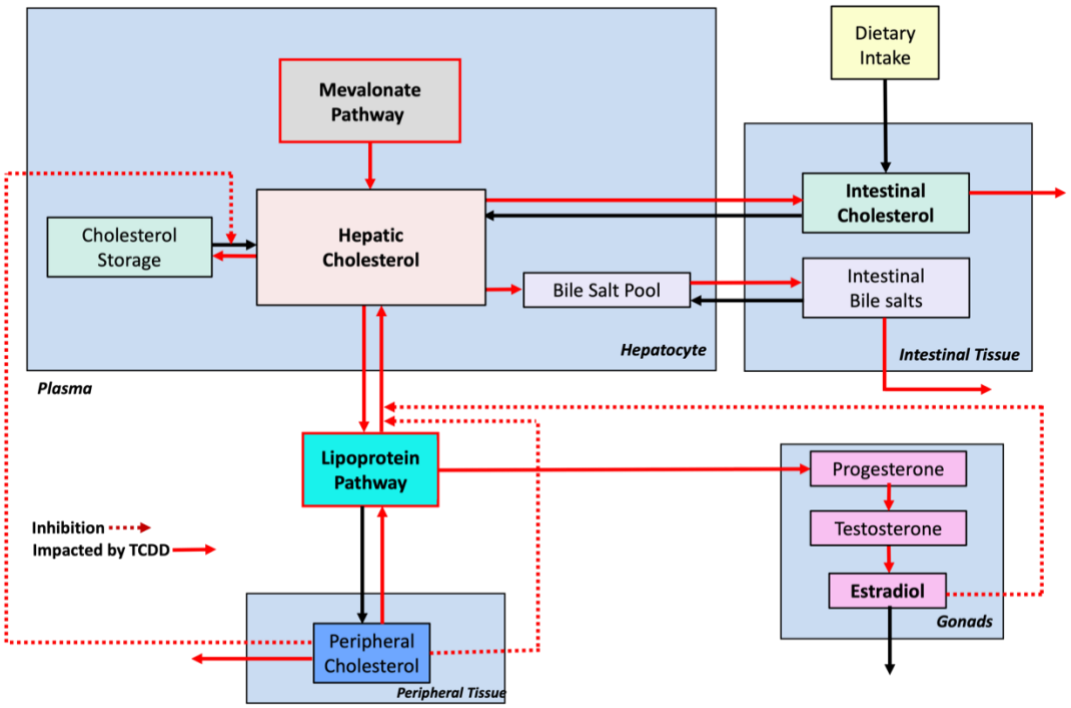

Figure 5.1: Organ systems forming the basis for the template model of cholesterol dynamics under TCDD exposure. Processes affected by TCDD exposure are indicated by red arrows.

In the analysis of the template model, all variables are informed by output from the anchor models, thereby allowing a global assessment of the effects of dioxin on the human body, which is novel and otherwise difficult to achieve.

5.1 Methods

5.1.1 Theoretical considerations regarding the structure of T&A models

We have been using T&A models in a straightforward manner, according to the intuitive notion of the template as a high-level, coarse-grained umbrella structure and the anchors as models elucidating parts of the template in greater detail. At first glance, the mathematical structures of template and anchor models seem to be simple variations of the same theme. Closer inspection, however, reveals an interesting combination of differences and correspondences between template and anchor models in general. This combination is most easily seen for a dynamic system operating at a steady state. At this prominent state, the two types of models have the structures of a regular directed graph (anchor model) and an edge-to-vertex dual graph (template model), respectively [85]. In the language of graph theory, the dual graph G* of a primal (line) graph G is constructed by exchanging edges and vertices. For directed graphs, which are most pertinent here, the vertex set of G* corresponds to the edge set of G, and every directed edge in G* corresponds to an instance in G where the head of an edge e_i meets the tail of another edge e_j. Figure 5.2 shows a generic example.

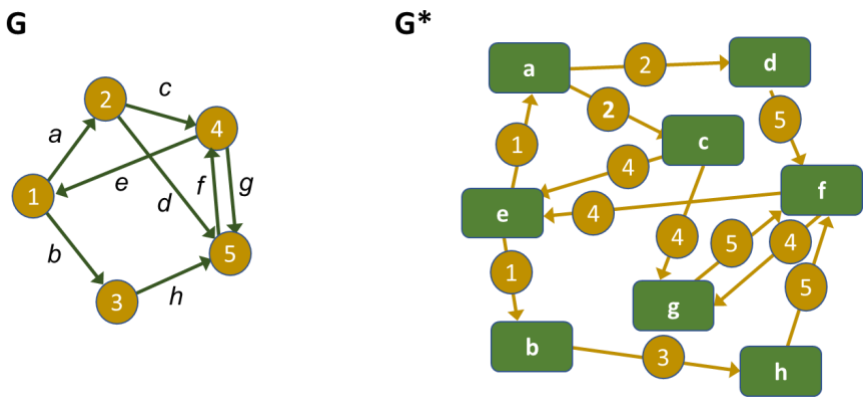

Figure 5.2: Example of a directed line graph G and its (edge-to-vertex) dual graph G*. The vertices of G* correspond directly to the edges in G, as indicated by letters a – h. The edges of G* correspond to vertices in G if one edge is entering this vertex and another one is leaving it. For instance, vertex 2 in G is represented in the directed dual graph G* through the edges from a to c and from a to d, because these edges meet head to tail at vertex 2 in G.

In graph theory, the different types of graph duality have been a topic of discussion for many years (*e.g.*, [85]). In contrast, the literature on dual dynamic models is scattered, with rather different concepts using the term "dual" (*e.g.*, [160-162]). Closest in spirit to the situation of T&A models is an article on flux duality [163], where the exchange of variables and fluxes in certain types of primal and dual differential equation models was investigated.

A typical anchor model has the underlying graph structure of a common metabolic or physiological model. In particular, the variables (vertices) are metabolites and the fluxes (directed edges) among them represent (regulated) biochemical reactions, transport steps, or the formation or disassociation of complexes; a typical example is the system of

cholesterol biosynthesis model in Figure 2.1. This type of diagram represents the biosynthesis anchor well and, as a natural consequence of the model design, there is perfect flux balance at steady state: the fluxes into any of the variables collectively equal the fluxes leaving this variable in magnitude.

Surprisingly, these fundamental features are not the same in a template model. The variables (vertices) in a template model are usually physiological or bio-chemical processes, or conglomerations of such processes. In the case of the cholesterol template, for example, the variables are cholesterol biosynthesis through the mevalonate pathway, cholesterol storage, the dynamics of (cholesterol-containing) plasma lipids, and so on (Figure 2.1), which are all processes altering the concentration of free or bound cholesterol. Concomitantly, the directed edges in the template model do not represent material fluxes. Rather, they indicate modifying effects that may increase or decrease the activity of another template variable. These effects either consist of handing molecules like cholesterol from one subsystem to another or they represent direct or indirect modulations. Importantly, there is no material flow between template variables in a strict sense, because “Biosynthesis” does not become “Plasma Dynamics,” in analogy to, for instance, “Lanosterol” becoming “Cholesterol” in the anchor model. Instead, the variable “Diet” increases the amounts of cholesterol in the variables “Plasma Dynamics” and “Storage,” and the variable “Biosynthesis” indirectly affects an increase in the input to the template variable “Steroid Hormone Production.” Furthermore, material may be generated or disappear within boxes. For instance, in the template box “Biosynthesis,” cholesterol is seemingly created out of nothing. Analogously, cholesterol disappears

within the box “Steroid Hormone Production,” because it is converted into testosterone, estradiol, and other steroids.

Thus, a more accurate, although slightly awkward depiction of the cholesterol template is shown in Figure 5.3; it is instructive to compare this figure with Figure 5.1. It is of note that the template representation actually runs counter to the standards of typical biological diagrams [10]. As an example, consider the signal emitted by a box like “Peripheral Tissue Utilization” on “Storage” within this diagram: It signifies that increased use of cholesterol in the peripheral tissues indirectly triggers a release of cholesterol from storage in the liver.

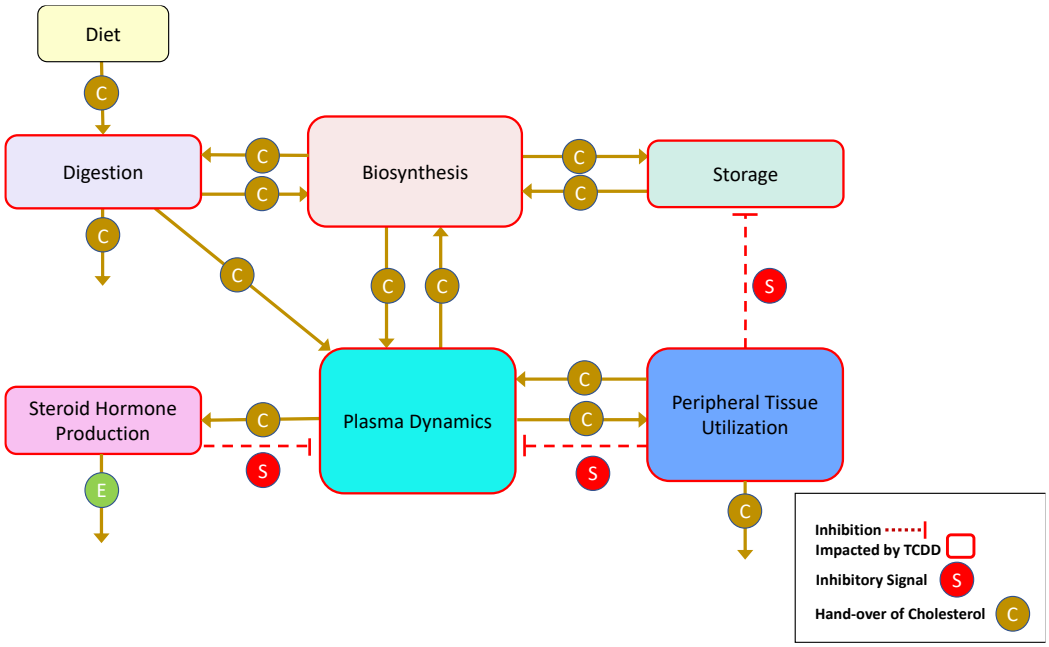

Figure 5.3: Cholesterol template model as a dual graph. In this novel and unusual representation, the variables are in truth processes and the edges either represent the moving of cholesterol C among processes or indicate (possibly indirect) inhibitory signals S Note that the arrows defy the standards of typical proper model diagrams [10].

The stark difference in model structures has implications for the stacking of sub-models for different biological levels during the zooming between templates and anchors. Specifically, it is possible that "anchors" associated with a template model in fact have the structure of lower-level templates. As an example different from cholesterol handling, suppose a high-level template represents some aspect of cellular physiology. The anchors then could represent mitochondrial energy dynamics, protein synthesis, generation of reactive oxygen species, and features like cell contraction. These anchors clearly have the structure of template models, as they represent systems of processes, rather than processes whose variables are biological entities like metabolites. Thus, in typical T&A models, the variables of a template models might be true anchor models, which are usually not further reducible to sub-models, or they are themselves lower-level template models with variables that may either be further templates or true anchors. For some psychological reasons, we tend to think downward from a template to anchors. Here, it might be more convenient to start with pure anchors at the lowest level of interest, which become the variables of templates at a higher level, which in turn are integrated in template models at even higher levels until one reaches an overarching umbrella template at the desired level.

As another example, consider again a typical physiologically based pharmacokinetic (PBPK) model (Figure 1.1). At first glance, the variables appear to be organs, but a slightly misleading moniker like "Liver" in truth means the concentration of a drug being processed by this organ at some point in time. The value of this variable is not only driven by the influx of the drug from the arterial blood and its efflux into the venous blood but also by the enzymatic, transport, and storage activities that alter (*e.g.*,

bind, degrade or excrete) some of this drug within the organ. Without accounting for this enzymatic activity or excretion, there is no valid flux balance at a steady state. This situation is reconciled if one recognizes that the variable "Liver" represents a system of processes in which the overall influx is converted into the overall efflux. In other words, this situation of a PBPK model is typical for a template model, whose anchor "Liver" is a lower-level template that contains as anchors subsystems of biosynthesis, metabolism, degradation, excretion, or storage. At the same time, each apparent flux in the PBPK model in truth represents the concentration of the drug being transported from one organ to another. As yet a different example, we recently proposed a template model for cystic fibrosis, where the variables at first glance appear to be organs (*e.g.*, intestine), but in reality consist of processes, such as digestion [164].

Taken together, anchors have the structure of typical biomathematical models. Their constituents are pools or vertices (*e.g.*, organic compounds) and arrows or edges (*e.g.*, enzymatic reactions, transport processes). By contrast, typical template models have the structure of dual systems: The vertices are processes, and the edges are entities like chemical compounds or signals. In the relationship between templates and anchors, the template variables become anchor models. These anchors may be true anchors or new, lower-level template models. A true anchor, like "Biosynthesis" in Figure 2.1, contains variables that are molecules (*e.g.*, lanosterol), which are handed off from one vertex to the next. Its processes are fluxes in the truest sense, as lanosterol is converted into—and thus becomes—cholesterol. However, if an anchor is a new template at a lower level, its variables are again processes or systems of processes. The edges of a template model, whether at the highest or a lower level, consist of signals or of entities (molecules)

that are handed from one anchor to the next. Thus, the multiscale organization effort is complete once all template variables are true anchors with variables that are entities rather than processes.

There are bound to be exceptions to this sweeping generalization of the T&A structure, but the feature of duality in typical T&A models highlights the fundamental difference between templates and anchors. It is unclear whether the recognition of this duality has practical ramifications beyond academic insights, but it does demonstrate that the two model types in T&A structures contain intrinsic differences. These differences offer guideposts for an effective hierarchical model design that spans different levels.

5.1.2 Model formulation of the template model

The pathway system in Figure 5.3 is slightly simplified toward the diagram in Figure 5.4 and mathematically represented with nonlinear ordinary differential equations (ODEs). It would be difficult to devise true mechanistic formulations of the edges connecting the variables, but it is comparatively straightforward to use generic approximations and, in particular, the format of a Generalized Mass Action (GMA) system from Biochemical Systems Theory (BST)) [68-70] and one of its special cases, Mass-Action Kinetics. Because the variables in the template model are processes, their steady-state values correspond to the steady-state fluxes of the anchor models; they may be directly affected by other template variables. The edges and their mathematical representations capture how the change in one template box (process system) affects a neighboring box. As the boxes are now directly affected by signals, these signals are represented slightly differently than in typical anchor-like models. The resulting GMA equations are

presented below. As is typical, they contain two types of parameters: (1) non-negative rate constants (v_i) of production and degradation, and (2) kinetic orders (a_j), whose signs directly align with the modeled function: activating or augmenting processes are modeled with positive kinetic orders, while inhibitory or diminishing processes are modeled with negative kinetic orders.

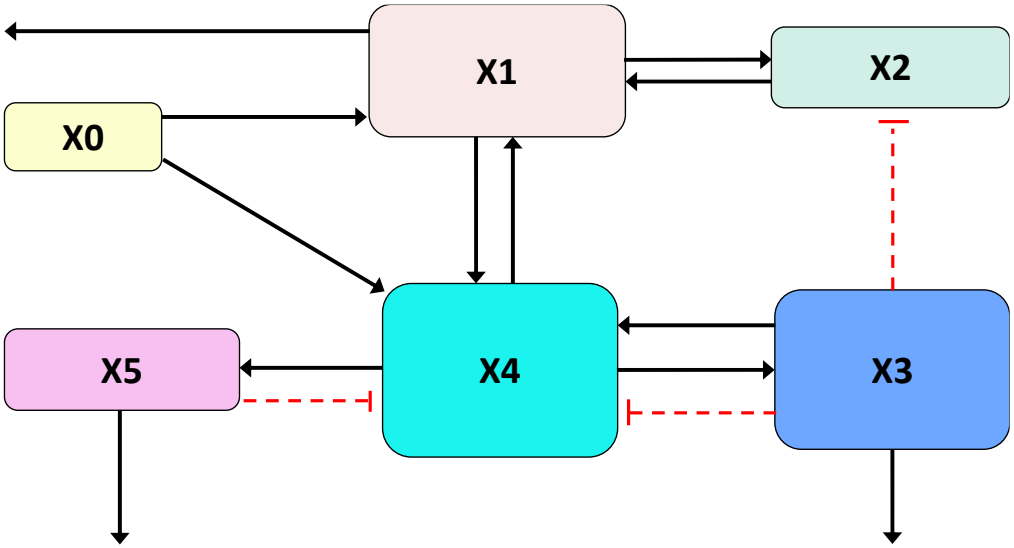

Figure 5.4: Simplified template model corresponding to variable names in the ODEs.

The GMA representation of the template model in Figure 5.4 thus has the following format:

Biosynthesis

$$\mathrm{X1}' = v_{01} \cdot \mathrm{X0}^{a1} + v_{21} \cdot \mathrm{X2} \cdot \mathrm{X3}^{a3} * DR_1 + v_{41} \cdot \mathrm{X4} \cdot \mathrm{X5}^{a2} \cdot \mathrm{X3}^{a4} * DR_2$$
$$-v_{14} \cdot \mathrm{X1} * DR_3 - v_{12} \cdot \mathrm{X1} * DR_4 - v_{1E} \cdot \mathrm{X1} * DR_5$$

Storage

$$\mathrm{X2}' = v_{12} \cdot \mathrm{X1} * DR_4 - v_{21} \cdot \mathrm{X2} \cdot \mathrm{X3}^{a3} * DR_1$$

Peripheral Tissue Utilization

$$\mathrm{X3}' = v_{43} \cdot \mathrm{X4} * DR_6 - v_{34} \cdot \mathrm{X3} * DR_7 - v_{30} \cdot \mathrm{X3}$$

Plasma Dynamics

$$\mathrm{X4}' = v_{34} \cdot \mathrm{X3} * DR_7 - v_{43} \cdot \mathrm{X4} * DR_8 - v_{41} \cdot \mathrm{X4} \cdot \mathrm{X5}^{a2} \cdot \mathrm{X3}^{a3} * DR_9 + \mathrm{X0}^{a4}$$
$$+v_{14} \cdot \mathrm{X1} * DR_3 - v_{45} \cdot \mathrm{X4} * DR_{10}$$

Steroid Hormone Production

$$\mathrm{X5}' = v_{45} \cdot \mathrm{X4} * DR_{10} - v_{40} \cdot \mathrm{X5}$$

Here, the quantities DR_i represent the effects of dioxin on a given flux. At the baseline, they all have a value of 1. For different dioxin exposure scenarios, the DR_i are numerically adjusted according to dose-response curves developed in the anchor models.

5.1.3 Global effects of TCDD on cholesterol dynamics

As documented in the CTD database and compiled in Table 5.1, the expression of numerous genes is affected by dioxin; shown here are only genes directly associated with dioxin and the organ systems in the anchors.

To set up a representative template model, the amount of cholesterol produced under continuous exposure to a TCDD dose of interest is extracted from the dose-response relationships obtained from the anchor models that had been produced previously (Chapters 2-4) and are now handed off to other variables of the template model. In other words, dose-response relationships are used as TCDD-dependent modulators of the healthy baseline fluxes (TCDD = 0; all $DR_i = 1$) between the various template variables, such as the flux of mevalonate into the biosynthesis pathway and hepatic cholesterol export into the bloodstream (see Figure 2.1).

Once implemented as an independent variable, the dioxin dose can be increased incrementally across all known affected processes, where different degrees of dioxin effect can be represented with varying fold changes ($DR_i > 1$ or $DR_i < 1$) and signs reflecting augmenting or diminishing effects. The template model thus allows us to gain a comprehensive understanding of dioxin's systemic impact on affected processes at a global level.

5.1.4 Parameter determination and model evaluation

To parameterize the template model, the input/output relationships obtained from the previously established anchor models (Chapters 2-4) were used to inform steady-state values of the template variables and the connections between them. Kinetic order parameters which, for instance, describe the influence of estradiol signaling and

peripheral tissue utilization on cholesterol uptake in hepatocytes, as well as hepatic cholesterol storage, were adjusted to render outputs consistent with published steady state concentration data.

The original anchor model of steroid hormone production represented the dynamics of estradiol production and utilization throughout the menstrual cycle, as detailed in Chapter 4. For the purposes of the overall template, we simplify this anchor here, thereby demonstrating how different anchor models of a subsystem may be swapped without affecting other anchors. Specifically, we assume for purposes of the template model analysis, an average steady-state level of estradiol obtained +/- 3 days around the time of ovulation [165]. This average level represents a value consistent with concentrations commonly referenced in clinical practice.

Upon calibrating the model parameters to match the steady-state concentrations that have been reported for the anchor models (Chapters 2-4) the output of the template model at baseline (TCDD = 0) exhibits strong correspondence with the anchors, as documented in Table 5.2.

Table 5.1: Flux values simulated in the template model compared to the values obtained from the anchor models.

	Anchor Models Flux (μM/day)	Simulation Flux (μM/day)
Biosynthesis	32	31.95
Storage	0.56	0.57
Peripheral Tissue Utilization	266.03	265.68
Plasma Dynamics	3266.37	3266.96
Steroid Hormone Production	1.34	1.34

5.2 Simulation Results

5.2.1 Sensitivity analysis for the template model

Sensitivity analysis of parameters for hepatic cholesterol and plasma cholesterol, which was selected due to its high connectivity within the template model. The sensitivity analysis was performed by increasing and decreasing one parameter at a time by 10% from the default value and calculating the percentage change of LDL HDL, and total plasma cholesterol. The relative sensitivity coefficient was calculated by averaging the ratios of the percentage change of the cholesterol concentrations to 10% in both directions. In the model, the parameter that exerts the most influence includes the rate constant v_01 reflecting the influx of cholesterol to the liver. However, the analysis revealed that variations of ±10% in each of the 16 parameters yielded changes in the steady-state values of less than 10% in magnitude (absolute values of relative sensitivity <1; Figure 5.5). Therefore, all parameters were deemed to exhibit low sensitivity, thus indicating a robust system response to parameter fluctuations.

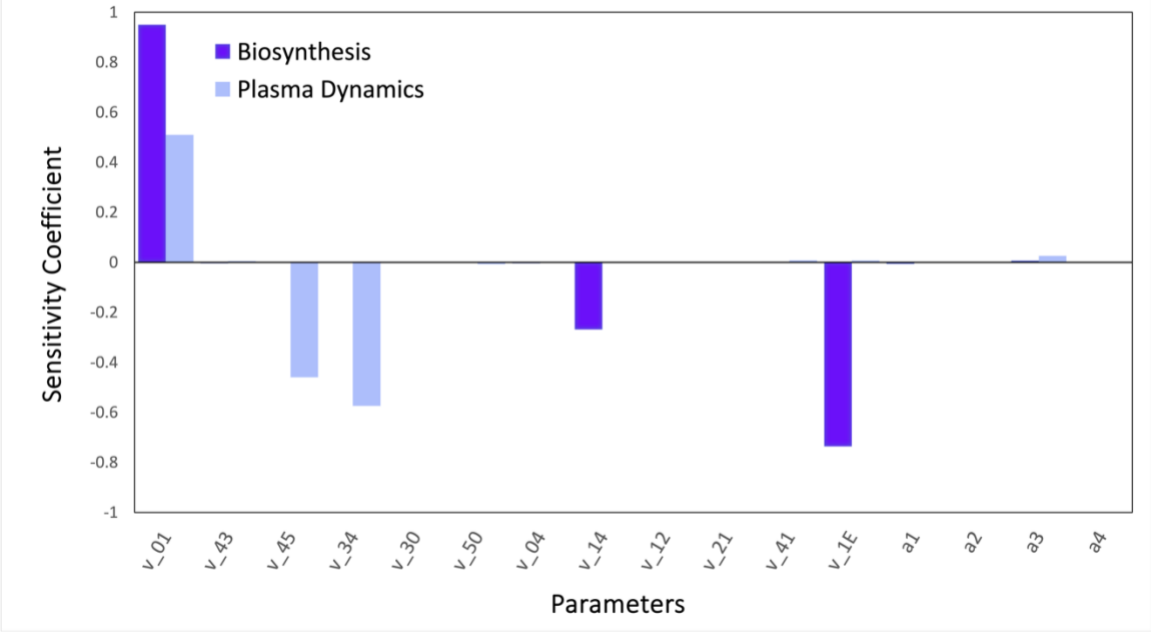

Figure 5.5: Sensitivity analysis fpr the template model. All parameters values exhibit changes in the steady-state values of less than 10% in magnitude (absolute values of relative sensitivity <1.

5.2.2 Overall Impact of dioxin on the template model

To quantify the impact of TCDD on cholesterol biosynthesis in the template model, we analyzed the effects of different doses of TCDD ranging from 0 to 50 μg/kg body weight. As reported in the cholesterol biosynthesis anchor model (Chapter 2, Figure2.4) the effect of TCDD on the rate of hepatic cholesterol biosynthesis, as reported previously [80], was implemented into the template model. Specifically, the rate constants of each edge known to be effected by dioxin were adjusted through the different DR_i according to the percent changes obtained from the previously reported anchor-based dose-response curves. The hepatic cholesterol biosynthesis rates resulting from these alterations were recorded and used to construct a template-based dose-response relationship (Figure 5.6), which is very similar to what was produced previously in Chapter 2 .

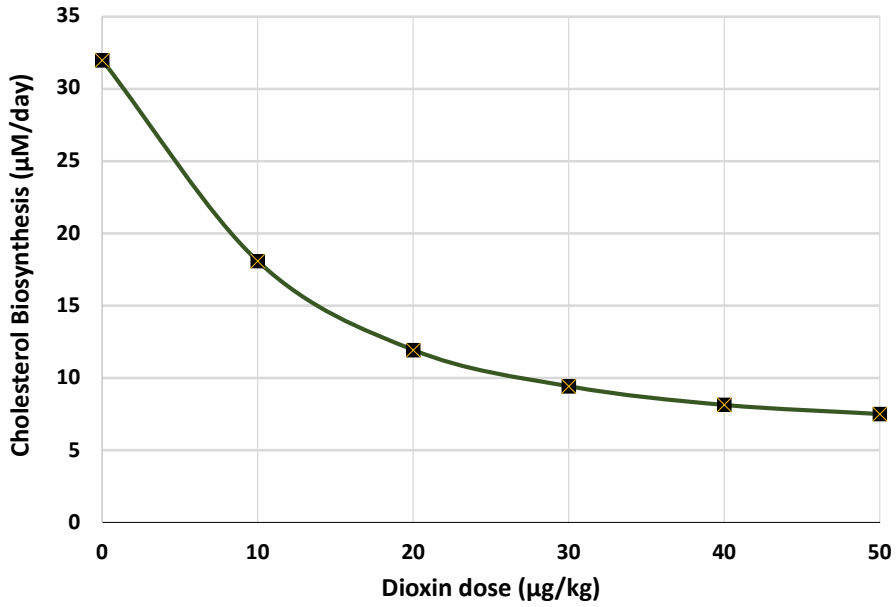

Figure 5.6: Dose response curve of dioxin vs cholesterol biosynthesis. The trend is ssimilar to what was previously reported in Figure 2.4.

By implementing the dose-response-curve of cholesterol biosynthesis rate *versus* dioxin in the template model, we were able to predict the overall effects of dioxin on the various processes comprising the template model (Table 5.3).

Table 5.2: Dose-response-curve of the processes *versus* dioxin dose. Grey highlighted sections represent simulated outcomes generated by applying the dose-response curve for cholesterol biosynthesis to the template model.

	Dioxin Dose					
	0 ug/kg	10 ug/kg	20 ug/kg	30 ug/kg	40 ug/kg	50 ug/kg
Biosynthesis	31.9	18.1	11.9	10.4	8.93	7.49
Storage	0.57	0.13	0.05	0.03	0.03	0.018
Peripheral Tissue Utilization	266	496	808	960	1186	1554
Plasma Dynamics	3267	3354	3481	3547	3648	3827
Steroid Hormone Production	1.34	0.76	0.5	0.44	0.37	0.31

The values for biosynthesis outlined in the table correspond to the dose-response curve information presented in Figure 5.6. The grey highlighted sections in Table 5.3

represent simulated outcomes generated by applying the dose-response curve for cholesterol biosynthesis to the template model. Thus, the table illustrates the global impact of dioxin on cholesterol biosynthesis and the resulting effects on hepatic cholesterol storage, peripheral tissue usage, plasma dynamics, and steroid hormone production.

With increasing doses of dioxin, the rate of cholesterol biosynthesis decreases, as was demonstrated previously in the literature (e.g., [81] and anchor simulations in Chapter 2. The observed decline can be explained by the suppressed expression of multiple genes involved in biosynthesis, including those encoding HMGCR, FDPS, SQS, and LSS.

Increasing doses of dioxin are predicted by the template to raise peripheral cholesterol utilization and plasma dynamics, while concurrently causing a reduction in hepatic storage and steroid hormone production. It is not known whether these predictions are correct.

The decrease in hepatic storage is attributed to the decreased expression of ACAT [166]. This observation is paralleled by a decrease in sex hormone production, which aligns with animal studies that indicate a reduction in estradiol production and with epidemiological studies that associate a decrease in estradiol levels with exposure to dioxin in humans [157]. Additionally, the model predicts an increase in the utilization of cholesterol in peripheral tissues, a change that is consistent with findings from studies indicating that exposure to dioxin promotes myocardial growth in female rodents [167]. This funding can also be related to human health, where such exposure has been linked to

the development of ischemic heart disease [168], a condition precipitated by the accumulation of cholesterol within the coronary artery lining [169].

5.2.3 Impact of diet in the template model

The template model allows us to assess the role of dietary cholesterol intake and its interaction with dioxin exposure on a broader scale. We begin with the effect of dioxin at the baseline of TCDD = 0.

As described previously (Chapter 2), the recommended range of dietary cholesterol intake is approximately 200mg/day [89]. The template model indicates that an increase in cholesterol intake results in a decrease of cholesterol synthesis in the liver. A possible explanation is that the increase in hepatic cholesterol, as a result of increased dietary cholesterol intake, promotes the reduction of cholesterol synthesis enzymes through the down-regulation of SREBP [170].

Our simulations with the template model demonstrate this relationship of increased cholesterol in diet and decreased biosynthesis rate, which is consistent with the results found in the cholesterol biosynthesis anchor model detailed in Chapter 2. Exact values can be seen in Table 5.4.

Table 5.3: The impact of diet on the various processes of the template model. The grey highlighted sections represent simulated outcomes generated by applying the dose-response curve for cholesterol biosynthesis to the template model.

Diet (mg)	Biosynthesis	Storage	Peripheral Tissue Utilization	Plasma Dynamics	Steroid Hormone Production
200	31.9	0.57	266	3267	1.34
400	26.8	0.47	223	2739	1.12
600	23.9	0.41	199	2442	1.00

Overall, our model indicates a wide-spread decrease across all outlined processes including storage, peripheral cholesterol utilization, plasma dynamics, and steroid hormone production. An explanation for this apparently counterintuitive decrease in flux rates is the availability of cholesterol from diet: The body does not need to produce as much cholesterol *de novo* if it receives it "for free" from diet. Additional considerations involve the correlation between elevated dietary cholesterol and diminished estradiol production [90]. There is also a documented link between heightened dietary cholesterol intake and the suppression of LDL receptor (LDLR) activity, which mediates the transport of cholesterol between the plasma and liver [171]. With the rise in cholesterol levels, a concurrent suppression in the transportation of LDL cholesterol to peripheral tissues has been found, likely due to increased levels of cholesterol in those tissues [112]. Moreover, it has been found that heightened dietary cholesterol intake is correlated with an elevation of cholesterol in peripheral tissues [172]. It is postulated that this elevation may serve as a feedback inhibitor to cholesterol storage, thereby mitigating any further accumulation of cholesterol within these peripheral tissues.

5.2.4 Overall Impact of dietary cholesterol and dioxin exposure

We used template simulations to explore the effects of combinations of dietary intake and TCDD exposure. Without TCDD exposure, the rate of hepatic cholesterol synthesis under a normal daily consumption of ~200 mg cholesterol is about 32 μM/day (Table 5.5). As expected, the synthesis of hepatic cholesterol levels decreases with both increased dietary intake and increasing doses of TCDD due to the accumulation of hepatic cholesterol (Figure 5.7). For the recommended cholesterol intake, the model predicts a decrease in the synthesis rate of cholesterol to about 7.5 μM/day, if an individual is exposed to a high

dose (~50 μg/kg) of TCDD. For the same dose of TCDD, but with 600 mg/day of dietary cholesterol intake, the model predicts a synthesis rate of approximately 5.47 μM/day as seen in Table 5.5.

Table 5.4: The impact of diet and dioxin on the processes comprising the template model. Grey highlighted sections represent simulated outcomes generated by applying the dose-response curve for cholesterol biosynthesis to the template model.

	Dioxin Dose					
	0 ug/kg	10 ug/kg	20 ug/kg	30 ug/kg	40 ug/kg	50 ug/kg
200 mg Cholesterol						
Biosynthesis	31.9	18.1	11.9	10.4	8.93	7.49
Storage	0.57	0.13	0.05	0.03	0.03	0.018
Peripheral Tissue Utilization	266	496	808	960	1186	1554
Plasma Dynamics	3267	3354	3481	3547	3648	3827
Steroid Hormone Production	1.34	0.76	0.5	0.44	0.37	0.31
400 mg Cholesterol						
Biosynthesis	26.8	14.8	9.71	8.45	7.21	5.99
Storage	0.47	0.10	0.04	0.03	0.02	0.01
Peripheral Tissue Utilization	223	407	660	782	961	1248
Plasma Dynamics	2739	2750	2841	2886	2955	3072
Steroid Hormone Production	1.12	0.62	0.41	0.36	0.30	0.25
600 mg Cholesterol						
Biosynthesis	23.9	11.1	8.85	7.71	6.58	5.47
Storage	0.41	0.06	0.04	0.03	0.02	0.01
Peripheral Tissue Utilization	198.6	460	605	718	883	1150
Plasma Dynamics	2442	2547	2603	2648	2716	2830
Steroid Hormone Production	1.01	0.47	0.37	0	0.28	0.23

As in an earlier table, the sections highlighted in grey within Table 5.3 present the simulation results generated by the simultaneous introduction of dioxin and increased dietary cholesterol intake. As a visualization, Figure 5.7 depicts a sample dose-response curve of the synergistic effects of dioxin and dietary cholesterol on cholesterol biosynthesis (first data row in Table 5.5).

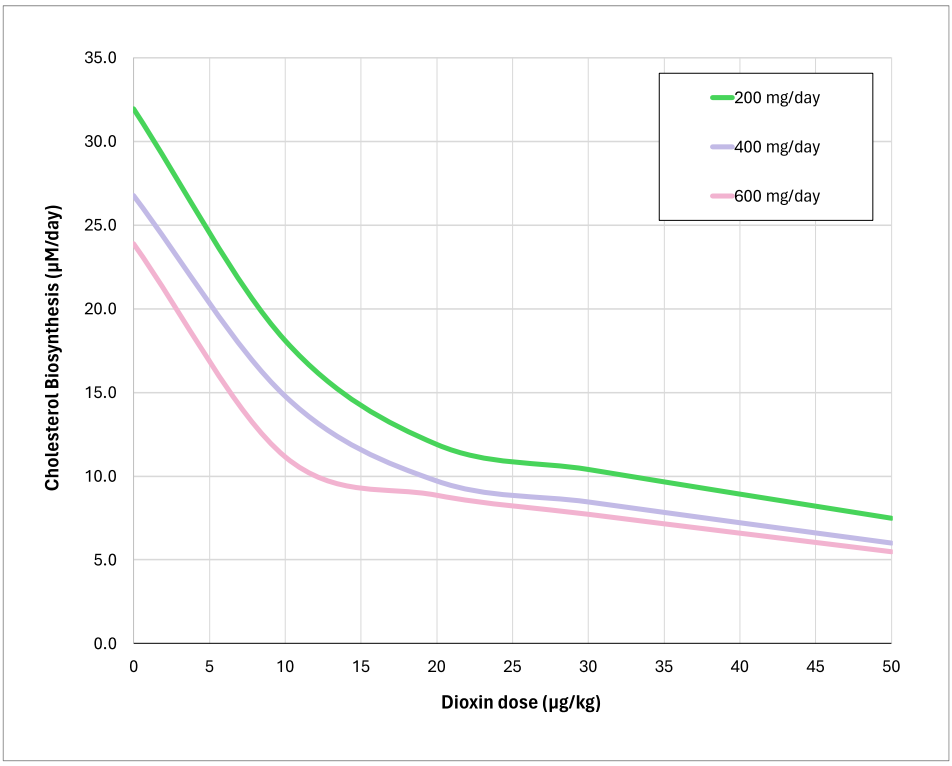

Figure 5.7 Dose response curve of the impact of diet and dioxin vs cholesterol biosynthesis

5.3 Discussion

5.3.1 Summary of findings

The template model within the template-and-anchor (T&A) framework serves as a macroscopic representation, offering a high-level overview of physiological processes impacted by external agents like dioxin. This overarching model captures the dynamics of various systems, such as cholesterol biosynthesis, lipoprotein transport, and steroid hormone production, which are all influenced by TCDD exposure. Within the template model, the variables, represent processes, while the edges indicate modifying effects among them. Each of these variables, in turn, is explored in detail through the more fine-grained anchor models. For instance, anchor models might cover specific aspects such as the synthesis of estradiol in the gonads or the dynamics of cholesterol-containing lipoproteins in plasma. The overall input/output relationships of the anchors are what informs the template model.

The dichotomy of anchors targeting concentrations as opposed to templates targeting processes is in some sense similar to the dichotomy between dynamic metabolic pathway models and approaches like flux-balance analysis[173] In contrast to FBA, a template model is still dynamic, and while FBA does not permit statements regarding metabolite concentrations, the variables of the template model, *e.g.*, altered by dioxin, can be returned to the anchor models as altered influxes and used to compute resulting steady-state concentrations.

The template model does well in encapsulating the comprehensive effects of dioxin as partially found in the literature. Specifically, the template demonstrates a dose-dependent reduction in cholesterol synthesis, concurrent with a reduction in estradiol

production, highlighting the systemic influence of dioxin exposure. At the same time, plasma transport and utilization in tissues are increased. As the combined biosynthesis-plasma anchor model showed, the result is an overall increase of cholesterol in the liver, leading, in extreme cases, to non-alcoholic fatty liver disease.

5.3.2 Advantages and drawbacks of T&A modeling

If sufficient data are available, the T&A approach offers substantial benefits without unduly losing resolution. First, the divide-and-conquer approach greatly increases computational efficiency, as the anchors are analyzed with methods devised for their specific levels; in other words, problems of data heterogeneity are substantially reduced. Second, since anchor models can be designed and analyzed in isolation, the T&A structure can be developed gradually by utilizing output information from increasingly more anchors, while ill-defined components of the template remain as simple variables. Thus, the approach offers flexible guidance for setting up a multiscale model and for the definition of variables and processes at the different stages of the modeling process. Third, in contrast to other multiscale approaches, there is no need to analyze anchors repeatedly together with other anchors and the template. Instead, each anchor is analyzed separately for all applicable scenarios and the main output consists of a functional record of all pertinent input-output relationships, which are later used to inform other anchors and to calibrate the template model. Fourth, the anchor models can be "hot-swapped" in a sense that they may be replaced, if deemed necessary, with more or less detailed models, while other anchors and the template remain intact. We indicated this by developing a detailed estradiol synthesis model, which we then simplified for the template analysis.

Given the novelty of the T&A modeling paradigm as it is proposed here, there is clear realization that this approach is still developing. More refinements will be necessary to fully harness its potential. Future directions may include enhancing the granularity of the anchor models to improve accuracy of input-output relationships used to inform the template model, incorporating more comprehensive data at the genetic level to better estimate the impact of dioxin on each process, and accounting for the heterogeneity found in different species or physiological conditions. Finally, as the template focuses on processes, results must be translated back to concentrations, which appears to necessitate a return to the anchor models.

Overall, the approach has other drawbacks and limitations, which are discussed in the future chapter.

CHAPTER 6 CONCLUSIONS AND FUTURE DIRECTIONS

6.1 Summary and Novelty of the Presented Research

The T&A modeling approach was originally proposed over two decades ago for the purpose of discerning sets of common design concepts from different implementations modeling [27]. The authors addressed with this approach the system of posture and movement, which must adhere to fundamental principles of biomechanics but at the same time permits drastically different modes of locomotion among terrestrial species, from ants to antelopes and cockroaches to crocodiles. The authors pursued this goal by creating a model on a conceptual low-dimensional manifold describing the key aspects of locomotion. This invariant manifold was conceived as being embedded within a much-higher-dimensional space describing the various observed modes of locomotion, and all species-specific implementations were seen as intersecting in the subspace of the common design [27, 28, 174].

Here, the T&A paradigm is used for a different purpose, namely for analyzing multiscale biomedical models in an effective manner. As demonstrated, the approach provides a systematic and intuitively organized strategy for multi-level analysis of complex biological systems. The template model serves as a high-level, coarse-grained representation that focuses on the main physiological components of a system and entails a minimal set of variables and parameters. It acts as an overarching representation of the entire system, providing an encompassing view of the dynamic interactions among its core constituents. By contrast, the anchor models provide a more detailed and finely grained view of specific biological details and mechanisms within the system. They allow the user to zoom into individual variables within the template, thereby permitting an

account of intricate aspects of the underlying processes. Furthermore, as discussed earlier, the approach is not restricted to two levels, but permits refinements in several steps. Together, the template and anchor models form a hierarchical structure, allowing for both broad overviews and in-depth analyses, thereby offering a versatile tool for multiscale modeling.

To demonstrate the practical application of the T&A model, we detail how dioxin exposure influences a range of processes integral to cholesterol dynamics across multiple organs. We have established three anchor models that are embedded in the template model. These include models for hepatic cholesterol biosynthesis, lipoprotein transport, and sex hormone synthesis. The models demonstrate at the organismal level the impact of dioxin on hepatic and plasma cholesterol (including LDL IDL VLDL and HDL cholesterol) and reveal how intestinal cholesterol increases while hepatic cholesterol storage decreases. They furthermore show how estradiol synthesis is reduced, thereby resulting in a lengthened menstrual cycle and a delay in ovulation.

The T&A modeling approach carries distinct advantages in handling multiscale problems. In particular, the method enhances computational efficiency through a divide-and-conquer strategy and provides a flexible structure for model setup and the definition of variables across different levels. In contrast to other multiscale approaches, each anchor is separately analyzed, yielding a comprehensive record of essential input-output relationships that inform other anchors and calibrate the template model, while allowing for the interchangeability of anchor models without affecting the overall template structure.

Of course, the T&A approach is no panacea, and our exposure-response model is obviously simplified, like any other model. For instance, we performed our analysis at the steady state of the pathway system, which may seem restrictive. However, it is expected that the dose-response curve we determined with each anchor model is similarly applicable to non-steady-state situations and that pathways within the human body operate close to the homeostatic steady state. Despite these possible limitations, the proposed approach appears to be sufficient for revealing the essence of a complex phenomenon, as in our example the impact of dioxin on cholesterol handling.

A different caveat is that even the best model is only as good as the supporting data, and the data need for a complete T&A analysis may greatly exceed reality. In our example, the amount of human data is scarce and our supplanting them with mouse data raises clear uncertainties. At a theoretical level, the duality between templates and anchors will require a deeper investigation and an exploration of its speculated generality.

Overall, multiscale models are clearly important, and the T&A approach is intended to provide a novel, effective tool for complex modeling tasks as it provides a comprehensive and holistic perspective that accommodates a range of organizational scales.

It is quite evident that an approach like T&A can readily be tailored toward many different research goals and applications, which could, for instance, support traditionally difficult extrapolations of *in vitro* to *in vivo* results [175] and the important translation of observations between different species [176]. For our example of TCDD exposure, this translation poses an interesting challenge, as some enzyme activities and the crucial TCDD-AhR mechanism are species-specific [65, 177]. More generically, the T&A

approach has the potential of serving as an effective tool for advancing computer-supported personalized medicine[178, 179] and in virtual clinical trials [180, 181].

6.2 Future Directions

6.2.1 Quantitative implementation of global dioxin-induced dysregulation

Dioxin notably impacts the expression of a wide range of genes involved across a spectrum of biological processes including cholesterol biosynthesis, lipoprotein transport, and steroid hormone production. In our T&A analysis, we adopted, by necessity, only a semi-quantitative approach to model the influence of dioxin on gene expression. The main reason was that the database CTD informs our model simply by indicating the directionality of gene expression changes in response to dioxin exposure, which we incorporate as estimated percentage adjustments to pertinent processes. A more precise understanding, including fold changes in gene expression in relation to dioxin dose-response curves, would presumably enhance our model's accuracy, possibly substantially. Although such data exist for certain genes within our scope, the information remains limited. Moreover, our current models are still simplified representations. In the future, with increasingly comprehensive availability of quantitative data, we envision fine-tuning the anchor models in our analysis to include more granular processes at the genetic and physiological levels, thereby enhancing the model's detail and predictive power.

6.2.2 Accounting for heterogeneity

6.2.2.1 Species differences in cholesterol biosynthesis

The pathways of cholesterol biosynthesis are known to exhibit significant variations among mammalian species. These manifest as alterations in parameter values within our generic model and appear to be specific to each species and possibly cell type. A particularly striking example that is pertinent to this work is the in vivo retention time of dioxin, which varies significantly between mice and humans [182].

Additionally, experimental findings indicate that dioxin exposure results in an increase in hepatic cholesterol and a concurrent decrease in plasma cholesterol in mice [40]. This pattern is not observed in humans, where epidemiological data suggest an increase in both hepatic and plasma cholesterol levels [42-46].

In constructing the Template and Anchor (T&A) model, we primarily relied on human data, integrating disruptions in gene expression from CTD when human-specific information was available. In the absence of such data, we had to resort to evidence derived from mouse studies. Given the differences in dioxin response between species, and the ethical impossibility of obtaining dose-response data from human subjects, it will be beneficial to develop a parallel whole-mouse model. Such a model would enable us to perform cross-species comparisons and enhance our mechanistic understanding of cholesterol dynamics and the effects of dioxin.

6.2.2.2 Account of hepatic zonation

The liver is divided into four lobes, namely the right, left, caudate, and quadrate lobe. Each lobe is divided into thousands of liver lobules that are composed of hepatocytes and other cells. Lobules are divided into three zones: periportal (zone 1), midzonal (zone 2), and centrilobular (zone 3). Each zone differs in hepatocellular enzymatic function and blood oxygenation. Importantly, key hepatic genes, many of them pertinent to this study, have been shown to be differentially expressed along the lobule axis. This is termed zonation.

For reasons of simplicity, the model design for the cholesterol biosynthesis anchor model (Chapter 2) ignores spatial heterogeneity and instead averages cholesterol biosynthesis via the mevalonate pathway over all hepatocytes. In addition to permit a simpler model, this averaging allows us to obtain corresponding parameter values from literature information. It is presently unknown whether future studies should indeed consider the well-known microanatomical zonation of liver lobules, thereby acknowledging the fact that gene expression and metabolic activity vary among the distinct layers of hepatocytes close to, and further away, from the central vein [183]. With respect to the overall effect of TCDD on cholesterol dynamics, which is of particular importance here, it is at present unclear whether the granularity of zonation is significant or whether averaging is sufficient, especially given the semi-qualitative nature of our study. Explicitly addressing the zonation of liver lobules could affect the input-output relationships of the different anchor models and their interactions, although the degree of effect is unclear. A gradually refined anchor model, to be embedded in the

overall template model of the effect of TCDD on cholesterol dynamics, could be set up in the future to answer this question when pertinent data become available.

One viable strategy for modeling liver zonation could be based on individually simulating each zone to reflect their unique volumes, specific kinetic parameters, and distinct transport mechanisms. Subsequently, a comprehensive macroscopic model could be developed to integrate all zones using weighted averages. Alternatively, one might consider modeling the dynamics of cholesterol flow through the various hepatic zones using partial differential equations. While this approach might be a natural default, it would seem to encounter substantial theoretical and practical challenges due to the heterogeneity of liver lobules. Instead, it appears to be more practical and effective to develop an agent-based model [14, 184], wherein hepatocytes would serve as agents, with differentiating properties according to their hepatic zones and appropriate definitions of interactions.

6.2.3 Expansion of the T&A model

6.2.3.1 Addition of anchor models

Dioxin exposure has been shown to dysregulate bile acid synthesis, a process integral to the digestion and elimination of cholesterol. Furthermore, bile acids, synthesized from cholesterol in the liver, promote the absorption of dietary lipids and provide an excretion mechanism for excess hepatic cholesterol [185]. Dioxin exposure has been shown to result in hepatic bile acid accumulation due to the increase of intestinal reabsorption to hepatocytes and decreased fecal excretion of bile acids, thus contributing to AhR-

mediated hepatotoxicity[65]. While our current T&A model accounts for the ingestion of dietary cholesterol and the elimination of hepatic cholesterol, its structure may be too coarse. As a remedy, expansions of the T&A model, for instance, with an added anchor that thoroughly tracks dietary cholesterol intake, absorption, and bile-mediated excretion, could provide deeper insights and enhance the model's predictability regarding dioxin-mediated effects on cholesterol dynamics.

6.2.3.2 Synergistic Impacts: Assessing the cumulative effects of multiple toxins within the T&A model

Humans are more often than not exposed to multiple environmental toxins simultaneously, which can have combined effects that differ from those of individual exposures. To reflect this complexity, we could expand the T&A model to encompass not only the impact of dioxin but also the synergistic effects of various other toxins on cholesterol dynamics. The CTD database [62] offers some insights into such interactions, including, for example, the downregulation of HMGCR when TCDD is co-treated with diethylhexyl phthalate. While the account for synergism appears to be intriguing, the practical feasibility and granularity of future models will largely hinge on the availability and richness of data on multi-toxin exposures.

6.2.4 T&A for personalized medicine and drug discovery

Looking ahead, the T&A framework holds potential for advancing personalized risk assessments and personalized medicine in general. By the same token, it could become relevant and effective for enhancing drug discovery and development. The current version of the model is mostly calibrated with average data, but also considers population variability, for instance, in menstrual cycle length, when modeling the dioxin-mediated

effects on estradiol (Chapter 4). For uses in personalized medicine, the model design would have to be readily customizable, allowing for the easy adjustment of relevant parameters based on personalized data [186, 187].

The proposed T&A strategy indicates how to study the impact of simultaneous external inputs such as dietary cholesterol and environmental toxins, notably dioxin. Obviously, the approach itself is independent of this application and it is quite evident that the T&A platform is versatile and can be expanded further to simulate the body's response to a wide array of pharmaceutical compounds, thereby potentially serving as a predictive tool for drug behavior and interactions within the body [188].

Furthermore, T&A presents an innovative potential approach in the context of virtual clinical trials. By simulating patient populations and drug responses, these models in the future will enable the prediction of drug dose-response outcomes, optimize dosing regimens, and identify the most promising therapeutic candidates. This application, as part of NAMs, not only streamlines the drug development process but also offers a more ethical approach by reducing the need for extensive animal testing. Through these diverse applications, T&A models offer a path toward more personalized, effective, and ethically responsible approaches to biomedical, public health and pharmaceutical research.

6.3 Closing Remarks

In this study, we address the well-known challenge of biomedical multiscale analysis with a novel, fundamentally different adaptation of the Template-and-Anchor (T&A) modeling paradigm. It considers a template as a high-level, coarse-grained model that focuses exclusively on the main physiological components of a system and involves correspondingly few variables, processes and parameters. The template contains as variables the anchor models, which are modules of component sub-systems that provide more elaborate descriptions of specific biological details. This conceptual framework

does not attempt to capture simultaneously all details within a single computable structure as many other multiscale models do. Instead, the often-overwhelming multilevel task is dissected into smaller, stand-alone models that are analyzed separately. This new adaptation of the T&A approach offers substantial advantages without losing resolution. First, the divide-and-conquer method enhances computational efficiency. Second, unlike other methods, each anchor is analyzed individually, producing a record of crucial input-output relationships that are ultimately used in the template model. Third, anchor models can be replaced with alternative representations without affecting the structure of the template or other anchors. Fourth, the T&A model provides flexible guidelines for its setup and for defining variables across scales.

Using the T&A approach, this work addresses the molecular basis for health implications caused by exposure to dioxin (specifically, 2,3,7,8-tetrachlorodibenzo-p-dioxin), a persistent organic pollutant that can severely affect health, depending on the magnitude of exposure. The template captures the overall effects of dioxin on the dynamics of cholesterol, a prominent target of dioxin. The anchor models serving as variables in the overall template model include hepatic cholesterol biosynthesis (via the mevalonate pathway), lipoprotein metabolism, and estrogen synthesis. The creation and combination of anchor and template models enables a holistic evaluation of the impact of dioxin, which can be translated into a tool for comprehensive computational health risk assessments.

On the theoretical side, this work discerns fundamental differences in the conceptual set-up of templates and anchors which may be viewed as dual structures of each other, as the variables in anchor models are material quantities, whereas the variables in template models are processes.

T&A modeling, and multiscale modeling in general, hold promise for a deeper understanding of complex systems and for advancing personalized medicine and risk assessment, interspecies translation, and the development of virtual clinical trials.

APPENDICES

A.1. T&A Model Design

The primary focus of the paper is the introduction of the T&A concept as a "new-approach methodology" (NAM). The actual implementation of this concept mandates the choice of a mathematical representation, which we selected from Mass-Action Kinetics and Biochemical Systems Theory [10, 69, 70, 189] because their tenets constitute a very effective and essentially unbiased compromise between biomedical realism and mathematical tractability. BST, along with MAK, which is a special case, always represents systems as sets of nonlinear ordinary differential equations (ODEs), in which each process v_i is formulated as a product of power-law functions that contain all variables X_j contributing to this term, each raised to a power f_{ikj}, called a *kinetic order*. In addition, a positive rate constant γ_{ik} determines the turnover rate of the process. Thus, each process representation has the format.

$$v_i = \gamma_{ik} \cdot X_1^{f_{ik1}} \cdot X_2^{f_{ik2}} \cdot \ldots \cdot X_n^{f_{ikn}}.$$

If a kinetic order is positive, it signifies a positive effect on the process, while a negative value signifies an inhibitory or diminishing effect. Typical kinetic orders vary between -1 and +2, while the rate constants may take any non-negative values. A rich literature has documented the theoretical underpinnings of BST as well as numerous applications. For a comprehensive review, see (Voit, 2013).

Applying the BST representation to the mevalonate pathway, we obtain the following set of differential equations; the complete code is available in Matlab and PLAS implementation at GitHub.com/LBSA-VoitLab/TCDD_Chol.

A.2. Dioxin Simulation

The effect of TCDD is coded either as positive or negative:

```
DEP = 1          // positive effect of TCDD if DEP > 1
DEN = 1          // negative effect of TCDD if DEN < 1
```

Specifically, DEP codes for a positive dioxin effect on some process and is implemented by an incremental increase in value, *i.e.*, 1.1, 1.2, 1.3… DEN codes for a negative dioxin effect on some process and is implemented by an incremental decrease in value, *i.e.*, 0.9, 0.8, 0.7… DEP and DEN are altered simultaneously. They affect the following rate constants:

```
r1 = 0.0012 * DEN
r7 = 0.0012 * DEN
r3 = 0.0012 * DEN
r5 = 0.0012 * DEN
r28 = 36.697 * DEN
r27 = 0.000356 * DEP
r30 = 0.7 * DEP
```

The specific values for DEP and DEN were taken from Figure S1, in which the trend line was deduced from (Lakshman *et al.* 1988, 1989). In these articles, the authors introduced various doses of dioxin in mice and determined the consequent synthetic rate of cholesterol in the liver.

Similarly, we matched our simulation results to the cholesterol synthesis rate found in the literature in order to determine dioxin dosage and the resulting concentration

of hepatic cholesterol (Figure 2.4 of the text). The synthetic rate was calculated as percent of control. For instance, given that our control is 11,200 μM hepatic cholesterol, 80% of our control corresponds to 8,960 μM hepatic cholesterol.

A.3. Simulations of dioxin exposure and cholesterol intake from diet

The default dietary intake of cholesterol is set at the recommended value of 200 mg/day, which corresponds to 517.26 μmol/day. High cholesterol diet is coded as 400 mg/day or 1030 μmol/day, while extremely high cholesterol diet is modeled as 600 mg/day = 1552 μmol/day.

To account for diet and dioxin exposure simultaneously, one changes both the parameter value accounting for dietary change ***Diet*** and the parameter values for the dioxin effects **DEN** and **DEP**.

Dietary parameters are set in the computer code as:

- Normal cholesterol diet: *200mg or 0.2g / day ~ 517.26*, which is implemented as *dD= (517.26/SF)/ VL*
- High cholesterol diet: *0.4g/day ~ 1030*
- Extremely high cholesterol diet: *0.6g/day ~ 1552*

A.4. Cholesterol Biosynthesis Anchor Model Equations

HMGCR mRNA

$$\dot{HMr} = r_1 * SRp^{a01} - r_2 * HMr$$

FDPS mRNA

$$\dot{FDPSr} = r_3 * SRp^{a02} - r_4 * FDPSr$$

Lanosterol synthase mRNA

$$\dot{LSr} = r_5 * SRp^{a03} - r_6 * LSr$$

Squalene Synthase mRNA

$$\dot{SQSr} = r_7 * SRp^{a04} - r_8 * SQSr$$

SREBP

$$\dot{SRp} = r_9 * C^{a6} - r_{10} * SRp$$

HMG-CoA Reductase

$$\dot{HRp} = r_{11} * HMr^{a05} - r_{12} * HRp * GPP^{a1} * FPP^{a2} * L^{a3} * C^{a4}$$

Farnesyl diphosphate synthase

$$\dot{FDPSp} = r_{13} * FDPSr^{a06} - r_{14} * FDPSp$$

Lanosterol Synthase

$$\dot{LSp} = r_{15} * LSr^{a07} - r_{16} * LSp$$

Squalene Synthase

$$\dot{SQSp} = r_{17} * SQSr^{a08} - r_{18} * SQSp * C^{a09}$$

HMG-CoA

$$\dot{HC} = (r_{19} - r_{20} * HC * HR^{a5} * FDPS^{a8}) * \text{SF}$$

Geranyl-PP

$$\dot{GPP} = (r_{20} * HC - HR^{a5} * FDPS^{a8} - r_{21} * \text{GPP} * FDPS^{a9} - r_{32} * GPP) * SF$$

Farnesyl-PP

$$\dot{FPP} = (r_{21} * \text{GPP} * FDPS^{a9} - r_{22} * \text{FPP} - r_{23} * \text{FPP} * SQS^{a7}) * \text{SF}$$

Squalene

$$\dot{SQ} = (r_{23} * FPP * SQS^{a7} - r_{24} * \mathrm{SQ} * LS^{a10}) * \mathrm{SF}$$

Lanosterol

$$\dot{L} = (r_{24} * \mathrm{SQ} * LS^{a10} - r_{25} * L) * \mathrm{SF}$$

Hepatic cholesterol

$$\dot{C} = (r_{25} * \mathrm{L} + r_{26} - r_{27} * \mathrm{C} - r_{28} * C^{a11} + r_{29} * CP + r_{33} * S - r_{34} * C) * SF$$

Plasma cholesterol

$$\dot{Cp} = r_{28} * C^{a11} - r_{29} * CP - r_{30} * CP + r_{31}$$

Cholesterol storage

$$\dot{S} = r_{34} * C - r_{33} * S$$

A.5. Summary of the Parameters Used in the Cholesterol Biosynthesis Anchor Model

Parameter	Value	Description
r1	0.0012	Influx HMGCR mRNA
r2	0.0012	Efflux HMGCR mRNA
r3	0.0012	Influx FDPS mRNA
r4	0.0012	Efflux FDPS mRNA
r5	0.0012	Influx Lanosterol synthase mRNA
r6	0.0012	Efflux Lanosterol synthase mRNA
r7	0.0012	influx Squalene Synthase mRNA
r8	0.0012	Efflux Squalene Synthase mRNA
r9	1150	Influx SREBP
r10	0.0023	Efflux SREBP
r11	0.0023	Influx HMG CoA Reductase
r12	1.90E-07	Efflux HMG CoA Reductase
r13	0.0017	Influx Farnesyl diphosphate synthase
r14	0.0023	Efflux Farnesyl diphosphate synthase
r15	0.0023	Influx Lanosterol Synthase
r16	0.0023	Efflux Lanosterol Synthase
r17	0.0023	Influx Squalene Synthase
r18	4.70E-07	Efflux Squalene Synthase
r19	18150	Influx HMGCoA
r20	39.192	Influx Geranyl-PP
r21	35.216	Influx Farnesyl- PP
r22	255.6	Efflux Farnesyl- PP
r23	0.09656	Influx Squalene
r24	0.06215	Influx lanesterol
r25	0.4005	Influx cholesterol
r26	6.16	Influx Diet
r27	0.000356	Efflux Bile
r28	37.76	Efflux cholesterol into the plasma
r29	0.7	Influx plasma cholesterol to hepatic cholesterol pool
r30	0.006	Efflux plasma cholesterol
r31	0.6	Influx to plasma cholesterol pool
r32	0.000009	Efflux Geranyl-PP
r33	0.00025	Efflux cholesterol storage
r34	0.000005	Influx cholesterol storage
a01	1	Kinetic order in HMr synthesis
a02	1	Kinetic order in FDPSr synthesis
a03	1	Kinetic order in LSr synthesis
a04	1	Kinetic order in SQSr synthesis
a05	1	Kinetic order in HRp synthesis
a06	1	Kinetic order in FDPSp synthesis
a07	1	Kinetic order in LSp synthesis
a08	1	Kinetic order in SQSp synthesis
a09	1	Kinetic order in SQSp degradation
a1	0.5	Kinetic order in P_HR degradation
a2	0.5	Kinetic order in P_HR degradation
a3	0.5	Kinetic order in P_HR degradation
a4	0.5	Kinetic order in P_HR degradation
a5	0.5	Kinetic order in HC degradation
a6	-1	Kinetic order in SREBP influx
a7	0.5	Kinetic order in FPP degradation
a8	0.5	Kinetic order in HC degradation
a9	0.5	Kinetic order in GPP degradation
a10	0.5	Kinetic order in SQ dergradation

A.6. Lipoprotein Metabolism and Cholesterol Transport Anchor Model Equations

Mevalonate Pathway

$$\dot{x}_0 = v_0 * x_1^{k_0} * DR_{1-}v_{01} * x_0^{k_1}$$

Hepatic Cholesterol

$$\dot{x}_1 = Diet + v_{01} * x_0 - v_{14} * x_1 * DR_2 - v_{10} * x_1 * DR_3 - v_{12} * x_1 * DR_3 - v_{21} * x_2 * DR_4 - v_{31} * x_3 * DR_5 - v_{51} * x_5 * DR_6 - v_{61} * x_6 * DR_7 + v_{41} * x_4$$

VLDL

$$\dot{x}_2 = b_{12} * x_1 - b_{21} * x_2 - v_{23} * x_2 * DR_8 + v_{62} * x_6 * DR_7$$

IDL

$$\dot{x}_3 = v_{23} * x_2 - v_{31} * x_3 * DR_8 - v_{35} * IDL * DR_{11}$$

Cholesterol Storage

$$\dot{x}_4 = v_{14} * x_1 * DR_2 - v_{41} * x_4$$

LDL

$$\dot{x}_5 = v_{65} * x_6 * DR_9 - v_{51} * x_5 * DR_6 + v_{35} * x_3 * DR_{11} - v_{57} * x_5 * DR_{12}$$

HDL

$$\dot{x}_6 = v_{76} * x_7 * DR_{10} - v_{61} * x_6 - v_{65} * x_6 * DR_9 - v_{62} * x_6 * DR_7$$

Peripheral Tissue

$$\dot{x}_7 = v_{57} * x_5 * DR_{12} - v_{76} * x_7 * DR_{10} - v_{70} * x_7$$

A.7. Summary of the Parameters Used in the Lipoprotein Metabolism and Cholesterol Transport Anchor Model

Parameter	Values
v0	0.05
v01	0.001
v14	0.000047964
v10	0.0002221
v41	0.0001708282
v12	0.28066
v21	2.3077
v31	1.00
v51	0.2988
v61	0.000163
v23	1.801
v65	0.000283
v62	0.0000180
v76	0.6
v35	2.64
v57	0.10286078
v41	265.4
k0	-0.5

A.8. MATLAB Code: Steroidogenesis Anchor Model

A.8.1. Steroidogenesis Anchor Model ODEs

```
function dydt = Steroidogenesis_model_ODE(t, y, option, p)


   Chol= y(1); %Cholesterol in ovary
   P5  = y(2); %Pregnenolone
   P4  = y(3); %Progesterone
   A4  = y(4); %Androstenedione
   T   = y(5); %Testosterone
   E2  = y(6); %Estradiol
   E2p = y(7); %Estradiol in plasma
   P4p = y(8); %Progesterone in plasma
   LH  = y(9); %LH in pituitary
   LHp = y(10); %LH in plasma
   CL  = y(11); %Corpus Luteum
   AF  = y(12); %Growing antral follicles
   S   = y(13); %Bistable signal S mediating E2p positive feedback onto LH release
   S1  = y(14); %Bistable signal S1 mediating LH surge-triggered AF collapse and CL formation
   S2  = y(15); %Intermediate promoting CL atresia
   FSH  = y(16); %FSH in pituitary
   FSHp = y(17); %FSH in plasma



 % Define the system of ODEs
   dydt = zeros(length(y),1);

   %Chol
   %dydt(1) = p.k1 * AF * p.Cholp + p.k33 * CL * p.Cholp - p.k2 * Chol;
   dydt(1) = 0; %p.k1 * p.Cholp + p.k33 * p.Cholp - p.k2 * Chol;
```

```
    %P5
    %dydt(2) = p.k2 * Chol - p.k3 * P5 - p.k11 * P5;
    dydt(2) = p.k2 * (p.k2a*AF + p.k2b*CL) * Chol - p.k3 * P5 - p.k11 * P5;

    %P4
    dydt(3) = p.k3 * P5 - p.k4 * CL * P4 - p.k5 * P4;

    %A4
    dydt(4) = p.k5 * P4 - p.k6 * A4 + p.k7 * T - p.k12 * A4;

    %T
    dydt(5) = p.k6 * A4 - p.k7 * T - p.k8 * T - p.k13 * T;

    %E2
    dydt(6) = p.k8 * T - p.k9 * E2 - p.k22 * LHp^p.n22/(p.J22^p.n22+LHp^p.n22) * E2;

    %E2p
    dydt(7) = p.scale_E2p * p.k9 * E2 - p.k10 * E2p;

    %P4p
    dydt(8) = p.scale_P4p * p.k4 * CL * P4 - p.k14 * P4p;

    %LH
    dydt(9) = p.k15 - p.k25 * S^p.n25/(p.J25^p.n25+S^p.n25) * LH - p.k18 * LH;

    %LHp
    dydt(10) = p.k25 * S^p.n25/(p.J25^p.n25+S^p.n25) * LH + p.k18 * LH - p.k17 * LHp;

    %CL
    dydt(11) = p.k29 * S1^p.n29/(p.J29^p.n29+S1^p.n29) - p.k20 * CL - p.k32 * S2^p.n32 /
(p.J32^p.n32 + S2^p.n32) * CL;

    %AF
```

```
    dydt(12) = p.k21 * AF^2 * (1 - AF/p.AFmax) - p.k29 * S1^p.n29/(p.J29^p.n29+S1^p.n29) * AF;
%Logistic function to describe exponential growth when AF is small and stop growing when AF is
large

    %S
    dydt(13) = p.k160 + p.k16 * S^p.n16 / ((p.J16/(p.k24+E2p))^p.n16 +  S^p.n16 ) - p.k23*S;

    %S1
    dydt(14) = p.k190 + p.k19 * S1^p.n19 / ((p.J19/(p.k26+p.k28*LHp))^p.n19 +  S1^p.n19 ) -
p.k27*S1;

    %S2
    dydt(15) = p.k30 * S1^p.n30 / (p.J30^p.n30 + S1^p.n30) - p.k31*S2;

    %FSH
    %dydt(16) = p.k34 - p.k37 * S^p.n37/(p.J37^p.n37+S^p.n37) * FSH - p.k35 * FSH;
    dydt(16) = p.k34 * p.J34^p.n34/(p.J34^p.n34+P4p^p.n38) * p.k38 *
p.J38^p.n38/(p.J38^p.n38+E2p^p.n38) - p.k37 * S^p.n37/(p.J37^p.n37+S^p.n37) * FSH - p.k35 *
FSH;

    %FSHp
    dydt(17) = p.k37 * S^p.n37/(p.J37^p.n37+S^p.n37) * FSH + p.k35 * FSH - p.k36 * FSHp;



end

%% ------------------------ DEFAULT PARAMETERS -----------------------------%%
%Hormone half-lives: https://www.kup.at/kup/pdf/4975.pdf
p.k1 = log(2)/(1/60);
p.k2 = log(2)/(1/60); %Assuming the conversion from Chol to P5 is fast such that the half-life of
Chol is 1 minute.
p.k2a = 1;
```

```
p.k2b = 1;
p.k3 = log(2)/(1/60); %Assuming the conversion from P5 to P4 is fast such that the half-life of P5 is 1 minute.
p.k4 = 0.015 * log(2)/(1/60)*0.5; %Assuming the loss of P4 due to conversion to A4 and to secretion into circulation is fast such that the half-life of P4 is 1 minute, and the split is 50/50.
p.k5 = log(2)/(1/60)*0.5;
p.k6 = log(2)/(1/60); %k6 and k7 are set this way so the difference between the two fluxes will be equal to k5 flux to maintain flux balance when A4 and T are both at 1.
p.k7 = log(2)/(1/60)*0.5;
p.k8 = log(2)/(1/60)*0.5;
p.k9 = log(2)/(1/60)*0.5;
p.k10 = 2*log(2)/2; % Estradiol half-life in circulation is 2 hours.
p.k11 = 0;
p.k12 = 0*log(2)/(1/60)*0.5;
p.k13 = 0;
p.k14 = 0.125*log(2)/(5/60); %Progesterone half-life in circulation is about 5 min according to wikipedia
p.k15 = 2*1/1.45;
p.k17 = 2*log(2)/1; % LH half-life in circulation is 1 hour.
p.k18 = 0.1 * p.k15;
p.k19 = 10*log(2)/0.1;
p.k20 = log(2)/4;
p.k21 = 0.85*log(2)/5;
p.k22 = 2 * p.k9;
p.k23 = log(2)/1; % S half-life is 1 hour.
p.k24 = 1;
p.k25 = 1e4;
p.k26 = 3;
p.k27 = log(2)/0.1; % S1 half-life is 0.1 hour.
p.k28 = 40;
p.k29 = 2;
p.k31 = 0.25;
p.k30 = 10*p.k31;
```

```
p.k32 = 10*p.k20;
p.k33 = log(2)/(1/60);
p.k34 = 1/1.45;
p.k35 = 3.5*0.1 * p.k34;
p.k36 = log(2)/2;
p.k37 = 1e4;
p.k38 = 4;
p.k16 = 10 * p.k23;
p.k160 = p.k23;
p.k190 = 0.01*log(2)/0.1;
p.J16 = 15;
p.J19 = 16;
p.J22 = 3;
p.J25 = 5;
p.J29 = 5;
p.J30 = 1;
p.J32 = 9;
p.J34 = 3;
p.J37 = 5;
p.J38 = 5;
p.n16 = 5;
p.n19 = 5;
p.n22 = 100;
p.n25 = 100;
p.n29 = 10;
p.n30 = 5;
p.n32 = 10;
p.n34 = 1;
p.n37 = 100;
p.n38 = 1;
p.AFmax = 7.5;
p.Cholp = 1;
p.scale_E2p = 1/60; %Used to scale E2p to 1.
```

```
p.scale_P4p = 1/2.5; %Used to scale E2p to 1.
default_p = p;

%% ------------------------ INITIAL CONDITION----------------------------%%
init.Chol= 1; %Cholesterol in ovary
init.P5  = 1; %Pregnenolone
init.P4  = 1; %Progesterone
init.A4  = 1; %Androstenedione
init.T   = 1; %Testosterone
init.E2  = 1; %Estradiol
init.E2p = 2; %Estradiol in plasma
init.P4p = 0; %Progesterone in plasma
init.LH  = 10; %LH in pituitary
init.LHp = 1; %LH in plasma
init.CL  = 0; %Corpus Luteum
init.AF  = 1; %Growing antral follicle
init.S   = 1; %Bistable signal S mediating E2p positive feedback onto LH release
init.S1   = 0; %Bistable signal S1 mediating LH surge-triggered AF collapse and CL formation
init.S2  = 0; %Intermediate promoting CL atresia
init.FSH  = 15; %FSH in pituitary
init.FSHp = 4; %FSH in plasma

default_init = init;

%% ------------------------ DEFAULT (AVERAGE MODEL) SIMULATION --------------------------%%
p = default_p;
init = default_init;

y0 = cell2mat(struct2cell(init));
tspan = [0:0.1:28];
options = [];
[t,y] = ode15s('Steroidogenesis_model_ODE',tspan, y0, options, p);
```

```
Chol= y(:,1); %Cholesterol in ovary
P5  = y(:,2); %Pregnenolone
P4  = y(:,3); %Progesterone
A4  = y(:,4); %Androstenedione
T   = y(:,5); %Testosterone
E2  = y(:,6); %Estradiol
E2p = y(:,7); %Estradiol in plasma
P4p = y(:,8); %Progesterone in plasma
LH  = y(:,9); %LH in pituitary
LHp = y(:,10); %LH in plasma
CL  = y(:,11); %Corpus Luteum
AF  = y(:,12); %Growing antral follicle
S   = y(:,13); %Bistable signal S mediating E2p positive feedback onto LH release
S1  = y(:,14); %Bistable signal S1 mediating LH surge-triggered AF collapse and CL formation
S2  = y(:,15); %Intermediatepromoting CL atresia
FSH  = y(:,16); %FSH in pituitary
FSHp = y(:,17); %FSH in plasma

figure(100)
plot(t, E2p, 'r', 'LineWidth',2, 'DisplayName','E2') %Plasma estradiol
hold on
plot(t, P4p, 'b', 'LineWidth',2,  'DisplayName','P4') %Plasma progesterone
plot(t, LHp, 'g', 'LineWidth',2,  'DisplayName','LH') %Plasma LH
plot(t, FSHp, 'm', 'LineWidth',2,  'DisplayName','FSH') %Plasma FSH
%plot(t, AF, 'c', 'DisplayName','AF') %Antral follicle
%plot(t, CL, 'm', 'DisplayName','CL') %Corpus luteum
%plot(t, LH, 'm', 'DisplayName','LH') %Pituitary LH
%plot(t, FSH, 'm', 'DisplayName','FSH') %Pituitary FSH
%plot(t, S, 'k', 'DisplayName','S') %S
%plot(t, S1, 'k.', 'DisplayName','S1') %S
%plot(t, S2, 'k-', 'DisplayName','S2') %S
xlabel('Time (day)')
ylabel('Hormone level')
```

```
xticks([0:7:28])
legend

% figure(110)
% plot(t, LH, 'r') %Pituitary LH
% hold on
% xlabel('Time (day)')
% ylabel('Hormone level')
% legend('Pituitary LH')
%
% figure(120)
% plot(t, Chol, 'r')
% hold on
% plot(t, P5, 'g')
% plot(t, P4, 'b')
% plot(t, A4, 'k')
% plot(t, T, 'c')
% plot(t, E2, 'm')
% xlabel('Time (day)')
% ylabel('Metabolite level')
% legend('Chol', 'P5', 'P4', 'A4', 'T', 'E2')
%
%    figure(130)
%     plot(t, y(:,11), 'r') %corpus luteum
%     hold on
%     xlabel('Time (day)')
%     ylabel('corpus luteum')
%     legend('corpus luteum')

%Find the follicular phase length
[LHpmax,idx] = max(LHp)
LH_peak_time_default = t(idx)
```

```
%% ------------------------ Sensitivity Analysis for follicular phase length ----------%
percent_change = 0.1;
sensitivity_coeff_follicular_phase_length = [];

%Run model at default parameter values
p = default_p;
init = default_init;

y0 = cell2mat(struct2cell(init));
tspan = [0:0.1:28];
options = [];
[t1,y1] = ode15s('Steroidogenesis_model_ODE',tspan, y0, options, p);
LHp1 = y1(:,10); %LH in plasma


%Find the follicular phase length
[LHpmax1,idx1] = max(LHp1)
LH_peak_time_default = t(idx1);


%----------Run model at modified parameter values

%Compile parameter list for sensitivity analysis;
param_cell = struct2cell(default_p);
param_names = fieldnames(default_p);

for n = 1:length(param_cell)
   n

   %Increase the parameter value
      p = default_p;
      init = default_init;
      if n ~= (length(param_cell)+1)
```

```
        eval(strcat('p.', param_names{n}, '=', num2str(param_cell{n}), '*(1 + percent_change);'));
    end
    y0 = cell2mat(struct2cell(init));
    [t2,y2] = ode15s('Steroidogenesis_model_ODE',tspan, y0, options, p);
    LHp2 = y2(:,10); %LH in plasma

    %Find the follicular phase length
    [LHpmax2,idx2] = max(LHp2);
    LH_peak_time_up = t(idx2);


  %Decrease the parameter value
    p = default_p;
    init = default_init;
    if n ~= (length(param_cell)+1)
        eval(strcat('p.', param_names{n}, '=', num2str(param_cell{n}), '*(1 - percent_change);'));
    end
    y0 = cell2mat(struct2cell(init));
    [t3,y3] = ode15s('Steroidogenesis_model_ODE',tspan, y0, options, p);
    LHp3 = y3(:,10); %LH in plasma

    %Find the follicular phase length
    [LHpmax3,idx3] = max(LHp3)
    LH_peak_time_down = t(idx3);

  %Calculate sensitivity coefficient
    sensitivity_coeff_follicular_phase_length(n) = mean([(LH_peak_time_up -
LH_peak_time_default)/LH_peak_time_default/percent_change, (LH_peak_time_default -
LH_peak_time_down)/LH_peak_time_default/percent_change])
end

%  tornado plot;
```

```
[~,idx] = sort(abs(sensitivity_coeff_follicular_phase_length), 'ascend'); % Obtain index after sorting
by absolute values;
param_names_follicular_phase_length = param_names(idx);
figure(1001)
barh(sensitivity_coeff_follicular_phase_length(idx));
ylim([0.5,length(param_cell)+1.5]);
xlabel('sensitivity coefficient (follicular phase length)');
yticks([1:1:length(param_cell)+1])
yticklabels(param_names_follicular_phase_length);
pbaspect([0.75 1 1])

%% ------------------------ MONTE CARLO POPULATION SIMULATION --------------------------%%
num_indv    = 100; %100 women

p = default_p;
init = default_init;

init_E2p_out = [];
init_P4p_out = [];
init_LHp_out = [];
init_FSHp_out = [];
J16_out = [];
k10_out = [];
k14_out = [];
k21_out = [];
k18_out = [];

out   = {};
for n = 1:1:num_indv
   n


   %Initial E2p
```

```
    m = default_init.E2p; %Mean
    v = (m*0.1)^2; %variance
    E2p_mean = log((m^2)/sqrt(v+m^2));
    E2p_sd = sqrt(log(v/(m^2)+1));
    init.E2p = lognrnd(E2p_mean, E2p_sd, 1);
    init_E2p_out = [init_E2p_out; init.E2p];
%
%     %Initial P4p
%     m = default_init.P4p; %Mean
%     v = (m*0.1)^2; %variance
%     P4p_mean = log((m^2)/sqrt(v+m^2));
%     P4p_sd = sqrt(log(v/(m^2)+1));
%     init.P4p = lognrnd(P4p_mean, P4p_sd, 1);
%     init_P4p_out = [init_P4p_out; init.P4p];

    %Initial LHp
    m = default_init.LHp; %Mean
    v = (m*0.1)^2; %variance
    LHp_mean = log((m^2)/sqrt(v+m^2));
    LHp_sd = sqrt(log(v/(m^2)+1));
    init.LHp = lognrnd(LHp_mean, LHp_sd, 1);
    init_LHp_out = [init_LHp_out; init.LHp];

    %Initial FSHp
    m = default_init.FSHp; %Mean
    v = (m*0.1)^2; %variance
    FSHp_mean = log((m^2)/sqrt(v+m^2));
    FSHp_sd = sqrt(log(v/(m^2)+1));
    init.FSHp = lognrnd(FSHp_mean, FSHp_sd, 1);
    init_FSHp_out = [init_FSHp_out; init.FSHp];


    %k10 sampling for plasma E2 clearance
```

```
m      = default_p.k10; %Mean
v = (m*0.05)^2; %variance 0.1
k10_mean = log((m^2)/sqrt(v+m^2));
k10_sd = sqrt(log(v/(m^2)+1));
p.k10 = lognrnd(k10_mean, k10_sd, 1);
k10_out = [k10_out; p.k10];

%k14 sampling for plasma P4 clearance
m      = default_p.k14; %Mean
v = (m*0.05)^2; %variance 0.1
k14_mean = log((m^2)/sqrt(v+m^2));
k14_sd = sqrt(log(v/(m^2)+1));
p.k14 = lognrnd(k14_mean, k14_sd, 1);
k14_out = [k14_out; p.k14];

%k21 sampling for AF growth rate
m      = default_p.k21; %Mean
v = (m*0.05)^2; %variance 0.1
k21_mean = log((m^2)/sqrt(v+m^2));
k21_sd = sqrt(log(v/(m^2)+1));
p.k21 = lognrnd(k21_mean, k21_sd, 1);
k21_out = [k21_out; p.k21];


%k18 sampling for different amount of pituitary LH stored such that the LH surge can reach
different peak levels
m      = default_p.k18; %Mean
v = (m*0.2)^2; %variance
k18_mean = log((m^2)/sqrt(v+m^2));
k18_sd = sqrt(log(v/(m^2)+1));
p.k18 = lognrnd(k18_mean, k18_sd, 1);
k18_out = [k18_out; p.k18];
```

```
%J16 sampling for E2 threshold triggering LH surge
m      = default_p.J16; %Mean
v = (m*0.05)^2; %variance
J16_mean = log((m^2)/sqrt(v+m^2));
J16_sd = sqrt(log(v/(m^2)+1));
p.J16 = lognrnd(J16_mean, J16_sd, 1);
J16_out = [J16_out; p.J16];




y0 = cell2mat(struct2cell(init));
tspan = [0:0.1:28];
options = [];
[t,y] = ode15s('Steroidogenesis_model_ODE',tspan, y0, options, p);

Chol= y(:,1); %Cholesterol in ovary
P5  = y(:,2); %Pregnenolone
P4  = y(:,3); %Progesterone
A4  = y(:,4); %Androstenedione
T   = y(:,5); %Testosterone
E2  = y(:,6); %Estradiol
E2p = y(:,7); %Estradiol in plasma
P4p = y(:,8); %Progesterone in plasma
LH  = y(:,9); %LH in pituitary
LHp = y(:,10); %LH in plasma
CL  = y(:,11); %Corpus Luteum
AF  = y(:,12); %Growing antral follicle
S   = y(:,13); %Bistable signal S mediating E2p positive feedback onto LH release
S1  = y(:,14); %Bistable signal S1 mediating LH surge-triggered AF collapse and CL formation
S2  = y(:,15); %Intermediatepromoting CL atresia
FSH  = y(:,16); %FSH in pituitary
FSHp = y(:,17); %FSH in plasma
```

```
    out.P4p(:,n) = P4p;
    out.E2p(:,n) = E2p;
    out.LHp(:,n) = LHp;
    out.FSHp(:,n) = FSHp;

%     %Plasma E2
%     figure(199)
%     plot(t, E2p, 'DisplayName','Plasma E2') %Plasma estradiol
%     hold on
%     %plot(t, P4p, 'b', 'DisplayName','P4p') %Plasma progesterone
%     %plot(t, LHp, 'g', 'DisplayName','LHp')
%     %plot(t, AF, 'c', 'DisplayName','AF')
%     %plot(t, CL, 'm', 'DisplayName','CL')
%     plot(t, LH, 'm', 'DisplayName','LH')
%     %plot(t, S, 'k', 'DisplayName','S')
%     %plot(t, S1, 'k.', 'DisplayName','S1')
%     %plot(t, S2, 'k-', 'DisplayName','S2')
%     xlabel('Time (day)')
%     ylabel('Hormone level')
%     legend
%
%     %Plasma P4
%     figure(210)
%     plot(t, P4p, 'DisplayName','Plasma P4')
%     hold on
%     xlabel('Time (day)')
%     ylabel('Hormone level')
%     legend
%
%     %Plasma LH
%     figure(220)
%     plot(t, LHp, 'DisplayName','Plasma LH')
%     hold on
```

```
%     xlabel('Time (day)')
%     ylabel('Hormone level')
%     legend

end

%Time-course figures
%Plasam E2
figure(200)
plot(t,out.E2p(:,1:end), 'Color', [0.7 0.7 0.7])
hold on
xlabel('Day')
ylabel('Plasam E2')
percentile_E2p = prctile(out.E2p',[2.5,50,97.5])';
%plot(t,percentile_E2p(:,2), 'Color', 'blue' ,'LineWidth',3)
plot(t,percentile_E2p(:,[1,3]), 'b--', 'LineWidth',3)
plot(t,mean(out.E2p'), 'Color', 'blue' ,'LineWidth',3)
title('Plasma E2')
xlim([0 28])

%Plasam P4
figure(210)
plot(t,out.P4p(:,1:end), 'Color', [0.7 0.7 0.7])
hold on
xlabel('Day')
ylabel('Plasam P4')
percentile_P4p = prctile(out.P4p',[2.5,50,97.5])';
%plot(t,percentile_P4p(:,2), 'Color', 'blue' ,'LineWidth',3)
plot(t,percentile_P4p(:,[1,3]), 'b--', 'LineWidth',3)
plot(t,mean(out.P4p'), 'Color', 'blue' ,'LineWidth',3)
title('Plasma P4')
xlim([0 28])
```

```
%Plasam LH
figure(220)
plot(t,out.LHp(:,1:end), 'Color', [0.7 0.7 0.7])
hold on
xlabel('Day)')
ylabel('Plasma LH')
percentile_LHp = prctile(out.LHp',[2.5,50,97.5])';
%plot(t,percentile_LHp(:,2), 'Color', 'blue' ,'LineWidth',3)
plot(t,percentile_LHp(:,[1,3]), 'b--', 'LineWidth',3)
plot(t,mean(out.LHp'), 'Color', 'blue' ,'LineWidth',3)
title('Plasma LH')
xlim([0 28])

%Plasam FSH
figure(230)
plot(t,out.FSHp(:,1:end), 'Color', [0.7 0.7 0.7])
hold on
xlabel('Day)')
ylabel('Plasma LH')
percentile_FSHp = prctile(out.FSHp',[2.5,50,97.5])';
%plot(t,percentile_FSHp(:,2), 'Color', 'blue' ,'LineWidth',3)
plot(t,percentile_FSHp(:,[1,3]), 'b--', 'LineWidth',3)
plot(t,mean(out.FSHp'), 'Color', 'blue' ,'LineWidth',3)
title('Plasma FSH')
xlim([0 28])

%Capture the follicular phase length
LH_peak_time =[];
for n = 1:1:num_indv
    %Find the LH time
    [LHpmax,idx] = max(out.LHp(:,n))
    LH_peak_time = [LH_peak_time, t(idx)]; %code is breaking so run outside of loop or change
tspan
```

```
end
figure(240)
h = histogram(LH_peak_time,'Normalization','probability','BinWidth',0.5);
hold on
%nbins = h.NumBins to find number of bins
probability = h.Values;
days = h.BinEdges(1:end-1);
xlabel('Folliclular phase length (day)')
ylabel('Probability')
mean_folliclular_phase_length   = mean(LH_peak_time);
sd_folliclular_phase_length    = std(LH_peak_time);
percentile_folliclular_phase_length = prctile(LH_peak_time,[2.5,50,97.5]);
median_folliclular_phase_length   = median(LH_peak_time);
title('Distribution of Folliclular Phase Length')
text(16, 0.14, strcat('mean=', num2str(round(mean_folliclular_phase_length,1)), '+/-',
num2str(round(sd_folliclular_phase_length,1))));

%% ------------------------ DIOXIN EFFECT ON AVERAGE MODEL ---------------------------%%
p = default_p;
init = default_init;

p.k2 = default_p.k2 * 0.8;

%p.k6 = default_p.k6 * 0.01;

y0 = cell2mat(struct2cell(init));
tspan = [0:0.1:28];
options = [];
[t,y] = ode15s('Steroidogenesis_model_ODE',tspan, y0, options, p);

Chol= y(:,1); %Cholesterol in ovary
P5  = y(:,2); %Pregnenolone
P4  = y(:,3); %Progesterone
```

```
A4  = y(:,4); %Androstenedione
T   = y(:,5); %Testosterone
E2  = y(:,6); %Estradiol
E2p = y(:,7); %Estradiol in plasma
P4p = y(:,8); %Progesterone in plasma
LH  = y(:,9); %LH in pituitary
LHp = y(:,10); %LH in plasma
CL  = y(:,11); %Corpus Luteum
AF  = y(:,12); %Growing antral follicle
S   = y(:,13); %Bistable signal S mediating E2p positive feedback onto LH release
S1  = y(:,14); %Bistable signal S1 mediating LH surge-triggered AF collapse and CL formation
S2  = y(:,15); %Intermediatepromoting CL atresia
FSH  = y(:,16); %FSH in pituitary
FSHp = y(:,17); %FSH in plasma


%Find the follicular phase length
[LHpmax,idx] = max(LHp)
LH_peak_time_dioxin = t(idx)
```

A.8.2. Population Model: Monte Carlo Simulation

```
%% ------------------------ MONTE CARLO POPULATION SIMULATION ---------------------------%%
num_indv    = 100; %100 women

p = default_p;
init = default_init;

init_E2p_out = [];
init_P4p_out = [];
init_LHp_out = [];
```

```
init_FSHp_out = [];
J16_out = [];
k10_out = [];
k14_out = [];
k21_out = [];
k18_out = [];

out   = {};
for n = 1:1:num_indv
   n



   %Initial E2p
   m = default_init.E2p; %Mean
   v = (m*0.1)^2; %variance
   E2p_mean = log((m^2)/sqrt(v+m^2));
   E2p_sd = sqrt(log(v/(m^2)+1));
   init.E2p = lognrnd(E2p_mean, E2p_sd, 1);
   init_E2p_out = [init_E2p_out; init.E2p];
%
%    %Initial P4p
%    m = default_init.P4p; %Mean
%    v = (m*0.1)^2; %variance
%    P4p_mean = log((m^2)/sqrt(v+m^2));
%    P4p_sd = sqrt(log(v/(m^2)+1));
%    init.P4p = lognrnd(P4p_mean, P4p_sd, 1);
%    init_P4p_out = [init_P4p_out; init.P4p];

   %Initial LHp
   m = default_init.LHp; %Mean
   v = (m*0.1)^2; %variance
   LHp_mean = log((m^2)/sqrt(v+m^2));
   LHp_sd = sqrt(log(v/(m^2)+1));
```

```
init.LHp = lognrnd(LHp_mean, LHp_sd, 1);
init_LHp_out = [init_LHp_out; init.LHp];

%Initial FSHp
m = default_init.FSHp; %Mean
v = (m*0.1)^2; %variance
FSHp_mean = log((m^2)/sqrt(v+m^2));
FSHp_sd = sqrt(log(v/(m^2)+1));
init.FSHp = lognrnd(FSHp_mean, FSHp_sd, 1);
init_FSHp_out = [init_FSHp_out; init.FSHp];



%k10 sampling for plasma E2 clearance
m      = default_p.k10; %Mean
v = (m*0.05)^2; %variance 0.1
k10_mean = log((m^2)/sqrt(v+m^2));
k10_sd = sqrt(log(v/(m^2)+1));
p.k10 = lognrnd(k10_mean, k10_sd, 1);
k10_out = [k10_out; p.k10];

%k14 sampling for plasma P4 clearance
m      = default_p.k14; %Mean
v = (m*0.05)^2; %variance 0.1
k14_mean = log((m^2)/sqrt(v+m^2));
k14_sd = sqrt(log(v/(m^2)+1));
p.k14 = lognrnd(k14_mean, k14_sd, 1);
k14_out = [k14_out; p.k14];

%k21 sampling for AF growth rate
m      = default_p.k21; %Mean
v = (m*0.05)^2; %variance 0.1
k21_mean = log((m^2)/sqrt(v+m^2));
k21_sd = sqrt(log(v/(m^2)+1));
```

```
p.k21 = lognrnd(k21_mean, k21_sd, 1);
k21_out = [k21_out; p.k21];


%k18 sampling for different amount of pituitary LH stored such that the LH surge can reach different peak levels
m      = default_p.k18; %Mean
v = (m*0.2)^2; %variance
k18_mean = log((m^2)/sqrt(v+m^2));
k18_sd = sqrt(log(v/(m^2)+1));
p.k18 = lognrnd(k18_mean, k18_sd, 1);
k18_out = [k18_out; p.k18];

%J16 sampling for E2 threshold triggering LH surge
m      = default_p.J16; %Mean
v = (m*0.05)^2; %variance
J16_mean = log((m^2)/sqrt(v+m^2));
J16_sd = sqrt(log(v/(m^2)+1));
p.J16 = lognrnd(J16_mean, J16_sd, 1);
J16_out = [J16_out; p.J16];



y0 = cell2mat(struct2cell(init));
tspan = [0:0.1:28];
options = [];
[t,y] = ode15s('Steroidogenesis_model_ODE',tspan, y0, options, p);

Chol= y(:,1); %Cholesterol in ovary
P5  = y(:,2); %Pregnenolone
P4  = y(:,3); %Progesterone
A4  = y(:,4); %Androstenedione
T   = y(:,5); %Testosterone
```

```
    E2  = y(:,6); %Estradiol
    E2p = y(:,7); %Estradiol in plasma
    P4p = y(:,8); %Progesterone in plasma
    LH  = y(:,9); %LH in pituitary
    LHp = y(:,10); %LH in plasma
    CL  = y(:,11); %Corpus Luteum
    AF  = y(:,12); %Growing antral follicle
    S   = y(:,13); %Bistable signal S mediating E2p positive feedback onto LH release
    S1  = y(:,14); %Bistable signal S1 mediating LH surge-triggered AF collapse and CL formation
    S2  = y(:,15); %Intermediatepromoting CL atresia
    FSH  = y(:,16); %FSH in pituitary
    FSHp = y(:,17); %FSH in plasma

    out.P4p(:,n) = P4p;
    out.E2p(:,n) = E2p;
    out.LHp(:,n) = LHp;
    out.FSHp(:,n) = FSHp;

%     %Plasma E2
%     figure(199)
%     plot(t, E2p, 'DisplayName','Plasma E2') %Plasma estradiol
%     hold on
%     %plot(t, P4p, 'b', 'DisplayName','P4p') %Plasma progesterone
%     %plot(t, LHp, 'g', 'DisplayName','LHp')
%     %plot(t, AF, 'c', 'DisplayName','AF')
%     %plot(t, CL, 'm', 'DisplayName','CL')
%     plot(t, LH, 'm', 'DisplayName','LH')
%     %plot(t, S, 'k', 'DisplayName','S')
%     %plot(t, S1, 'k.', 'DisplayName','S1')
%     %plot(t, S2, 'k-', 'DisplayName','S2')
%     xlabel('Time (day)')
%     ylabel('Hormone level')
%     legend
```

```
%
%    %Plasma P4
%    figure(210)
%    plot(t, P4p, 'DisplayName','Plasma P4')
%    hold on
%    xlabel('Time (day)')
%    ylabel('Hormone level')
%    legend
%
%    %Plasma LH
%    figure(220)
%    plot(t, LHp, 'DisplayName','Plasma LH')
%    hold on
%    xlabel('Time (day)')
%    ylabel('Hormone level')
%    legend

end

%Time-course figures
%Plasam E2
figure(200)
plot(t,out.E2p(:,1:end), 'Color', [0.7 0.7 0.7])
hold on
xlabel('Day')
ylabel('Plasam E2')
percentile_E2p = prctile(out.E2p',[2.5,50,97.5])';
%plot(t,percentile_E2p(:,2), 'Color', 'blue' ,'LineWidth',3)
plot(t,percentile_E2p(:,[1,3]), 'b--', 'LineWidth',3)
plot(t,mean(out.E2p'), 'Color', 'blue' ,'LineWidth',3)
title('Plasma E2')
xlim([0 28])
```

```
%Plasam P4
figure(210)
plot(t,out.P4p(:,1:end), 'Color', [0.7 0.7 0.7])
hold on
xlabel('Day')
ylabel('Plasam P4')
percentile_P4p = prctile(out.P4p',[2.5,50,97.5])';
%plot(t,percentile_P4p(:,2), 'Color', 'blue' ,'LineWidth',3)
plot(t,percentile_P4p(:,[1,3]), 'b--', 'LineWidth',3)
plot(t,mean(out.P4p'), 'Color', 'blue' ,'LineWidth',3)
title('Plasma P4')
xlim([0 28])

%Plasam LH
figure(220)
plot(t,out.LHp(:,1:end), 'Color', [0.7 0.7 0.7])
hold on
xlabel('Day)')
ylabel('Plasma LH')
percentile_LHp = prctile(out.LHp',[2.5,50,97.5])';
%plot(t,percentile_LHp(:,2), 'Color', 'blue' ,'LineWidth',3)
plot(t,percentile_LHp(:,[1,3]), 'b--', 'LineWidth',3)
plot(t,mean(out.LHp'), 'Color', 'blue' ,'LineWidth',3)
title('Plasma LH')
xlim([0 28])

%Plasam FSH
figure(230)
plot(t,out.FSHp(:,1:end), 'Color', [0.7 0.7 0.7])
hold on
xlabel('Day)')
ylabel('Plasma LH')
percentile_FSHp = prctile(out.FSHp',[2.5,50,97.5])';
```

```
%plot(t,percentile_FSHp(:,2), 'Color', 'blue' ,'LineWidth',3)
plot(t,percentile_FSHp(:,[1,3]), 'b--', 'LineWidth',3)
plot(t,mean(out.FSHp'), 'Color', 'blue' ,'LineWidth',3)
title('Plasma FSH')
xlim([0 28])

%Capture the follicular phase length
LH_peak_time =[];
for n = 1:1:num_indv
   %Find the LH time
   [LHpmax,idx] = max(out.LHp(:,n))
   LH_peak_time = [LH_peak_time, t(idx)]; %code is breaking so run outside of loop or change
tspan
end
figure(240)
h = histogram(LH_peak_time,'Normalization','probability','BinWidth',0.5);
hold on
%nbins = h.NumBins to find number of bins
probability = h.Values;
days = h.BinEdges(1:end-1);
xlabel('Folliclular phase length (day)')
ylabel('Probability')
mean_folliclular_phase_length   = mean(LH_peak_time);
sd_folliclular_phase_length    = std(LH_peak_time);
percentile_folliclular_phase_length = prctile(LH_peak_time,[2.5,50,97.5]);
median_folliclular_phase_length   = median(LH_peak_time);
title('Distribution of Folliclular Phase Length')
text(16, 0.14, strcat('mean=', num2str(round(mean_folliclular_phase_length,1)), '+/-',
num2str(round(sd_folliclular_phase_length,1))));

%% ------------------------ DIOXIN EFFECT ON AVERAGE MODEL --------------------------%%
p = default_p;
init = default_init;
```

```
p.k2 = default_p.k2 * 0.8;

%p.k6 = default_p.k6 * 0.01;

y0 = cell2mat(struct2cell(init));
tspan = [0:0.1:28];
options = [];
[t,y] = ode15s('Steroidogenesis_model_ODE',tspan, y0, options, p);

Chol= y(:,1); %Cholesterol in ovary
P5  = y(:,2); %Pregnenolone
P4  = y(:,3); %Progesterone
A4  = y(:,4); %Androstenedione
T   = y(:,5); %Testosterone
E2  = y(:,6); %Estradiol
E2p = y(:,7); %Estradiol in plasma
P4p = y(:,8); %Progesterone in plasma
LH  = y(:,9); %LH in pituitary
LHp = y(:,10); %LH in plasma
CL  = y(:,11); %Corpus Luteum
AF  = y(:,12); %Growing antral follicle
S   = y(:,13); %Bistable signal S mediating E2p positive feedback onto LH release
S1  = y(:,14); %Bistable signal S1 mediating LH surge-triggered AF collapse and CL formation
S2  = y(:,15); %Intermediatepromoting CL atresia
FSH  = y(:,16); %FSH in pituitary
FSHp = y(:,17); %FSH in plasma

figure(301)
plot(t, E2p, 'r', 'LineWidth',2, 'DisplayName','E2') %Plasma estradiol
hold on
plot(t, P4p, 'b', 'LineWidth',2,  'DisplayName','P4') %Plasma progesterone
plot(t, LHp, 'g', 'LineWidth',2,  'DisplayName','LH') %Plasma LH
```

```
plot(t, FSHp, 'm', 'LineWidth',2,  'DisplayName','FSH') %Plasma FSH
%plot(t, AF, 'c', 'DisplayName','AF') %Antral follicle
%plot(t, CL, 'm', 'DisplayName','CL') %Corpus luteum
%plot(t, LH, 'm', 'DisplayName','LH') %Pituitary LH
%plot(t, FSH, 'm', 'DisplayName','FSH') %Pituitary FSH
%plot(t, S, 'k', 'DisplayName','S') %S
%plot(t, S1, 'k.', 'DisplayName','S1') %S
%plot(t, S2, 'k-', 'DisplayName','S2') %S
xlabel('Time (day)')
ylabel('Hormone level')
xticks([0:7:28])
legend

% figure(110)
% plot(t, LH, 'r') %Pituitary LH
% hold on
% xlabel('Time (day)')
% ylabel('Hormone level')
% legend('Pituitary LH')
%
% figure(120)
% plot(t, Chol, 'r')
% hold on
% plot(t, P5, 'g')
% plot(t, P4, 'b')
% plot(t, A4, 'k')
% plot(t, T, 'c')
% plot(t, E2, 'm')
% xlabel('Time (day)')
% ylabel('Metabolite level')
% legend('Chol', 'P5', 'P4', 'A4', 'T', 'E2')
%
%    figure(130)
```

```
%     plot(t, y(:,11), 'r') %corpus luteum
%     hold on
%     xlabel('Time (day)')
%     ylabel('corpus luteum')
%     legend('corpus luteum')

%Find the follicular phase length
[LHpmax,idx] = max(LHp)
LH_peak_time_dioxin = t(idx)

%% ------------------------ DIOXIN EFFECT ON MONTE CARLO POPULATION SIMULATION ------
----------------------%%
num_indv    = 100; %100 women

p = default_p;
init = default_init;

TCDD_vector = [1,10,100,1000,10000];
a= 0.77
Ki = 100 %ppt
n = 0.5
mean_folliclular_phase_length_vector = [];
sd_folliclular_phase_length_vector = [];
for i = 1:length(TCDD_vector)
   i
   TCDD = TCDD_vector(i);
   k2_fold_change = a + (1-a) * Ki^n / (Ki^n + TCDD^n)
   p.k2 = default_p.k2 * k2_fold_change;



   init_E2p_out = [];
   init_P4p_out = [];
   init_LHp_out = [];
```

```
init_FSHp_out = [];
J16_out = [];
k10_out = [];
k14_out = [];
k21_out = [];
k18_out = [];

out   = {};
for j = 1:1:num_indv
   j


   %Initial E2p
   m = default_init.E2p; %Mean
   v = (m*0.1)^2; %variance
   E2p_mean = log((m^2)/sqrt(v+m^2));
   E2p_sd = sqrt(log(v/(m^2)+1));
   init.E2p = lognrnd(E2p_mean, E2p_sd, 1);
   init_E2p_out = [init_E2p_out; init.E2p];
%
%    %Initial P4p
%    m = default_init.P4p; %Mean
%    v = (m*0.1)^2; %variance
%    P4p_mean = log((m^2)/sqrt(v+m^2));
%    P4p_sd = sqrt(log(v/(m^2)+1));
%    init.P4p = lognrnd(P4p_mean, P4p_sd, 1);
%    init_P4p_out = [init_P4p_out; init.P4p];

   %Initial LHp
   m = default_init.LHp; %Mean
   v = (m*0.1)^2; %variance
   LHp_mean = log((m^2)/sqrt(v+m^2));
   LHp_sd = sqrt(log(v/(m^2)+1));
```

```
init.LHp = lognrnd(LHp_mean, LHp_sd, 1);
init_LHp_out = [init_LHp_out; init.LHp];

%Initial FSHp
m = default_init.FSHp; %Mean
v = (m*0.1)^2; %variance
FSHp_mean = log((m^2)/sqrt(v+m^2));
FSHp_sd = sqrt(log(v/(m^2)+1));
init.FSHp = lognrnd(FSHp_mean, FSHp_sd, 1);
init_FSHp_out = [init_FSHp_out; init.FSHp];


%k10 sampling for plasma E2 clearance
m  = default_p.k10; %Mean
v = (m*0.05)^2; %variance 0.1
k10_mean = log((m^2)/sqrt(v+m^2));
k10_sd = sqrt(log(v/(m^2)+1));
p.k10 = lognrnd(k10_mean, k10_sd, 1);
k10_out = [k10_out; p.k10];

%k14 sampling for plasma P4 clearance
m  = default_p.k14; %Mean
v = (m*0.05)^2; %variance 0.1
k14_mean = log((m^2)/sqrt(v+m^2));
k14_sd = sqrt(log(v/(m^2)+1));
p.k14 = lognrnd(k14_mean, k14_sd, 1);
k14_out = [k14_out; p.k14];

%k21 sampling for AF growth rate
m  = default_p.k21; %Mean
v = (m*0.05)^2; %variance 0.1
k21_mean = log((m^2)/sqrt(v+m^2));
k21_sd = sqrt(log(v/(m^2)+1));
```

```
p.k21 = lognrnd(k21_mean, k21_sd, 1);
k21_out = [k21_out; p.k21];


%k18 sampling for different amount of pituitary LH stored such that the LH surge can reach
different peak levels
m  = default_p.k18; %Mean
v = (m*0.2)^2; %variance
k18_mean = log((m^2)/sqrt(v+m^2));
k18_sd = sqrt(log(v/(m^2)+1));
p.k18 = lognrnd(k18_mean, k18_sd, 1);
k18_out = [k18_out; p.k18];

%J16 sampling for E2 threshold triggering LH surge
m  = default_p.J16; %Mean
v = (m*0.05)^2; %variance
J16_mean = log((m^2)/sqrt(v+m^2));
J16_sd = sqrt(log(v/(m^2)+1));
p.J16 = lognrnd(J16_mean, J16_sd, 1);
J16_out = [J16_out; p.J16];



y0 = cell2mat(struct2cell(init));
tspan = [0:0.1:28];
options = [];
[t,y] = ode15s('Steroidogenesis_model_ODE',tspan, y0, options, p);

Chol= y(:,1); %Cholesterol in ovary
P5  = y(:,2); %Pregnenolone
P4  = y(:,3); %Progesterone
A4  = y(:,4); %Androstenedione
T   = y(:,5); %Testosterone
```

```
        E2  = y(:,6); %Estradiol
        E2p = y(:,7); %Estradiol in plasma
        P4p = y(:,8); %Progesterone in plasma
        LH  = y(:,9); %LH in pituitary
        LHp = y(:,10); %LH in plasma
        CL  = y(:,11); %Corpus Luteum
        AF  = y(:,12); %Growing antral follicle
        S   = y(:,13); %Bistable signal S mediating E2p positive feedback onto LH release
        S1  = y(:,14); %Bistable signal S1 mediating LH surge-triggered AF collapse and CL
formation
        S2  = y(:,15); %Intermediatepromoting CL atresia
        FSH  = y(:,16); %FSH in pituitary
        FSHp = y(:,17); %FSH in plasma

        out.P4p(:,j) = P4p;
        out.E2p(:,j) = E2p;
        out.LHp(:,j) = LHp;

    %     %Plasma E2
    %     figure(200)
    %     plot(t, E2p, 'DisplayName','Plasma E2') %Plasma estradiol
    %     hold on
    %     %plot(t, P4p, 'b', 'DisplayName','P4p') %Plasma progesterone
    %     %plot(t, LHp, 'g', 'DisplayName','LHp') %Plasma LH
    %     %plot(t, AF, 'c', 'DisplayName','AF') %Plasma LH
    %     %plot(t, CL, 'm', 'DisplayName','CL') %Plasma LH
    %     %plot(t, LH, 'm', 'DisplayName','LH') %Plasma LH
    %     %plot(t, S, 'k', 'DisplayName','S') %S
    %     %plot(t, S1, 'k.', 'DisplayName','S1') %S
    %     %plot(t, S2, 'k-', 'DisplayName','S2') %S
    %     xlabel('Time (day)')
    %     ylabel('Hormone level')
    %     legend
```

```
%
%    %Plasma P4
%    figure(210)
%    plot(t, P4p, 'DisplayName','Plasma P4')
%    hold on
%    xlabel('Time (day)')
%    ylabel('Hormone level')
%    legend
%
%    %Plasma LH
%    figure(220)
%    plot(t, LHp, 'DisplayName','Plasma LH')
%    hold on
%    xlabel('Time (day)')
%    ylabel('Hormone level')
%    legend

end

%Time-course figures
%Plasam E2
figure(400)
plot(t,out.E2p(:,1:end), 'Color', [0.7 0.7 0.7])
hold on
xlabel('Day')
ylabel('Plasam E2')
percentile_E2p = prctile(out.E2p',[2.5,50,97.5])';
%plot(t,percentile_E2p(:,2), 'Color', 'blue' ,'LineWidth',3)
plot(t,percentile_E2p(:,[1,3]), 'b--', 'LineWidth',3)
plot(t,mean(out.E2p'), 'Color', 'blue' ,'LineWidth',3)
title('Plasma E2')
xlim([0 28])
```

```
%Plasam P4
figure(410)
plot(t,out.P4p(:,1:end), 'Color', [0.7 0.7 0.7])
hold on
xlabel('Day')
ylabel('Plasam P4')
percentile_P4p = prctile(out.P4p',[2.5,50,97.5])';
%plot(t,percentile_P4p(:,2), 'Color', 'blue' ,'LineWidth',3)
plot(t,percentile_P4p(:,[1,3]), 'b--', 'LineWidth',3)
plot(t,mean(out.P4p'), 'Color', 'blue' ,'LineWidth',3)
title('Plasma P4')
xlim([0 28])

%Plasam LH
figure(420)
plot(t,out.LHp(:,1:end), 'Color', [0.7 0.7 0.7])
hold on
xlabel('Day)')
ylabel('Plasma LH')
percentile_LHp = prctile(out.LHp',[2.5,50,97.5])';
%plot(t,percentile_LHp(:,2), 'Color', 'blue' ,'LineWidth',3)
plot(t,percentile_LHp(:,[1,3]), 'b--', 'LineWidth',3)
plot(t,mean(out.LHp'), 'Color', 'blue' ,'LineWidth',3)
title('Plasma LH')
xlim([0 28])

%Capture the follicular phase length
LH_peak_time =[];
for j = 1:1:num_indv
    %Find the LH time
    [LHpmax,idx] = max(out.LHp(:,j))
    LH_peak_time = [LH_peak_time, t(idx)]; %code is breaking so run outside of loop or change
tspan
```

```
    end
    figure(430)
    h = histogram(LH_peak_time,'Normalization','probability','BinWidth',0.5);
    hold on
    %nbins = h.NumBins to find number of bins
    probability = h.Values;
    days = h.BinEdges(1:end-1);
    xlabel('Follicular phase length (day)')
    ylabel('Probability')
    mean_follicular_phase_length   = mean(LH_peak_time);
    mean_follicular_phase_length_vector = [mean_follicular_phase_length_vector,
mean_follicular_phase_length];
    sd_follicular_phase_length    = std(LH_peak_time);
    sd_follicular_phase_length_vector = [sd_follicular_phase_length_vector,
sd_follicular_phase_length];
    percentile_follicular_phase_length = prctile(LH_peak_time,[2.5,50,97.5]);
    median_follicular_phase_length   = median(LH_peak_time);
    title('Cumulative Distribution of Follicular Phase Length')
    text(16, 0.14, strcat('mean=', num2str(round(mean_follicular_phase_length,1)), '+/-',
num2str(round(sd_follicular_phase_length,1))));

    %Cumulative probability plot
    figure(440)
    hold on
    h = cdfplot(LH_peak_time)

end

figure(450)
errorbar(TCDD_vector, mean_follicular_phase_length_vector+14,
sd_follicular_phase_length_vector)
xlabel('TCDD serum level (ppt)')
ylabel('Mean Follicular Phase Length')
```

A.9. Summary of Parameters Used in the Steroidogenesis Anchor Model

Parameter	Value
k1	log(2)/(1/60)
k2	log(2)/(1/60).
k2a	1
k2b	1
k3	log(2)/(1/60)
k4	0.015 * log(2)/(1/60)*0.5
k5	log(2)/(1/60)*0.5
k6	log(2)/(1/60)
k7	log(2)/(1/60)*0.5
k8	log(2)/(1/60)*0.5
k9	log(2)/(1/60)*0.5
k10	2*log(2)/2
k11	0
k12	0*log(2)/(1/60)*0.5
k13	0
k14	0.125*log(2)/(5/60)
k15	2*1/1.45
k17	2*log(2)/1
k18	0.1 * k15
k19	10*log(2)/0.1
k20	log(2)/4
k21	0.85*log(2)/5
k22	2 * k9
k23	log(2)/1
k24	1
k25	1e4
k26	3
k27	log(2)/0.1
k28	40
k29	2
k31	0.25
k30	10*k31
k32	10*k20
k33	log(2)/(1/60)
k34	1/1.45
k35	3.5*0.1 * k34
k36	log(2)/2
k37	1e4
k38	4
k16	10 * k23
k160	k23
k190	0.01*log(2)/0.1
J16	15
J19	16
J22	3
J25	5
J29	5
J30	1
J32	9
J34	3
J37	5

A.10. Sample PLAS Code for the Mevalonate Model

Differential Equations

---

mRNAs

HMGCR mRNA

HMr' = r1 * SRp - r2 * HMr

FDPS mRNA

FDPSr' = r3 * SRp - r4 * FDPSr

Lanosterol Synthase mRNA

LSr' = r5* SRp - r6 * LSr

Squalene Synthase mRNA

SQSr' = r7 * SRp - r8 * SQSr

Proteins

SREBP

SRp' = r9 * C ^ a6 - r10 * SRp

HMG CoA Reductase

HRp' = r11 * HMr - r12 * HRp * GPP ^ a1 * FPP ^ a2 * L ^ a3 * C ^ a4

Farnesyl Diphosphate Synthase

FDPSp' = r13 * FDPSr - r14 * FDPSp

Lanosterol Synthase

LSp' = r15 * LSr - r16 * LSp

Squalene Synthase

SQSp' = r17 * SQSr - r18 * SQSp * C

Metabolites

HMGCoA

HC' = (r19 - r20 * HC * HRp^ a5 * FDPSp ^ a8) * SF

Geranyl-PP

GPP' = (r20 * HC   * HRp ^ a5 * FDPSp ^ a8 - r21 * GPP * FDPSp ^ a9 - r32 * GPP) * SF

Farnesyl- PP

FPP' = (r21 * GPP * FDPSp ^ a9 - r22 * FPP - r23 * FPP * SQSp ^ a7) * SF

Squalene

SQ' = (r23 FPP * SQSp ^ a7 - r24 * SQ * LSp ^ a10) * SF

Lanosterol

L' = (r24 * SQ * LSp ^ a10 - r25 * L) * SF

Hepatic Cholesterol

C' = (r25 * L + r26 - r27 * C - r28 * C ^ a11 + r29 * CP + r33 *S - r34 * C) * SF

Plasma Cholesterol

CP' = r28 * C ^ a11 - r29 * CP - r30 * CP + r31

Cholesterol Storage

S' = r34 * C - r33* S

Timescale factor

SF = 1000/23

Initial Values

---

mRNAs

HMr = 100

FDPSr = 100

LSr = 100

SQSr = 100

Enzymes/Proteins

SRp = 100

HRp = 100

FDPSp =100

LSp = 100

SQSp = 100

Metabolites

HC = 29.08138

GPP = 88.89034

FPP = 70.88889

SQ = 73.48281

L = 76.90346

C = 10993.27

CP = 5608.411

S = 2000

Parameter Values

VL = 1.93 // liver volume (L)

VP = 3.2 // plasma volume (L)

Rate Constants

r1 = 0.0012 * DEN

r2 = 0.0012

r3 = 0.0012 * DEN

r4 = 0.0012

r5 = 0.0012 * DEN

r6 = 0.0012

r7 = 0.0012 * DEN

r8 = 0.0012

r9 = 1150

r10 = 0.0023

r11 = 0.0023

r12 = 1.9E-7

r13 = 0.0017

r14 = 0.0023

r15 = 0.0023

r16 = 0.0023

r17 = 0.0023

r18 = 4.7E-7

r19 = 18150

r20 = 39.192

r21 = 35.216

r22 = 255.6

r23 = 0.09656

r24 = 0.06215

r25 = 0.4005

Diet

This is accounted for by the term r26

Normal Diet is considered as 200 mg/day, which corresponds to a micromole/day level of 517.26

High cholesterol diet: 400 mg/day, corresponding to 1030

Extremely high cholesterol diet: 600 mg/day, corresponding to 1552

r26 = (517.26/SF)/ VL

Cholesterol to Bile

r27 = 0.000356 * DEP

Interaction with Plasma

vHP

r28 = 36.697 * DEN

VPH

r29 = 0.7 * DEP

r30 = 0.006

r31 = 0.6

r32 = 0.000009

Cholesterol Storage

vHS

r33 = 0.00025 * DEN

vHS

r34 = 0.00001* 0.5 * DEN

Kinetic Orders

a1= 0.5

a2= 0.5

a3 = 0.5

a4 = 0.5

a5= 0.5

a6= -1

a7 = 0.5

a8 = 0.5

a9 = 0.5

a10 = 0.5

a11= 0.5

Specific Simulation Settings

Dioxin Effect

DEP = 1 // positive effect as a percent increase

DEN = 1 // negative effect as a percent decrease

Example: To account for a 10% change we set DEP = 1.1 and DEN = 0.9 simultaneously

Solution Parameters

---

t0= 0

tf = 60000

hr= 1

REFERENCES

1. Schnell, S., R. Grima, and P. Maini, *Multiscale Modeling in Biology.* American Scientist - AMER SCI, 2007. **95**.
2. Savageau, M.A., *The challenge of reconstruction.* New Biol, 1991. **3**(2): p. 101-2.
3. Savageau, M.A., *Reconstructionist molecular biology.* New Biol, 1991. **3**(2): p. 190-7.
4. Kreeger, P.K. and D.A. Lauffenburger, *Cancer systems biology: a network modeling perspective.* Carcinogenesis, 2009. **31**(1): p. 2-8.
5. Shurin, M.R., *Cancer as an immune-mediated disease.* Immunotargets Ther, 2012. **1**: p. 1-6.
6. Goetz, L.H. and N.J. Schork, *Personalized medicine: motivation, challenges, and progress.* Fertil Steril, 2018. **109**(6): p. 952-963.
7. Anderson, A.R. and V. Quaranta, *Integrative mathematical oncology.* Nat Rev Cancer, 2008. **8**(3): p. 227-34.
8. Millar-Wilson, A., et al., *Multiscale modeling in the framework of biological systems and its potential for spaceflight biology studies.* iScience, 2022. **25**(11): p. 105421.
9. Voit, E.O., *The Inner Workings of Life: Vignettes in Systems Biology*. 2016: Cambridge University Press.
10. Voit, E., *A First Course in Systems Biology (2nd ed.). Garland Science*. 2017.
11. Liu, R., et al., *A Physiologically Based Pharmacokinetic (PBPK) Modeling Framework for Mixtures of Dioxin-like Compounds.* Toxics, 2022. **10**(11).
12. Wilensky, U. and W. Rand, *An Introduction to Agent-Based Modeling Modeling Natural, Social, and Engineered Complex Systems with NetLogo*. 2015: The MIT Press.
13. Versypt, A.N.F., *Multiscale modeling in disease.* Curr Opin Syst Biol, 2021. **27**.
14. Glen, C.M., M.L. Kemp, and E.O. Voit, *Agent-based modeling of morphogenetic systems: Advantages and challenges.* PLOS Computational Biology, 2019. **15**(3): p. e1006577.
15. Kasereka, S., N. Kasoro, and P. Chokki, *A hybrid model for modeling the spread of epidemics: Theory and simulation*. 2014.
16. Bardini, R., et al., *Multi-level and hybrid modelling approaches for systems biology.* Comput Struct Biotechnol J, 2017. **15**: p. 396-402.
17. Garbey, M., S. Casarin, and S.A. Berceli, *A versatile hybrid agent-based, particle and partial differential equations method to analyze vascular adaptation.* Biomechanics and Modeling in Mechanobiology, 2019. **18**(1): p. 29-44.
18. Cruz, D.A. and M.L. Kemp, *Hybrid computational modeling methods for systems biology.* Progress in Biomedical Engineering, 2022. **4**(1): p. 012002.
19. Cassidy, R., et al., *Mathematical modelling for health systems research: a systematic review of system dynamics and agent-based models.* BMC Health Services Research, 2019. **19**(1): p. 845.
20. Lättilä, L., P. Hilletofth, and B. Lin, *Hybrid simulation models – When, Why, How?* Expert Systems with Applications, 2010. **37**(12): p. 7969-7975.
21. Bodine, E.N., et al., *Agent-Based Modeling and Simulation in Mathematics and Biology Education.* Bulletin of Mathematical Biology, 2020. **82**(8): p. 101.

22. Liao, J.C. and E.N. Lightfoot, Jr., *Lumping analysis of biochemical reaction systems with time scale separation.* Biotechnol Bioeng, 1988. **31**(8): p. 869-79.
23. Savageau, M.A., *Growth of complex systems can be related to the properties of their underlying determinants.* Proceedings of the National Academy of Sciences, 1979. **76**(11): p. 5413-5417.
24. Gunawardena, J., *Time-scale separation--Michaelis and Menten's old idea, still bearing fruit.* Febs j, 2014. **281**(2): p. 473-88.
25. Ferreira, A.E.N., A.M. Ponces Freire, and E.O. Voit, *A quantitative model of the generation of N(epsilon)-(carboxymethyl)lysine in the Maillard reaction between collagen and glucose.* Biochem J, 2003. **376**(Pt 1): p. 109-21.
26. Collier, M.L., et al., *Calcium-induced calcium release in smooth muscle: loose coupling between the action potential and calcium release.* J Gen Physiol, 2000. **115**(5): p. 653-62.
27. Full, R.J. and D.E. Koditschek, *Templates and anchors: neuromechanical hypotheses of legged locomotion on land.* J Exp Biol, 1999. **202**(Pt 23): p. 3325-32.
28. Kvalheim, M., and Revzen, S, *Templates and Anchors; in M.A.* Bioinspired Legged Locomotion. Models, Concepts, Control and Applications, ed. S.a.A. Seyfarth. 2017, Oxford, UK.
29. Poland, A. and A. Kende, *2,3,7,8-Tetrachlorodibenzo-p-dioxin: environmental contaminant and molecular probe.* Fed Proc, 1976. **35**(12): p. 2404-11.
30. Institute of Medicine, B.o.t.H.o.S.P., *Committee to Evaluate the Potential Exposure of Agent Orange/TCDD Residue and Level of Risk of Adverse Health Effects for Aircrew of Post-Vietnam C-123 Aircraft; Board on the Health of Select Populations; Institute of Medicine. Post-Vietnam Dioxin Exposure in Agent Orange-Contaminated C-123 Aircraft.* . National Academies Press (US), 2015.
31. *Evaluation of certain food additives and contaminants. Eightieth report of the Joint FAO/WHO Expert Committee on Food Additives.* World Health Organ Tech Rep Ser, 2016(995): p. 1-114, back cover.
32. Marinković, N., et al., *Dioxins and human toxicity.* Arh Hig Rada Toksikol, 2010. **61**(4): p. 445-53.
33. Medicine., B.o.t.H.o.S.P.I.o., *Committee to Evaluate the Potential Exposure of Agent Orange/TCDD Residue and Level of Risk of Adverse Health Effects for Aircrew of Post-Vietnam C-123 Aircraft; Board on the Health of Select Populations; Institute of Medicine. Post-Vietnam Dioxin Exposure in Agent Orange-Contaminated C-123 Aircraft.* National Academies Press (US, 2015.
34. Eskenazi, B., et al., *Dioxin exposure associated with fecundability and infertility in mothers and daughters of Seveso, Italy.* Hum Reprod, 2021. **36**(3): p. 794-807.
35. Fracchiolla, N.S., et al., *2,3,7,8-Tetrachlorodibenzo-p-dioxin (TCDD) role in hematopoiesis and in hematologic diseases: A critical review.* Toxicology, 2016. **374**: p. 60-68.
36. Greene, J.F., S. Hays, and D. Paustenbach, *Basis for a proposed reference dose (RfD) for dioxin of 1-10 pg/kg-day: a weight of evidence evaluation of the human and animal studies.* J Toxicol Environ Health B Crit Rev, 2003. **6**(2): p. 115-59.
37. Cole, P., et al., *Dioxin and cancer: a critical review.* Regul Toxicol Pharmacol, 2003. **38**(3): p. 378-88.

38. Tuomisto, J.T., et al., *Soft-tissue sarcoma and dioxin: A case-control study.* Int J Cancer, 2004. **108**(6): p. 893-900.
39. Viinamakelainen. *Increase of dioxin concentrations by age in humans*. 2019; Available from: https://commons.wikimedia.org/wiki/File:Dioxin_concentration_by_age.png.
40. Angrish, M.M., C.Y. Dominici, and T.R. Zacharewski, *TCDD-elicited effects on liver, serum, and adipose lipid composition in C57BL/6 mice.* Toxicol Sci, 2013. **131**(1): p. 108-15.
41. Dornbos, P., et al., *Characterizing the Role of HMG-CoA Reductase in Aryl Hydrocarbon Receptor-Mediated Liver Injury in C57BL/6 Mice.* Scientific Reports, 2019. **9**(1): p. 15828.
42. Martin, J.V., *Lipid abnormalities in workers exposed to dioxin.* Br J Ind Med, 1984. **41**(2): p. 254-6.
43. Pelclová, D., et al., *Lipid metabolism and neuropsychological follow-up study of workers exposed to 2,3,7,8- tetrachlordibenzo-p-dioxin.* International Archives of Occupational and Environmental Health, 2002. **75**(1): p. 60-66.
44. Hu, S.W., et al., *Association between dioxins/furans exposures and incinerator workers' hepatic function and blood lipids.* J Occup Environ Med, 2003. **45**(6): p. 601-8.
45. Lee, C.C., et al., *Fatty liver and hepatic function for residents with markedly high serum PCDD/Fs levels in Taiwan.* J Toxicol Environ Health A, 2006. **69**(5): p. 367-80.
46. Pazderova-VejlupkovÁ, J., et al., *The Development and Prognosis of Chronic Intoxication by Tetrachlordibenzo-p-dioxin in Men.* Archives of Environmental Health: An International Journal, 1981. **36**(1): p. 5-11.
47. van der Zalm, A., et al., *A framework for establishing scientific confidence in new approach methodologies.* Archives of Toxicology, 2022. **96**(11): p. 2865-2879.
48. Magurany, K., et al., *A pragmatic framework for the application of new approach methodologies in one health toxicological risk assessment.* Toxicological Sciences, 2023. **192**(2): p. 155-177.
49. Westmoreland, C., et al., *Use of New Approach Methodologies (NAMs) in regulatory decisions for chemical safety: Report from an EPAA Deep Dive Workshop.* Regulatory Toxicology and Pharmacology, 2022. **135**: p. 105261.
50. Fabian, E., et al., *In vitro-to-in vivo extrapolation (IVIVE) by PBTK modeling for animal-free risk assessment approaches of potential endocrine-disrupting compounds.* Archives of Toxicology, 2019. **93**(2): p. 401-416.
51. Yang, H., et al., *Developing an In Vitro to In Vivo Extrapolation (IVIVE) Model to Predict Human Milk-to-Plasma Drug Concentration Ratios.* Molecular Pharmaceutics, 2022. **19**(7): p. 2506-2517.
52. Zhang, Q., et al., *Bridging the Data Gap From in vitro Toxicity Testing to Chemical Safety Assessment Through Computational Modeling.* Front Public Health, 2018. **6**: p. 261.
53. Seipel, J., et al., *Chapter 3 - Conceptual Models of Legged Locomotion,* in *Bioinspired Legged Locomotion*, M.A. Sharbafi and A. Seyfarth, Editors. 2017, Butterworth-Heinemann. p. 55-131.

54. Voit, E.O., *The best models of metabolism.* Wiley Interdiscip Rev Syst Biol Med, 2017. **9**(6).
55. Gao, J., et al., *A review of food contaminant 2,3,7,8-tetrachlorodibenzo-p-dioxin and its toxicity associated with metabolic disorders.* Curr Res Food Sci, 2023. **7**: p. 100617.
56. Dornbos, P., et al., *Characterizing the Role of HMG-CoA Reductase in Aryl Hydrocarbon Receptor-Mediated Liver Injury in C57BL/6 Mice.* Scientific Reports, 2019. **9**(1): p. 15828.
57. Beischlag, T.V., et al., *The aryl hydrocarbon receptor complex and the control of gene expression.* Crit Rev Eukaryot Gene Expr, 2008. **18**(3): p. 207-50.
58. Cano, R., et al., *Role of Endocrine-Disrupting Chemicals in the Pathogenesis of Non-Alcoholic Fatty Liver Disease: A Comprehensive Review.* Int J Mol Sci, 2021. **22**(9).
59. Vergeer, M., et al., *The HDL hypothesis: does high-density lipoprotein protect from atherosclerosis?* J Lipid Res, 2010. **51**(8): p. 2058-73.
60. Scott Kiss, R. and A. Sniderman, *Shunts, channels and lipoprotein endosomal traffic: a new model of cholesterol homeostasis in the hepatocyte.* J Biomed Res, 2017. **31**(2): p. 95-107.
61. Lim, E., et al., *T3DB: a comprehensively annotated database of common toxins and their targets.* Nucleic Acids Res, 2010. **38**(Database issue): p. D781-6.
62. Davis, A.P., et al., *Comparative Toxicogenomics Database: a knowledgebase and discovery tool for chemical-gene-disease networks*. Nucleic Acids Res, 2009. **37**(Database issue): p. D786-92.
63. Ye, W., et al., *AhR regulates the expression of human cytochrome P450 1A1 (CYP1A1) by recruiting Sp1*. Febs j, 2019. **286**(21): p. 4215-4231.
64. Matthews, J., *AHR toxicity and signaling: Role of TIPARP and ADP-ribosylation.* Current Opinion in Toxicology, 2017. **2**: p. 50-57.
65. Fader, K.A. and T.R. Zacharewski, *Beyond the Aryl Hydrocarbon Receptor: Pathway Interactions in the Hepatotoxicity of 2,3,7,8-Tetrachlorodibenzo-p-dioxin and Related Compounds.* Curr Opin Toxicol, 2017. **2**: p. 36-41.
66. Nault, R., et al., *Dose-Dependent Metabolic Reprogramming and Differential Gene Expression in TCDD-Elicited Hepatic Fibrosis.* Toxicol Sci, 2016. **154**(2): p. 253-266.
67. Lu, J., et al., *The role of CYP1A1/2 in cholesterol ester accumulation provides a new perspective for the treatment of hypercholesterolemia.* Acta Pharmaceutica Sinica B, 2023. **13**(2): p. 648-661.
68. Savageau, M.A., *Biochemical Systems Analysis: A Study of Function and Design in Molecular Biology*. 1976.
69. Voit, E.O., *Computational Analysis of Biochemical Systems: A Practical Guide for Biochemists and Molecular Biologists*. 2000, Cambridge, U.K.: Cambridge University Press.
70. Voit, E.O., *Characterizability of metabolic pathway systems from time series data.* Math Biosci, 2013. **246**(2): p. 315-25.
71. Alvarez-Vasquez, F., et al., *Simulation and validation of modelled sphingolipid metabolism in Saccharomyces cerevisiae.* Nature, 2005. **433**(7024): p. 425-30.

72. Chen, P.W., et al., *Dynamics of the Heat Stress Response of Ceramides with Different Fatty-Acyl Chain Lengths in Baker's Yeast.* PLoS Comput Biol, 2015. **11**(8): p. e1004373.
73. Dolatshahi, S., L.L. Fonseca, and E.O. Voit, *New insights into the complex regulation of the glycolytic pathway in Lactococcus lactis. II. Inference of the precisely timed control system regulating glycolysis.* Mol Biosyst, 2016. **12**(1): p. 37-47.
74. Faraji, M., et al., *A dynamic model of lignin biosynthesis in Brachypodium distachyon.* Biotechnol Biofuels, 2018. **11**: p. 253.
75. Mentewab, A., et al., *A dynamic compartment model for xylem loading and long-distance transport of iron explains the effect of kanamycin on metal uptake in Arabidopsis.* Frontiers in Plant Science, 2023. **14**.
76. Olivença, D.V., E.O. Voit, and F.R. Pinto, *ENaC regulation by phospholipids and DGK explained through mathematical modeling.* Scientific Reports, 2020. **10**(1): p. 13952.
77. Qi, Z., G.W. Miller, and E.O. Voit, *A mathematical model of presynaptic dopamine homeostasis: implications for schizophrenia.* Pharmacopsychiatry, 2008. **41 Suppl 1**: p. S89-98.
78. Voit, E., A.R. Neves, and H. Santos, *The intricate side of systems biology.* Proc Natl Acad Sci U S A, 2006. **103**(25): p. 9452-7.
79. Wade, J.D., et al., *Mechanistic Model of Signaling Dynamics Across an Epithelial Mesenchymal Transition.* Frontiers in Physiology, 2020. **11**.
80. Lakshman, M.R., et al., *Effects of 2,3,7,8-tetrachlorodibenzo-p-dioxin on lipid synthesis and lipogenic enzymes in the rat.* J Pharmacol Exp Ther, 1989. **248**(1): p. 62-6.
81. Lakshman, M.R., et al., *Effects of 2,3,7,8-tetrachlorodibenzo-p-dioxin (TCDD) on de novo fatty acid and cholesterol synthesis in the rat.* Lipids, 1988. **23**(9): p. 904-6.
82. Alves, R. and M.A. Savageau, *Comparing systemic properties of ensembles of biological networks by graphical and statistical methods.* Bioinformatics, 2000. **16**(6): p. 527-533.
83. Zhang, Q. and M.E. Andersen, *Dose Response Relationship in Anti-Stress Gene Regulatory Networks.* PLOS Computational Biology, 2007. **3**(3): p. e24.
84. Sharpe, L.J. and A.J. Brown, *Controlling cholesterol synthesis beyond 3-hydroxy-3-methylglutaryl-CoA reductase (HMGCR).* J Biol Chem, 2013. **288**(26): p. 18707-15.
85. Malhotra, P., et al., *Disturbances in Cholesterol Homeostasis and Non-alcoholic Fatty Liver Diseases.* Front Med (Lausanne), 2020. **7**: p. 467.
86. Lu, J., et al., *The role of CYP1A1/2 in cholesterol ester accumulation provides a new perspective for the treatment of hypercholesterolemia.* Acta Pharm Sin B, 2023. **13**(2): p. 648-661.
87. Nault, R., et al., *Lipidomic Evaluation of Aryl Hydrocarbon Receptor-Mediated Hepatic Steatosis in Male and Female Mice Elicited by 2,3,7,8-Tetrachlorodibenzo-p-dioxin.* Chem Res Toxicol, 2017. **30**(4): p. 1060-1075.

88. Calvert, G.M., et al., *Evaluation of serum lipid concentrations among U.S. workers exposed to 2,3,7,8-tetrachlorodibenzo-p-dioxin.* Arch Environ Health, 1996. **51**(2): p. 100-7.
89. Carson, J.e.a., *Dietary Cholesterol and Cardiovascular Risk: A Science Advisory From the American Heart Association.* Circulation, 2020. **141**(3): p. e39-e53.
90. Griffin, J.D. and A.H. Lichtenstein, *Dietary Cholesterol and Plasma Lipoprotein Profiles: Randomized-Controlled Trials.* Curr Nutr Rep, 2013. **2**(4): p. 274-282.
91. Duval, C., et al., *Chronic Exposure to Low Doses of Dioxin Promotes Liver Fibrosis Development in the C57BL/6J Diet-Induced Obesity Mouse Model.* Environ Health Perspect, 2017. **125**(3): p. 428-436.
92. Fernandez, M.L. and A.G. Murillo, *Is There a Correlation between Dietary and Blood Cholesterol? Evidence from Epidemiological Data and Clinical Interventions.* Nutrients, 2022. **14**(10).
93. Adams, C.M., et al., *Cholesterol and 25-Hydroxycholesterol Inhibit Activation of SREBPs by Different Mechanisms, Both Involving SCAP and Insigs**. Journal of Biological Chemistry, 2004. **279**(50): p. 52772-52780.
94. EPA, *Exposure and Human Health Reassessment of 2,3,7,8-Tetrachlorodibenzo-p-Dioxin (TCDD) and Related Compounds* https://cfpub.epa.gov/ncea/risk/recordisplay.cfm?deid=87843, 2004.
95. Emond, C., et al., *Comparison of the Use of a Physiologically Based Pharmacokinetic Model and a Classical Pharmacokinetic Model for Dioxin Exposure Assessments.* Environmental Health Perspectives, 2005. **113**(12): p. 1666-1668.
96. Liu, R., et al., *A Physiologically Based Pharmacokinetic (PBPK) Modeling Framework for Mixtures of Dioxin-like Compounds.* Toxics, 2022. **10**(11): p. 700.
97. Dai, L., et al., *Cholesterol Metabolism in Neurodegenerative Diseases: Molecular Mechanisms and Therapeutic Targets.* Molecular Neurobiology, 2021. **58**(5): p. 2183-2201.
98. Liu, J.-P., et al., *Cholesterol involvement in the pathogenesis of neurodegenerative diseases.* Molecular and Cellular Neuroscience, 2010. **43**(1): p. 33-42.
99. Feingold, K.R., *Introduction to Lipids and Lipoproteins*, in *Endotext*, K.R. Feingold, et al., Editors. 2000: South Dartmouth (MA).
100. Zampelas, A. and E. Magriplis, *New Insights into Cholesterol Functions: A Friend or an Enemy?* Nutrients, 2019. **11**(7).
101. Steyrer, E., et al., *The role of lecithin: cholesterol acyltransferase for lipoprotein (a) assembly. Structural integrity of low density lipoproteins is a prerequisite for Lp(a) formation in human plasma.* J Clin Invest, 1994. **94**(6): p. 2330-40.
102. Rahmany, S. and I. Jialal, *Biochemistry, Chylomicron*, in *StatPearls*. 2024: Treasure Island (FL).
103. Kirkley, A.G. and R.M. Sargis, *Environmental endocrine disruption of energy metabolism and cardiovascular risk.* Curr Diab Rep, 2014. **14**(6): p. 494.
104. Fling, R.R., et al., *2,3,7,8-Tetrachlorodibenzo-p-dioxin (TCDD) dysregulates hepatic one carbon metabolism during the progression of steatosis to steatohepatitis with fibrosis in mice.* Scientific Reports, 2020. **10**(1): p. 14831.

105. Kim, J.J. and Y.M. Choi, *Dyslipidemia in women with polycystic ovary syndrome.* Obstet Gynecol Sci, 2013. **56**(3): p. 137-42.
106. Kanat, M., et al., *Is lipid lowering treatment aiming for very low LDL levels safe in terms of the synthesis of steroid hormones?* Med Hypotheses, 2007. **69**(1): p. 104-12.
107. van de Sluis, B., M. Wijers, and J. Herz, *News on the molecular regulation and function of hepatic low-density lipoprotein receptor and LDLR-related protein 1.* Curr Opin Lipidol, 2017. **28**(3): p. 241-247.
108. Czarnecka, H. and S. Yokoyama, *Regulation of cellular cholesterol efflux by lecithin:cholesterol acyltransferase reaction through nonspecific lipid exchange.* J Biol Chem, 1996. **271**(4): p. 2023-8.
109. Ouimet, M., T.J. Barrett, and E.A. Fisher, *HDL and Reverse Cholesterol Transport.* Circ Res, 2019. **124**(10): p. 1505-1518.
110. Shen, W.J., S. Azhar, and F.B. Kraemer, *SR-B1: A Unique Multifunctional Receptor for Cholesterol Influx and Efflux.* Annu Rev Physiol, 2018. **80**: p. 95-116.
111. Hernell, O., J.E. Staggers, and M.C. Carey, *Physical-chemical behavior of dietary and biliary lipids during intestinal digestion and absorption. 2. Phase analysis and aggregation states of luminal lipids during duodenal fat digestion in healthy adult human beings.* Biochemistry, 1990. **29**(8): p. 2041-56.
112. Mc Auley, M.T., et al., *A whole-body mathematical model of cholesterol metabolism and its age-associated dysregulation.* BMC Syst Biol, 2012. **6**: p. 130.
113. Grassman, J.A., et al., *Animal models of human response to dioxins.* Environ Health Perspect, 1998. **106 Suppl 2**(Suppl 2): p. 761-75.
114. Bull, J.R., et al., *Real-world menstrual cycle characteristics of more than 600,000 menstrual cycles.* npj Digital Medicine, 2019. **2**(1): p. 83.
115. Grieger, J.A. and R.J. Norman, *Menstrual Cycle Length and Patterns in a Global Cohort of Women Using a Mobile Phone App: Retrospective Cohort Study.* J Med Internet Res, 2020. **22**(6): p. e17109.
116. Mcneilly, A.S., *The Control of Fsh-Secretion.* Acta Endocrinologica, 1988. **119**: p. 31-40.
117. Brown, J.B., *Pituitary control of ovarian function--concepts derived from gonadotrophin therapy.* Aust N Z J Obstet Gynaecol, 1978. **18**(1): p. 46-54.
118. Zeleznik, A.J., *The physiology of follicle selection.* Reprod Biol Endocrinol, 2004. **2**: p. 31.
119. Mesen, T.B. and S.L. Young, *Progesterone and the luteal phase: a requisite to reproduction.* Obstet Gynecol Clin North Am, 2015. **42**(1): p. 135-51.
120. Hillier, S.G., P.F. Whitelaw, and C.D. Smyth, *Follicular oestrogen synthesis: the 'two-cell, two-gonadotrophin' model revisited.* Mol Cell Endocrinol, 1994. **100**(1-2): p. 51-4.
121. Christenson, L.K. and L. Devoto, *Cholesterol transport and steroidogenesis by the corpus luteum.* Reprod Biol Endocrinol, 2003. **1**: p. 90.
122. Lavoie, H.A. and S.R. King, *Transcriptional regulation of steroidogenic genes: STARD1, CYP11A1 and HSD3B.* Exp Biol Med (Maywood), 2009. **234**(8): p. 880-907.

123. Stocco, D.M. and B.J. Clark, *Role of the steroidogenic acute regulatory protein (StAR) in steroidogenesis.* Biochem Pharmacol, 1996. **51**(3): p. 197-205.
124. Manna, P.R., et al., *Role of the steroidogenic acute regulatory protein in health and disease.* Endocrine, 2016. **51**(1): p. 7-21.
125. Yonemoto, J., *The effects of dioxin on reproduction and development.* Ind Health, 2000. **38**(3): p. 259-68.
126. Barsotti, D.A., L.J. Abrahamson, and J.R. Allen, *Hormonal alterations in female rhesus monkeys fed a diet containing 2, 3,7,8-tetrachlorodibenzo-p-dioxin.* Bull Environ Contam Toxicol, 1979. **21**(4-5): p. 463-9.
127. Valdez, K.E., et al., *Effect of chronic exposure to the aryl hydrocarbon receptor agonist 2,3,7,8-tetrachlorodibenzo-p-dioxin in female rats on ovarian gene expression.* Reprod Toxicol, 2009. **28**(1): p. 32-7.
128. Morán, F.M., et al., *2,3,7,8-tetrachlorodibenzo-p-dioxin decreases estradiol production without altering the enzyme activity of cytochrome P450 aromatase of human luteinized granulosa cells in vitro.* Biol Reprod, 2000. **62**(4): p. 1102-8.
129. Karman, B.N., et al., *2,3,7,8-Tetrachlorodibenzo-p-dioxin activates the aryl hydrocarbon receptor and alters sex steroid hormone secretion without affecting growth of mouse antral follicles in vitro.* Toxicol Appl Pharmacol, 2012. **261**(1): p. 88-96.
130. Li, X., D.C. Johnson, and K.K. Rozman, *Effects of 2,3,7,8-tetrachlorodibenzo-p-dioxin (TCDD) on estrous cyclicity and ovulation in female Sprague-Dawley rats.* Toxicol Lett, 1995. **78**(3): p. 219-22.
131. Eskenazi, B., et al., *Serum dioxin concentrations and menstrual cycle characteristics.* Am J Epidemiol, 2002. **156**(4): p. 383-92.
132. Buck Louis, G.M., et al., *Persistent organochlorine pollutants and menstrual cycle characteristics.* Chemosphere, 2011. **85**(11): p. 1742-8.
133. Morán, F.M., et al., *Molecular target of endocrine disruption in human luteinizing granulosa cells by 2,3,7,8-tetrachlorodibenzo-p-dioxin: inhibition of estradiol secretion due to decreased 17alpha-hydroxylase/17,20-lyase cytochrome P450 expression.* Endocrinology, 2003. **144**(2): p. 467-73.
134. Dasmahapatra, A.K., et al., *Demonstration of 2,3,7,8-tetrachlorodibenzo-p-dioxin attenuation of P450 steroidogenic enzyme mRNAs in rat granulosa cell in vitro by competitive reverse transcriptase-polymerase chain reaction assay.* Mol Cell Endocrinol, 2000. **164**(1-2): p. 5-18.
135. Karman, B.N., et al., *Dioxin exposure reduces the steroidogenic capacity of mouse antral follicles mainly at the level of HSD17B1 without altering atresia.* Toxicol Appl Pharmacol, 2012. **264**(1): p. 1-12.
136. Wright, A.A., et al., *Mechanistic model of hormonal contraception.* PLoS Comput Biol, 2020. **16**(6): p. e1007848.
137. Graham, E.J. and J.F. Selgrade, *A model of ovulatory regulation examining the effects of insulin-mediated testosterone production on ovulatory function.* J Theor Biol, 2017. **416**: p. 149-160.
138. Harris, L.A. and J.F. Selgrade, *Modeling endocrine regulation of the menstrual cycle using delay differential equations.* Math Biosci, 2014. **257**: p. 11-22.

139. Hendrix, A.O., C.L. Hughes, and J.F. Selgrade, *Modeling endocrine control of the pituitary-ovarian axis: androgenic influence and chaotic dynamics.* Bull Math Biol, 2014. **76**(1): p. 136-56.
140. Margolskee, A. and J.F. Selgrade, *A lifelong model for the female reproductive cycle with an antimüllerian hormone treatment to delay menopause.* J Theor Biol, 2013. **326**: p. 21-35.
141. Margolskee, A. and J.F. Selgrade, *Dynamics and bifurcation of a model for hormonal control of the menstrual cycle with inhibin delay.* Math Biosci, 2011. **234**(2): p. 95-107.
142. Selgrade, J.F., *Bifurcation analysis of a model for hormonal regulation of the menstrual cycle.* Math Biosci, 2010. **225**(2): p. 108-14.
143. Selgrade, J.F., L.A. Harris, and R.D. Pasteur, *A model for hormonal control of the menstrual cycle: Structural consistency but sensitivity with regard to data.* Journal of Theoretical Biology, 2009. **260**(4): p. 572-580.
144. Clark, L.H., P.M. Schlosser, and J.F. Selgrade, *Multiple stable periodic solutions in a model for hormonal control of the menstrual cycle.* Bull Math Biol, 2003. **65**(1): p. 157-73.
145. Röblitz, S., et al., *A mathematical model of the human menstrual cycle for the administration of GnRH analogues.* J Theor Biol, 2013. **321**: p. 8-27.
146. Hendrix, A.O. and J.F. Selgrade, *Bifurcation analysis of a menstrual cycle model reveals multiple mechanisms linking testosterone and classical PCOS.* J Theor Biol, 2014. **361**: p. 31-40.
147. Chen, C.Y. and J.P. Ward, *A mathematical model for the human menstrual cycle.* Math Med Biol, 2014. **31**(1): p. 65-86.
148. Reinecke, I. and P. Deuflhard, *A complex mathematical model of the human menstrual cycle.* J Theor Biol, 2007. **247**(2): p. 303-30.
149. Schlosser, P.M. and J.F. Selgrade, *A model of gonadotropin regulation during the menstrual cycle in women: qualitative features.* Environ Health Perspect, 2000. **108 Suppl 5**: p. 873-81.
150. Stricker, R., et al., *Establishment of detailed reference values for luteinizing hormone, follicle stimulating hormone, estradiol, and progesterone during different phases of the menstrual cycle on the Abbott ARCHITECT analyzer.* Clin Chem Lab Med, 2006. **44**(7): p. 883-7.
151. Groome, N.P., et al., *Measurement of dimeric inhibin B throughout the human menstrual cycle.* J Clin Endocrinol Metab, 1996. **81**(4): p. 1401-5.
152. Hutz, R.J., et al., *Environmental toxicants and effects on female reproductive function.* Tren Reprod Bio, 2006. **2**: p. 1-11.
153. Harlow, S.D., X. Lin, and M.J. Ho, *Analysis of menstrual diary data across the reproductive life span Applicability of the bipartite model approach and the importance of within-woman variance.* Journal of Clinical Epidemiology, 2000. **53**(7): p. 722-733.
154. Treloar, A.E., et al., *Variation of the human menstrual cycle through reproductive life.* Int J Fertil, 1967. **12**(1 Pt 2): p. 77-126.
155. Fehring, R.J., M. Schneider, and K. Raviele, *Variability in the phases of the menstrual cycle.* J Obstet Gynecol Neonatal Nurs, 2006. **35**(3): p. 376-84.

156. Reed, B.G. and B.R. Carr, *The Normal Menstrual Cycle and the Control of Ovulation*, in *Endotext*, K.R. Feingold, et al., Editors. 2000: South Dartmouth (MA).
157. Eskenazi, B., et al., *Serum dioxin concentrations and age at menopause.* Environ Health Perspect, 2005. **113**(7): p. 858-62.
158. Fader, K.A., et al., *2,3,7,8-Tetrachlorodibenzo-p-Dioxin Alters Lipid Metabolism and Depletes Immune Cell Populations in the Jejunum of C57BL/6 Mice.* Toxicol Sci, 2015. **148**(2): p. 567-80.
159. Vattulainen, I. and T. Rog, *Lipid simulations: a perspective on lipids in action.* Cold Spring Harb Perspect Biol, 2011. **3**(4).
160. Dassios, I. and F. Milano, *Singular dual systems of fractional-order differential equations.* Mathematical Methods in the Applied Sciences, 2021.
161. Rudolph, J., *Duality in time-varying linear systems: A module theoretic approach.* Linear Algebra and its Applications, 1996. **245**: p. 83-106.
162. Bruce, J.W. and F. Tari, *Duality and implicit differential equations.* Nonlinearity, 2000. **13**(3): p. 791.
163. Marin-Sanguino, A., E.R. Mendoza, and E.O. Voit, *Flux duality in nonlinear GMA systems: implications for metabolic engineering.* J Biotechnol, 2010. **149**(3): p. 166-72.
164. Olivença, D.V., et al., *Mathematical models of cystic fibrosis as a systemic disease.* WIREs Mech Dis, 2023: p. e1625.
165. Baird, L.L., *The Practical Utility of Measures of College Environments.* Review of Educational Research, 1974. **44**(3): p. 307-329.
166. Huang, K.T., et al., *Decreased PEDF Promotes Hepatic Fatty Acid Uptake and Lipid Droplet Formation in the Pathogenesis of NAFLD.* Nutrients, 2020. **12**(1).
167. Lind, P.M., et al., *The dioxin-like pollutant PCB 126 (3,3',4,4',5-pentachlorobiphenyl) affects risk factors for cardiovascular disease in female rats.* Toxicology Letters, 2004. **150**(3): p. 293-299.
168. Humblet, O., et al., *Dioxins and cardiovascular disease mortality.* Environ Health Perspect, 2008. **116**(11): p. 1443-8.
169. Varbo, A., M. Benn, and B.G. Nordestgaard, *Remnant cholesterol as a cause of ischemic heart disease: Evidence, definition, measurement, atherogenicity, high risk patients, and present and future treatment.* Pharmacology & Therapeutics, 2014. **141**(3): p. 358-367.
170. Moslehi, A. and Z. Hamidi-Zad, *Role of SREBPs in Liver Diseases: A Mini-review.* J Clin Transl Hepatol, 2018. **6**(3): p. 332-338.
171. Dietschy, J.M., *Dietary Fatty Acids and the Regulation of Plasma Low Density Lipoprotein Cholesterol Concentrations1,2.* The Journal of Nutrition, 1998. **128**(2): p. 444S-448S.
172. Barona, J. and M.L. Fernandez, *Dietary cholesterol affects plasma lipid levels, the intravascular processing of lipoproteins and reverse cholesterol transport without increasing the risk for heart disease.* Nutrients, 2012. **4**(8): p. 1015-25.
173. Orth, J.D., I. Thiele, and B.Ø. Palsson, *What is flux balance analysis?* Nature Biotechnology, 2010. **28**(3): p. 245-248.
174. Holmes, P., et al., *The Dynamics of Legged Locomotion: Models, Analyses, and Challenges.* SIAM Review, 2006. **48**(2): p. 207-304.

175. Zhang, Q., et al., *Bridging the Data Gap From in vitro Toxicity Testing to Chemical Safety Assessment Through Computational Modeling.* Frontiers in Public Health, 2018. **6**.
176. Brubaker, D.K., et al., *An interspecies translation model implicates integrin signaling in infliximab-resistant inflammatory bowel disease.* Sci Signal, 2020. **13**(643).
177. Schulz, T.G., et al., *Inducibility of cytochromes P-450 by dioxin in liver and extrahepatic tissues of the marmoset monkey (Callithrix jacchus).* Biochimica et Biophysica Acta (BBA) - Protein Structure and Molecular Enzymology, 1996. **1298**(1): p. 131-140.
178. Voit, E.O. and K.L. Brigham, *The Role of Systems Biology in Predictive Health and Personalized Medicine.* The Open Pathology Journal,, 2008. **2**: p. 68-70.
179. Davis, J.D., et al., *Dynamical systems approaches to personalized medicine.* Curr Opin Biotechnol, 2019. **58**: p. 168-174.
180. Brown, D., et al., *Trauma in silico: Individual-specific mathematical models and virtual clinical populations.* Science Translational Medicine, 2015. **7**(285): p. 285ra61-285ra61.
181. Craig, M., et al., *A practical guide for the generation of model-based virtual clinical trials.* Frontiers in Systems Biology, 2023. **3**.
182. Gasiewicz, T.A., et al., *Distribution, excretion, and metabolism of 2,3,7,8-tetrachlorodibenzo-p-dioxin in C57BL/6J, DBA/2J, and B6D2F1/J mice.* Drug Metab Dispos, 1983. **11**(5): p. 397-403.
183. Nault, R., et al., *Dose-dependent disruption of hepatic zonation by 2,3,7,8-tetrachlorodibenzo-p-dioxin in mice: integration of single-nuclei RNA sequencing and spatial transcriptomics.* bioRxiv, 2022: p. 2022.06.15.496321.
184. Dutta-Moscato, J., et al., *A Multiscale Agent-Based in silico Model of Liver Fibrosis Progression.* Front Bioeng Biotechnol, 2014. **2**: p. 18.
185. Fader, K.A., et al., *2,3,7,8-Tetrachlorodibenzo-p-dioxin (TCDD)-elicited effects on bile acid homeostasis: Alterations in biosynthesis, enterohepatic circulation, and microbial metabolism.* Sci Rep, 2017. **7**(1): p. 5921.
186. Chen, R. and M. Snyder, *Systems biology: personalized medicine for the future?* Curr Opin Pharmacol, 2012. **12**(5): p. 623-8.
187. Prague, M., D. Commenges, and R. Thiebaut, *Dynamical models of biomarkers and clinical progression for personalized medicine: the HIV context.* Adv Drug Deliv Rev, 2013. **65**(7): p. 954-65.
188. Schoeberl, B., *Quantitative Systems Pharmacology models as a key to translational medicine.* Current Opinion in Systems Biology, 2019. **16**: p. 25-31.
189. Savageau, M.A., *Biochemical systems analysis. I. Some mathematical properties of the rate law for the component enzymatic reactions.* J Theor Biol, 1969. **25**(3): p. 365-9.